Turun yliopisto
University of Turku

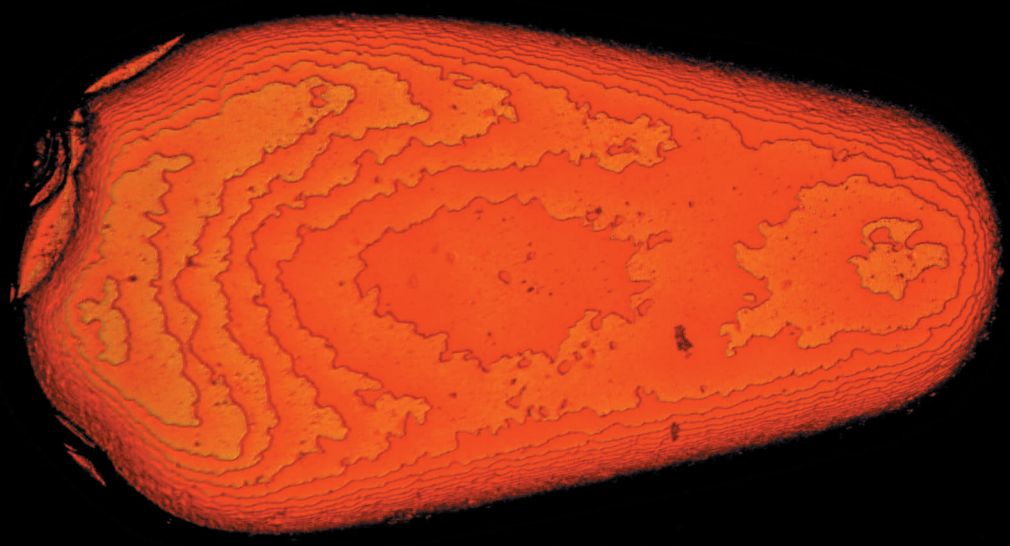

CHARACTERIZATION OF POROUS SILICON NANOPARTICLES FOR BIOMEDICAL APPLICATIONS

Martti Kaasalainen

TURUN YLIOPISTON JULKAISUJA – ANNALES UNIVERSITATIS TURKUENSIS
Sarja – ser. AI osa – tom. 557 | Astronomica – Chemica – Physica – Mathematica | Turku 2017

Turun yliopisto
University of Turku

CHARACTERIZATION OF POROUS SILICON NANOPARTICLES FOR BIOMEDICAL APPLICATIONS

Martti Kaasalainen

TURUN YLIOPISTON JULKAISUJA – ANNALES UNIVERSITATIS TURKUENSIS
Sarja - ser. A I osa - tom. 557 | Astronomica - Chemica - Physica - Mathematica | Turku 2017

University of Turku

Faculty of Mathematics and Natural Sciences
Department of Physics and Astronomy

Supervised by

Jarno Salonen
Docent
Department of Physics and Astronomy
University of Turku
Turku, Finland

Reviewed by

Miguel Manso Silván
Lecturer
Departmento de Física Aplicada
Facultad de Ciencias
Universidad Autónoma de Madrid
Madrid, Spain

Clive Prestidge
Professor
School of Pharmacy and Medical Science
University of South Australia
Adelaide, Australia

Opponent

Frédérique Cunin
CNRS Research scientist
Institut Charles Gerhardt Montpellier
Université de Montpellier
Montpellier, France

Cover image: Martti Kaasalainen

The originality of this thesis has been checked in accordance with the University of Turku quality assurance system using the Turnitin OriginalityCheck service.

ISBN 978-951-29-6811-4 (PRINT)
ISBN 978-951-29-6812-1 (PDF)
ISSN 0082-7002 (Print)
ISSN 2343-3175 (Online)
Painosalama Oy - Turku, Finland 2017

Acknowledgements

The Finnish dissertation defense tradition is an amazing end to a long project. Despite the fact that only one person is defending this thesis, it was not just born out of thin air. I have an amazing network of people around me who have made this possible. I would like to thank a few of you here, but at the same time, I regret that I cannot mention you all. For that, there is limited amount of space, time, and as you know me, memory capacity. So I start by thanking you all around me! Although I might sometimes be absent minded, I sense you are there, and I am extremely grateful for that.

It seems that in the future we are heading towards shorter graduation times. This may be a good direction, but we should also remember to think what is important. While you are wandering in an enormous, constantly changing, forest of information, it is time consuming to accumulate enough confidence to say that you know something, and perhaps even know where to go next. At the same time, the surrounding society reminds us to "think big" and "be creative." I agree that these may be important skills in the future, but thinking big does not happen itself, not without good general knowledge, and we need to understand that tight boundaries are destroying the creativity. Aaro Hellaakoski, Finnish poet and scientist, turned the same idea into an aphorism in 1946 in his collection of poems *Huojuvat keulat*:

Tietä käyden tien on vanki.

Vapaa on vain umpihanki.

A common translation is not too elegant, but the idea is that "You are a prisoner of the road you follow. Only the untrodden snowdrift is free."

For me, the duration of this project has been appropriate. I think that I know now something about thinking big and being creative, although there is still so much to learn. For this, I would like to thank Jarno and his hard pioneering work to buy people time to find their path. In addition, Jarno gave me a unique topic for my thesis and an amazing interdisciplinary and international collaboration network to support my project. I would also like to thank Vesa-Pekka for introducing me for the first time to zeta potential during my bachelor thesis and for all the support you have given me during these years.

In research, things often do not go as you wish. During these moments, collegial support is worth its weight in gold. The spirit in the Laboratory of Industrial Physics has been amazing and I have never felt that I am in this alone. Especially, I would like to thank Ermei for sharing all his knowledge, Tero for listening (and keeping me alive), Luke for amazing, honest discussions, Jorma for your uncompromising spirit, Joe for proof-reading and comments, and Jaani

and Matti for your subtle but solid support. Outi, Janne, Jaakko, OP, Rici, and all other great people in the laboratory in the past and today, thank you for your inspiring attitude and sorry if it seems that it does not stick. It does, but in small doses.

Collaborators, Jussi, Miia, Joakim, Vladimir, Eva, and all the others, your names and influence can be found from the following pages. Thank you for trusting me, teaching me, letting me use your expensive instruments, reviewing my manuscripts, and everything else. Trust based collaboration, which we have had, is the key if we really want to think big and be creative. I would also like to thank my pre-examiners Miguel Manso Silván and Clive Prestidge for their evaluation and comments.

In order to be able to do science, to learn and to study, the vital role of funding cannot be emphasized too much. I consider myself lucky in this sense since I received my first two year contract from a project of the Academy of Finland. Thank you for that. This funding was followed by an extraordinary National Graduate School in Nanoscience. Besides that I am grateful for the salary, I would like to thank all the people in the Nanoscience center for all those seminars in Jyväskylä with superior international speakers and a welcoming atmosphere. I would also like to thank the Finnish Cultural Foundation, the Turku University Foundation, and the Turku University Doctoral Programme in Physical and Chemical Sciences for your support and travel grants.

As much as I enjoy doing research, life cannot be all work. My productivity increases substantially if every now and then someone pulls me out of the wilderness, back to the civilized world and gives me a reason not to think on my research. In this sense, my family and friends have had a vital role in this project. Mom and dad, and my grandparents, thank you for making this possible and creating such a feeling of support that I have had chance to do things that are important to me. Thank you Elisa, that you have always been beside me and for all the strength and attitude that you have taught me. Thank you family Heinilä, for all the evenings in Huiluntie and your great company and food. All my god children, Frans, Aada, Valtteri and Otava, and Siiri of course, thank you for all the games and fun! And all my friends: Esa, Tuomas, Aleksi, Päivö, Maria, family Kankkio, and family Vehanen, and all other study friends from Delta, Ellipsis, and Society of Physical Pharmacy, thank you for sharing your experiences, opinions and giving your support.

And finally, Leila, you have been my colleague, collaborator, supervisor, friend, support—and my love—during these years. Thank you for everything we have gone through.

Turku, April 2017

Martti Kaasalainen

Abstract

Porous silicon (PSi) is an intriguing material for biomedical applications because a great variation of properties can be created by adjusting fabrication parameters. Physicochemical properties, including pore size, surface area, surface chemistry and material dimensions, are dictating PSi behavior in biological environments. Degradation rate and drug loading capacity, as well as interactions with cell membranes and blood proteins correlate with these properties. When material dimensions are approaching the nanoscale, significant benefits, like efficient biodistribution and permeation through biological membranes, can be achieved. Unfortunately, nanoscale objects are challenging to characterize because the physical models that explain regularities in the nanoscale world are significantly different compared with the macroscopic world. Thus, careful basic studies and linking material properties to its performance is important when designing functional materials for biomedical applications.

In this thesis, nanoparticle characterization with light scattering techniques and nanoparticle properties in biologically and pharmacologically relevant conditions are studied. During the research, we have found electrophoretic light scattering (ELS) and zeta potential to be a convenient way to characterize PSi nanoparticles' surface chemistry and colloidal stability. Multiangle light scatterings (dynamic and static light scattering) proved to be useful phenomena when structure, agglomeration, and size of mesoporous nanoparticles needed to be revealed in their natural colloidal form. ELS studies did also show that isotonic media and peptide adsorption play a pivotal role in the stability and zeta potential of PSi nanoparticles. These results highlight the importance of medium dependent characterization of nanoparticles and show the versatility of light scattering experiments for this purpose.

The role of medium in loading peptides into PSi nanoparticles has also been studied, and pH was found to have a significant effect. Despite the general assumption, the highest loading degree was achieved in pH conditions where the total charge of the peptide was close to zero. Peptide adsorption at low loading concentrations was found to be very strong, especially on hydrophobic particles, and part of the peptide payload was irreversibly adsorbed.

In *in vivo* studies, the loading of peptides into PSi nanoparticles sustained the peptide release in subcutaneous delivery from 26 min to more than 20 hours. Intravenously administered nanoparticles did not cause notable sustained release. These results are indicating that loading conditions may affect the release of peptides from PSi nanoparticles. The possibility to tune the peptide release by altering loading conditions makes PSi nanoparticles an interesting candidate for the sustained subcutaneous delivery of peptide drugs.

Tiivistelmä

Huokoisen piin (PSi) ominaisuuksia pystytään säätelemään helposti valmistusparametrien avulla ja tästä johtuen materiaalilla on lupaavia biolääketieteellisiä sovelluksia. Nämä fysikaaliset ja kemialliset ominaisuudet, kuten huokoskoko, pinta-ala, pintakemia ja yhden yksikön mittasuhteet, määrittelevät materiaalin käyttäytymistä biologisessa ympäristössä. Muutamia mainitakseni, ominaisuuksilla on vaikutusta PSi:n hajoamisnopeuteen ja lääkelatauskapasiteettiin, sekä sen vuorovaikutukseen solukalvon ja veren proteiinien kanssa. Kun yhden yksikön mittasuhteet lähestyvät nanomittakaavaa, voidaan biologisissa sovelluksissa saavuttaa huomattavia etuja. Näitä ovat esimerkiksi materiaalin tehokas leviäminen elimistössä ja kulkeutuminen biologisten esteiden läpi. Juuri tästä pienestä mittakaavasta johtuen materiaalin karakterisointi on kuitenkin haastavaa. Nanomittakaavan lainalaisuudet eroavat merkittävästi intuitiivisestä käsityksestämme materiaalin vuorovaikutuksesta ympäristön kanssa. Näin ollen perustutkimus, jonka tulosten perusteella materiaalin ominaisuuksia pyritään kytkemään materiaalin käyttäytymiseen biologisessa ympäristössä, on erittäin tärkeää.

Olen väitöskirjassani tutkinut nanopartikkelien karakterisointia valonsirontatekniikoiden avulla, sekä nanopartikkelien ominaisuuksia farmaseuttisesti ja biologisesti relevanteissa väliaineissa. Olemme tutkimuksessa huomanneet elektroforeettisen valonsironnan (ELS) ja tästä mittauksesta saatavan suureen, zeta potentiaalin, hyödyllisyyden PSi nanopartikkelien pintakemian ja kolloidisen stabiiliuden karakterisoinnissa. Monikulmasirontamenetelmät (dynaaminen ja staattinen valonsironta) osoittautuivat hyödyllisiksi mitattaessa mesohuokoisten nanopartikkelien rakennetta, kokoa ja agglomeroitumista niiden luonnollisessa kolloidisessa olomuodossa.

Valonsirontamittaukset osoittivat myös, että isotoninen väliaine ja peptidiadsorptio vaikuttavat oleellisesti nanopartikkelien stabiilisuuteen ja zeta potentiaaliin. Tämän innoittamana tutkimme väliaineen roolia myös peptidien latautumisessa ja tuloksena huomasimme pH:n suuren vaikutuksen latausasteeseen. Yleisesti oletettu käsitys on, että peptidit latautuvat parhaiten vastakkaismerkkisesti varautuneisiin nanopartikkeleihin. Varauksien erimerkkisyyden huomattiin kuitenkin olevan vain vähäisessä roolissa, sillä paras latausaste saavutettiin peptidien ollessa kokonaisvaraukseltaan mahdollisimman lähellä neutraalia. Adsorptio matalissa peptidikonsentraatioissa oli erittäin voimakasta erityisesti hydrofobisten partikkelien tapauksessa. Lisäksi huomattiin, että osa latautuneista peptideistä oli adsorboitunut irreversiibelisti.

In vivo -kokeissa peptidien ihonalainen annostelu PSi nanopartikkeleihin ladattuna hidasti peptidien vapautumista 26 minuutista yli 20 tuntiin. Suonensisäisesti annosteltuna nanopartikkelit eivät merkittävästi pidentäneet vapautu-

misaikaa. Tuloksista voidaan päätellä myös, että latausolosuhteet saattavat vaikuttaa peptidien vapautumiseen nanopartikkeleista. Mahdollisuus vaikuttaa peptidien vapautumiseen latausolosuhteita muuttamalla saattaa tulevaisuudessa auttaa hallitsemaan peptidien ihonalaista annostelua.

List of papers

This thesis consists of a review of the subject and the following original research articles. Paper I is reprinted with permission from Elsevier (© 2012). Paper II, III, IV are reprinted with permission from American Chemical Society (© 2012, 2013 and 2015, respectively). Paper V is published in open access journal.

I **Effect of Isotonic Solutions and Peptide Adsorption on Zeta Potential of Porous Silicon Nanoparticle Drug Delivery Formulations**
M. Kaasalainen, E. Mäkilä, J. Riikonen, M. Kovalainen, K. Järvinen, K.-H. Herzig, V.-P. Lehto, and J. Salonen, Int. J. Pharm. **431**, 230–236 (2012)

II **Amine Modification of Thermally Carbonized Porous Silicon with Silane Coupling Chemistry**
E. Mäkilä, L. M. Bimbo, M. Kaasalainen, B. Herranz, A. J. Airaksinen, M. Heinonen, E. Kukk, J. Hirvonen, H. A. Santos and J. Salonen, Langmuir **28**, 14045–14054 (2012)

III **Development of Porous Silicon Nanocarriers for Parenteral Peptide Delivery**
M. Kovalainen, J. Mönkäre, M. Kaasalainen, J. Riikonen, V.-P. Lehto, J. Salonen, K.-H. Herzig and K. Järvinen, Mol. Pharm. **10**, 353–359 (2013)

IV **Electrostatic Interaction on Loading of Therapeutic Peptide GLP-1 into Porous Silicon Nanoparticles**
M. Kaasalainen, J. Rytkönen, E. Mäkilä, A. Närvänen and J. Salonen, Langmuir **31**, 1722–1729 (2015)

V **Size, Stability, and Porosity of Mesoporous Nanoparticles characterized with light scattering**
M. Kaasalainen, V. Aseyev, E. von Haartman, D. Şen Karaman, E. Mäkilä, H. Tenhu, J. Rosenholm and J. Salonen, Nanoscale Res. Lett. **12**, 74 (2017)

Contents

1 Background

1.1 Establishment of nanotechnology

The story of nanoscience and nanotechnology differs from typical scientific narratives because it is a mix of science, popular science, and politics. Since all these approaches are important for the existence of this thesis and I feel that leaving some of these out would not be the whole truth, I will here describe my interpretation of the history of nanotechnology based on these three institutions.

The most significant political act in history of nanotechnology was the establishment of U.S. National Nanotechnology Initiative (NNI), an achievement of President Clinton in 2000, which directed significant amount of research funding to promote nanotechnology in the United States. The European Union followed right behind and in 2003, the 6th Framework Programme for Research and Technological Development was started, with nanotechnologies and nanosciences as one of the thematic areas[1]. Promises of nanotechnology, which we will get to know in more detail in next chapters, tempted Finnish scientists, also. The fastest response to this increasing interest came from University of Jyväskylä, where in 2001, nanoscientists, together with the university governance, decided to build a new building for the purpose of nano research [1]. This project was special on a global scale, as until then, a typical nanoscience center was only a virtual construction. This joint project, and the commitment of scientists and governance, established the role of the University of Jyväskylä in nanoscience. When the new National Graduate School in Nanoscience (NGS-NANO) started in 2006, the responsibility of coordination was given to the University of Jyväskylä.

The NNI defines the nanotechnology as follows[2]:

---

[1] The Sixth Framework Programme in brief, online citation 8.12.2016, https://ec.europa.eu/research/fp6/pdf/fp6-in-brief_en.pdf

[2] What is Nanotechnology?, online citation 8.12.2016, http://www.nano.gov/nanotech-101/what/definition

> Nanotechnology is science, engineering, and technology conducted at the nanoscale, which is about 1 to 100 nanometers. Nanoscience and nanotechnology are the study and application of extremely small things and can be used across all the other science fields, such as chemistry, biology, physics, materials science, and engineering.

This is quite a common definition, and it mentions two of the most guiding features of nanoscience and nanotechnology: the size scale and interdisciplinary nature of the field. Although both of them are, every now and then, argued.

When it comes to science and popular science, the official (as defined by NNI) privilege to be called the "father" of nanotechnology is commonly given to U.S. physicist Richard Feynman because of his famous talk, "There's Plenty of Room at the Bottom." The adaptation of the talk can be found for example, in reference [2]. In the talk, he envisions his idea of how much room there still is to decrease the size of machines before they are limited by the laws of physics. Feynman was a world known lecturer and physics Nobel Prize Winner, thus the talk was brilliant with no doubt, and might have even included some new perspectives. However, it is easy to agree with Toumey, who states in his column in Nature Nanotechnology special Feynman edition, that the scientific impact of the talk for the field of nanoscience was not that large [3]. One of the arguments that supports this opinion is that it took about 30 years before Feynman's ideas were discovered again and harnessed for use in the nanoscience narrative. Meanwhile, almost no attention to these predictions was given. The talk was published several times, but despite this, it gathered almost no citations during the first 20 years. This is especially significant since in 1950s, Feynman was already a recognized scientist, as indicated by the 160 citations[3] that one of his most successful articles [4] gained during first 20 years, even though the Second World War decreased the scientific efforts at the same time.

One of the earliest citations to Feynman's talk is in the article of Eric Drexler in 1981 [5]. He refines Feynman's idea about tiny machines and explains how it should be possible to create them with molecular engineering. In 1986, Drexler wrote a whole book, Engines of Creation [6], around this interesting idea, and it started gaining public attention. In Drexler's vision, in the near future, it should be possible to build nanomachines that could fabricate things in the macroscale and, in addition, replicate themselves. As one can imagine, these ideas, especially the idea of replication, had a lot of influence on science fiction, and the threats of nanoscience came into public discussion, before the actual field even existed.

[3] According to Google Scholar 28.11.2016

At the same time, with or without contribution from the nano hype, the advances towards the nanoscale were also made on the scientific side, especially on microscopy. Atomic-force microscopes were discovered in the 1980s [7]; this also enabled the first actual atom-by-atom structures fabricated in 1990 [8]. Also electron microscopes and especially sample fabrication procedures advanced during 1980s and 1990s from which one real life example considers myosin which was imaged on action, "walking" along F-actin [9].

One of the influential popularizer and educator in the field of the nanoscience is Richard Jones, whose book "Soft machines" was published in 2004 [10]. Jones placed molecular engineering in one of the three subfields of nanotechnology called radical nanotechnology. He also pointed out that it is important to understand the nanoscale physics, which could be very different from the physics in the macroscopic world. This was thought to be a limitation of Drexler's approach. Two other subfields were incremental nanotechnology and evolutionary nanotechnology. Incremental nanotechnology aims to improve materials through nanoscale modifications. One very recent advancement of this kind is UltraRope, developed by Kone[4]. The strong carbon (nano)fiber core enables longer elevators to higher buildings due to the lighter weight of the rope. Evolutionary nanotechnology aims towards developing more active materials such as nanoscale transistors and sensors. This kind of development on transistors has been evident for a long time, being accelerated by the strong commercial need for smaller microelectronics. When in the 1980s the size of the smallest feature on microprocessor could be decreased to under 1 μm [10]; it is now 14 nm in commercial processors[5].

In the scientific background of this work, there are three different disciplines which have something to do with the "nano". The first of them is perhaps most influenced by the hype of nanotechnology; since after the establishment of NNI, the number of nanopharmaceuticals have been rapidly growing [11,12]. This research is considered to originate from the studies of controlled drug delivery systems (DDS) which have been studied since the 1950s [13]. In the 1960s, polymer based DDSs were discovered, and in the 1970s, the research of nanoparticles, or colloidal particles (as they were called in those days), began to gain attention in the field. This takes us to the second tradition called colloid science.

Colloid scientists have a long tradition of characterizing nanoparticles in liquid medium, which is important when biological or pharmaceutical applications are considered. The political emergence of nanoscience has caused an espe-

[4] KONE UltraRope, online citation 8.12.2016, http://download.kone.com/ultrarope/index.htm
[5] Your Source for Intel® Product Specifications, online citation 8.12.2016, http://ark.intel.com/

cially strong identity crisis in the field of colloidal sciences [14]. Colloidal dispersion can be defined as a heterogeneous mixture of two or more substances, where at least one component occurs in non-continuous, dispersed, form and the other in form of continuous medium [15]. The size of dispersed objects can vary between 1 nm and 1 μm, by definition. It does not matter what is the actual state of the matter and almost all the three basic states occur. The only exception is gas as both the continuous and non-continuous components in one system. Mixtures of two immiscible liquids (like oil and water) are called emulsions, solid or liquid particles dispersed in gas (like smoke or fog) are called aerosol, and gas in liquid is called foam. Mixtures of solid particles and liquid medium are often called suspensions. Nanoparticles are, in most cases, well dispersed and stable in liquid medium, in which case, the terms colloidal dispersion or colloidal suspension can be used. For simplicity, the word suspension is used to describe this kind of system.

The third tradition is the development of porous materials. Again, even before nanoscience, researchers studied these materials, classifying by pore diameter into three different groups. The pores with diameter less than 2 nm are called micropores, 2-50 nm pores are mesopores and pores larger than 50 nm are called macropores [16]. With the same logic, a material can be defined micro-, meso- or macroporous. As we will see in the next chapter, the discovery of the material that I have mainly studied, porous silicon (PSi), dates back to the 1970s when the porosity was measured for the first time. Nevertheless, on those days, there was more than 200 years history of research on microporous materials called zeolites [17].

Therefore, when we are manipulating and applying different kind of pores on PSi, we are doing nanoscience by the definition of NNI. On the other hand, we are willing to utilize the interesting properties of this nanomaterial in particular forms in the DDS field. Because of this, we adapt the definition of nanoparticle from the field of colloidal science and nanopharmacy and work in the area well below 1 μm. This we do by keeping in mind as Richard Jones has written [18]:

> Perhaps Feynman can be credited, above all, for making nanotechnology a field driven by imagination and visions of the future. Something else that we might usefully take from his lecture is the importance of a spirit of play and the drive to achieve new technical feats just because you can. Ultimately, what's important is not what you can imagine, but what you can make.

1.2 Discovery of porous silicon

The discovery of porous silicon (PSi) dates back to 1956 with early electrochemical studies on silicon. While studying the electrolytic shaping of silicon, Arthur Uhlir and his wife Ingeborg Uhlir discovered the formation of a dark matte layer on a top of the silicon wafer [19]. This layer, which they thought to be silicon suboxide, was unwanted, and they did not notice its porosity. Two years later Turner, in his article concerning electrochemical anodization of silicon [20], stated as follows:

> At a critical current density, the thick film suddenly starts coming off and floats to the surface.

He had found out that the dark layer, which he actually suspected to be porous, was possible to detach by increasing the current density above the critical point, to the so-called electropolishing region. During the next ten years, different ways to form the same kind of films on top of the silicon substrate were discovered. These studies concerned mainly anodic oxidation, electropolishing, and chemical etching [21]. Puzzled by the colored stain films on top of the silicon, which followed by etching it in aqueous solution of hydrofluoric acid (HF) and nitric acid (HNO_3), Archer made the first thorough study on the technique called stain etching in 1960 [22]. The first light assisted (photoelectrochemical) etchings were made by Dalisa *et al.* in 1970 [23].

Finally in 1971, Watanabe *et al.* verified the porous nature of the film [24]. This discovery gave the first thrust to an increasing interest on PSi. The main applications for PSi in these early studies were limited mainly to the development of an insulating material on microelectronic circuits [25,26]. The next wave came along the discovery of Leigh Canham in 1990, when he noticed the visible photoluminescence of PSi at room temperature [27]. Right after this, the electroluminescence of PSi was also discovered [28]. The growing interest to new materials for light emitting diodes (LED) boosted the PSi research [29] and number of different fabrication techniques grew significantly. Despite the promising use of PSi in integrated circuits, the properties of the material were not good enough, and the PSi LED remained as a promise [30].

In 1995, the enormous impact of Leigh Canham to the research of PSi was sealed when he found the first hints of the biocompatible nature of the material [31]. He found that hydroxyapatite, the major constituent of bone, was growing to the surface of PSi in biologically relevant phosphate-buffered saline (PBS). In addition, PSi showed signs of degradation in physiological conditions. Soon after this, the ability of cells to adhere PSi surface was recognized [32]. These

findings initiated the research of PSi into a completely new area of medical applications, which was the final step giving PSi broad interest.

2 Fabrication of mesoporous nanoparticles

Until today, more than 30 different techniques to fabricate PSi with different structures and properties are known [33]. Despite the variety of fabrication techniques, the most used is still the electrochemical etching or anodization. The reason for this is the possibility to control the properties of PSi with the etching parameters.

2.1 Electrochemical anodization

During electrochemical etching, pores are formed due to the highly localized electrochemical dissolution of the crystalline silicon. Parameters affecting the formation rate and pore morphology are electrolyte composition, dopant type and concentration, crystal orientation, current density, temperature, and illumination [34]. In the simplest fabrication setup, only HF-compatible plastic vial, electrolyte, platinum counter electrode, anode connector, and power supply are needed. However, the homogeneity of the formed PSi layer depends on the quality of the contacts and the homogeneity of the formed electric field. Hence, in most cases the time or money is invested for design and manufacturing of the dedicated etching cell (Figure 1).

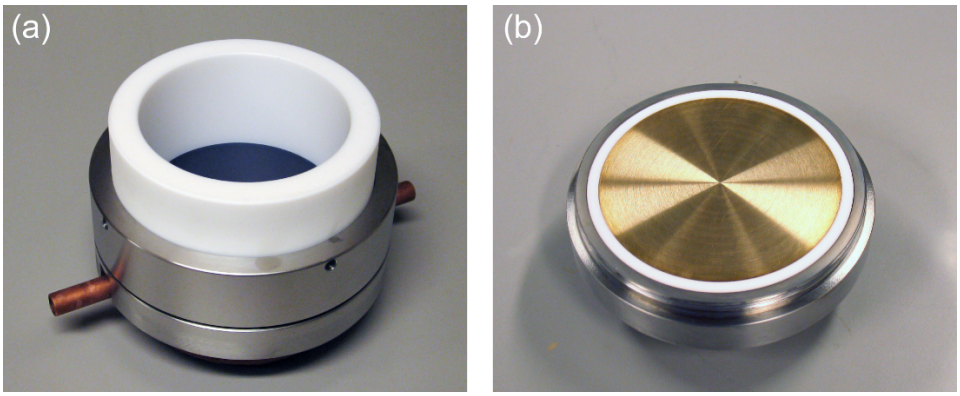

Figure 1. (a) A single tank PSi etching cell for 100 mm Si wafers, fabricated from Teflon with a stainless steel frame. (b) Lower part of the etching cell, showing the metallic back contact for the Si wafer. The set-up is published in reference [35]. The figure is constructed from original pictures with permission from Ermei Mäkilä.

The question, why the silicon dissolves in such a local fashion and the pore walls not, has intrigued scientists since the discovery of PSi. The basic idea of an electrochemical dissolution of silicon in HF-solution is explained in Figure 2. Silicon is stable in acidic aqueous solutions if they do not contain fluoride because a native oxide passivates the silicon surface. If the solution contains HF, slow isotropic dissolution occurs and can be accelerated by adding the oxidizing agent. On the anodic etching of PSi, the wafer is attached on the anode, covered with HF electrolyte and the counter electrode is placed in the electrolyte on the top of the wafer. The electrolyte contains HF, $(HF)_2$, and HF_2^- species and in p-type silicon the applied voltage causes the holes to drift towards the surface. As explained in the first panel in Figure 2, the hole enables the nucleophilic attack of HF_2^- to the Si atom. In the next phase, the nucleophilic attack takes place without the hole since the ionic balance of the Si—H bond changes as a consequence of highly electronegative fluoride on the other side. In this phase, the electron injection to silicon is thought to happen and hydrogen escapes in a gaseous form. Now, the even more pronounced ionic nature of silicon with two fluorides attached enables the nucleophilic attack of HF_2^- to silicone back-bonds and the silicon atom detaches from the surface in a form of silicon tetrafluoride. It immediately reacts with HF and forms a stable and liquid hexafluoride molecule SiF_6^{2-}. It should be noted that dissolution of silicon starts from the hydrogen terminated surface and results to the same situation.

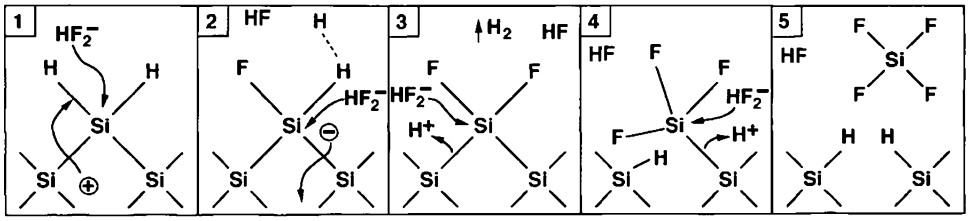

Figure 2. Anodic divalent dissolution of silicon in HF [21]. © 2002 Wiley-VCH Verlag GmbH. Reproduced with permission from Wiley Materials.

Another important phenomenon is that the first phase, where the hole is enabling the nucleophilic attack, is rate limiting. In the case of p-type silicon, holes are on material typically as a consequence of boron doping. In n-type silicon, charge carriers are electrons and the holes need to be created with a powerful illumination. This is the first factor affecting pore formation. In addition, there are several different theories, which all have their relevance in certain cases, but none conclusive, all explaining theory for formation mechanism has been formulated and agreed.

One of the explaining models is the crystal face selectivity. Pores tend to grow in <100> directions which is explained by the higher dissolution tendency of the (100) surface compared for example, with the (111) surface on pore walls [36]. Another explanation for the aligned pores is the charge carriers' route of the lowest resistance. Because the electrolyte is typically more conductive than the silicon substrate, the easiest way to the electrode is from the bottom tip of the pore. In addition, high curvature of the pore tip yields to the higher electric field and subsequent increase of the hole concentration and dissolution rate. On the other hand, the decreased hole concentration plays a role in decreased dissolution of pore walls. This is caused by the so-called space-charge region (SCR), which is formed near the silicon/electrolyte interface where the energy bands bend as a result of charge equilibration between the semiconductor and the electrolyte. This region is spatially so large that it can prevent the charge transport to the pore walls.

For drug delivery purposes, mesoporous structures are typically the most wanted outcome of anodization. For the etching process, the first thing that needs to be selected is the wafer's doping type and concentration. With highly doped n+, p+ or p++, it is possible to fabricate mesopores [21,36]. In the case of p-type silicon, the diameter of formed pores decreases when the dopant concentration decreases (Figure 3). For n-type silicon, the effect is typically the opposite.

In the following step, the electrolyte needs to be decided. Fluoride is naturally an important part of the electrolyte, but luckily, the etching is not too sensitive to this concentration as long as it is sufficiently high. During the etching, the fluoride concentration is harder to keep constant close to the surfaces and especially in pore tips. For this purpose, some etch pauses may need to apply. Local deficit of fluoride yields to the formation of insulating surface oxide which leads to pore widening and electropolishing. In addition, ethanol is used as a surfactant in the electrolyte in order to promote the evolving hydrogen bubbles' detachment from the surface.

The parameter which is the easiest to adjust, even during the etching, is the current density [37]. The current density does not significantly affect the pore size in the case of p-type silicon, but density of pores increases while the current density is increased (Figure 3).

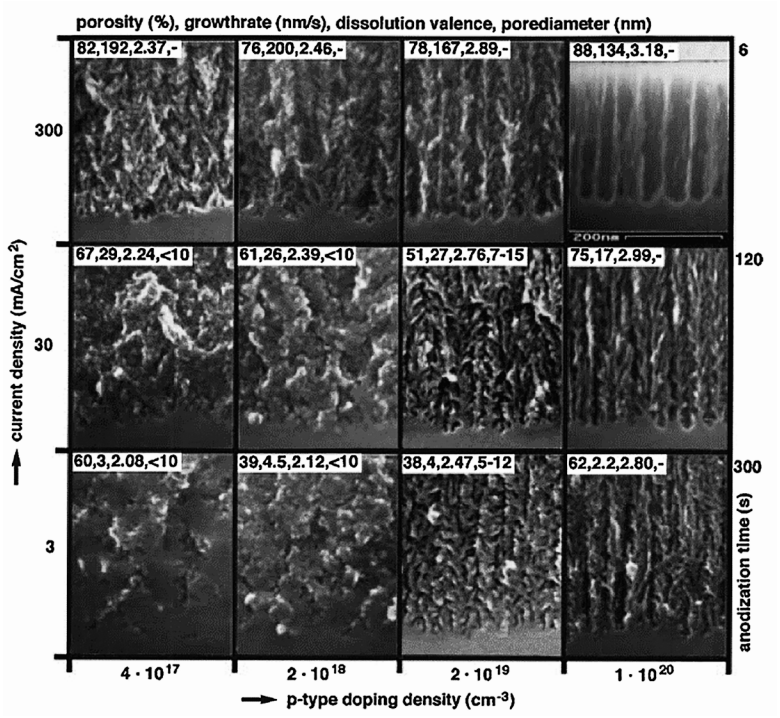

Figure 3. Cross-sectional SEM image of PSi layers etched in ethanoic HF with different current densities and p-type dopant concentrations. Reprinted from reference [38] with permission from Elsevier (© 2000).

2.2 Surface passivation

The etching process leaves the surface of PSi hydrogen terminated (Figure 2), which is prone to oxidation. The great benefit of the top-down nanomaterial such as PSi, which can be easily handled in the dry state, is the possibility to use thermal gas phase treatments for comprehensive stabilization of the surface.

2.2.1 Thermal oxidation

Oxidation is the most common way to stabilize the silicon surface owing to its simplicity and because of a versatile variety of chemical entities that would be possible to attach to the surface via siloxane bonds [36,39]. Oxidation can and will take place in ambient air as so called native oxidation and its rate highly depends on humidity and temperature [34]. Native oxidation is a slow process and does not provide decent chemical stability for most applications. Oxides that are more durable can be made with chemical treatments by boosting aqueous oxidation with an oxidizing agent like HNO_3 or in gas treatments where increased temperature is used to enable reactions that require more energy and speed up diffusion of the oxide into the crystalline silicon matrix. The latter is called thermal oxidation (TO), and it is commonly used in microelectronics industry for the production of high quality oxides on silicon wafers [36]. In thermal oxidation, the used atmosphere, temperature, and treatment time play a major role. The so called back-bone oxidation takes place in ambient air at temperatures above 250 °C [40]. The siloxane bridges are formed between silicon atoms at the surface and at the second atom layer (Si—O—Si—H) during this process [41]. Due to the slightly stronger nature of Si—H bond to resist oxidation, some surface hydrides still remain on the surface after the back-bond oxidation. When the temperature is raised to 700 °C, the hydrides are completely desorbed [39]. The drawback is that high treatment temperatures could cause reformation of the pores. The oxide structure on top of PSi resembles amorphous silica [42] which suffers from poor stability in alkaline media [43]. There are a lot of benefits to oxide passivated surfaces, but for some applications, like in sensors [44] and drug delivery [45], its stability against the dissolution may not be sufficient, and a longer degradation profile is needed.

2.2.2 Thermal carbonizations

When a more durable surface is needed, surface treatment with carbon is a commonly used method. This can also be done in a solution or in a dry state. The first method for the carbon stabilization was the so called hydrosilylation, which was

actively studied at the turn of the century. Lewis acid catalysis [46], white or UV-light [47], or increased temperature [48] was used in order to initialize a reaction between unsaturated organic molecules and silanes (Figure 4).

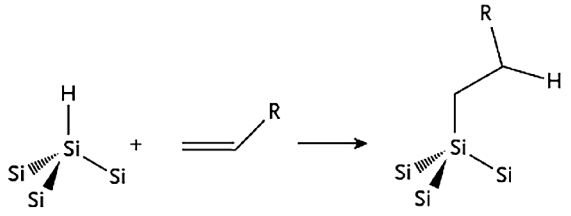

Figure 4. Hydrosilylation reaction of PSi surface hydride with double bond terminated alkene [36]. Reproduced with permission from Wiley-VCH Verlag & Co. KGaA (© 2012).

At the same time, thermal gas phase treatments were also developed to introduce carbon into the PSi structure. This so called thermal carbonization is carried out by pre-exposing the fresh etched PSi film to a mixture of inert carrier and carbon containing gas, such as a mixture of acetylene and nitrogen [49,50]. During the pretreatment, acetylene molecules are adsorbed to the PSi surface. Heating yields to the breaking of the double bond and disintegration of carbon atoms, but the high activation energy of desorption keeps molecules attached to the surface [51]. The treatment temperature has a significant impact on the hygroscopic properties of the formed surface [52], which is attributed to changes in surface chemistry [53,54]. When the treatment temperature is kept below 700 °C, the thermal energy cannot break all of the C—H bonds, and the surface stays covered with hydrophobic hydrocarbons. When the temperature is raised above 700 °C, all the hydrogen desorbs from the surface and carbon diffuses deeper into the structure [55]. This leaves a very thin, non-stoichiometric silicon carbide structure on the surface, which will become terminated with a thin oxide layer after the treatment is done and the films are taken back into ambient air [56]. The thin oxide layer makes the surface hydrophilic. In order to distinguish these significantly different surface chemistries, thermal carbonization (TC) refers to acetylene treatment at higher temperature, and thermal hydrocarbonization (THC) refers to acetylene treatment at lower temperature (Figure 5).

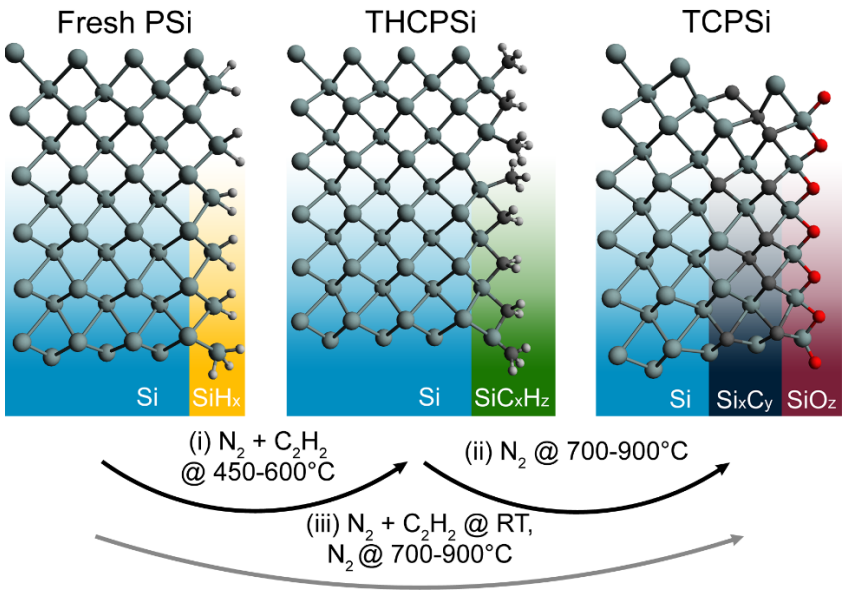

Figure 5. C_2H_2-based thermal carbonization treatments for fresh PSi. (i) THC process is done by exposing the PSi to C_2H_2 on a moderate temperature (450–600 °C). (ii) TC treatment is done in high temperature (700–900 °C) N_2 treatment immediately after the THCPSi treatment. (iii) Alternatively TCPSi treatment can be made directly to fresh PSi. Drawing was made as proposed in [35] and [56].

2.2.3 Functionalization of TC and THC surfaces

The benefit of thermal stabilization of PSi in the gas phase is the high surface coverage of the stabilizing layer. This layer, for the most part, determines the material stability against degradation and uncontrolled oxidation. Nevertheless, these surfaces are not necessarily optimal for biological applications and further modifications may be needed. Varieties of organosilanes can be attached to the silicon oxide surface via rather stable siloxane (—Si—O—Si—R) linkage [57,58]. One frequently used organosilane is APTES (3-aminopropyltriethoxysilane), which creates an amine termination and positive charge on the surface [59], and it is widely used to attach biomolecules to silica surfaces. As we have shown in Paper II, silane coupling chemistry can also be used with TC surfaces because carbon penetrates deeper into the structure and silicon oxide covers the surface. This can be changed to a hydroxyl termination simply by dipping the sample in a HF containing solution. Thermal carbonization makes structure of PSi durable against dissolution and can also increase the stability of amine treatment when compared to TOPSi (Paper II).

The situation is different when the functionalization needs to be made for a hydrophobic THCPSi surface. Now, the hydrocarbon groups terminate the surface and silane chemistry is not conveniently applied. Nevertheless, THCPSi surface provides superior stability against aqueous degradation, which is a desired property in some applications. In recent studies, functionalization of THCPSi surface has been managed to produce with the radical coupling of a dicarboxylic acid (sebacic acid) using a benzoyl peroxide initiator [60] and hydrosilylation resembling thermal reaction of unsaturated carboxylic acid (undecylenic acid) [61]. The strong C—C bond between the carbon on PSi surface and hydrocarbon chain shows excellent stability compared to many other surface chemistries [62] and also provides a route for further functionalization via carboxylic acid groups. Undecylenic acid functionalized THCPSi particles are herein abbreviated to Un-THCPSi.

2.3 Fracturing methods

Unlike most nanomaterials, PSi nanoparticles are fabricated with the top-down method, and different kinds of techniques for the disintegration of the nanoparticles from the PSi film have been developed. PSi can be a very fragile material at the nanoscale, and this fact was utilized when first PSi based nanoparticles were made in the beginning of the 1990s [63,64]. These nanoparticles appeared in ultrasonic treatments of highly porous silicon matrixes. According to Bley *et al.*, the size of these particles was typically below 50 nm, but the wide size range was explained by agglomeration of smaller Si crystallites in the size range of 2-11 nm. In this case, the concept of porous nanoparticles should not be used as it is evident that the original porous structure was destroyed during the treatment.

During the first five years of new millennium, the first reports of PSi particles being used for drug delivery purposes [65–67] were published. In these studies, microparticles were fabricated either by photolithographic method [65] or by milling with planetary ball mill [67]. For the photolithographic method, the silicon nitride layer is first deposited to the Si surface. This layer is covered with photoresist that is photolithographically patterned, and the formed template is plasma etched. The porous structure is etched with electrochemical anodization on the spots where silicon is exposed to the electrolyte, and a subsequent electropolishing pulse is used in order to detach the particles from the wafer. This method facilitates the etching of microparticles with rigorously controlled shape

and size [68]. Planetary ball milling, on the other hand, can be used for the production of much larger amounts of microparticles in one batch, but the control over shape and size is more complicated.

A few years later, the first paper concerning *in vivo* studies of the PSi nanoparticles was published. Particles were made with the ultrasonic treatment, but now with the production of PSi nanoparticles with actually porous structures [69]. A year later, ball milling was also used for the same purpose [70]. On the latter study, the possibility to control the size of PSi nanoparticles in one dimension by multilayer etching [71] was utilized for the first time. Despite the significant amount of studies on these top-down fabricated PSi nanoparticles, the fracturing methods are not well understood. In 2014, Qin *et al.* were able to achieve the size control and increased yield with multilayer etching of PSi and ultrasonic fracturing [72]. Nissinen *et al.* recently made a similar study with multilayer etching and ball milling. They noted that multilayers might increase the yield of the nanoparticle production, but the size control is hard to achieve [73]. One of the problems with fracturing methods is that the simultaneous creation of Si nanocrystals (<< 100 nm) is impossible to avoid [74], and these particles might cause problems in characterization and applications if they are not properly washed away on the separation process. Both of these fabrication methods result in a very wide particle size distribution, where particle size vary from nanoscale to micrometer regime. Thus the additional separation step, in order to extract the wanted fraction of nanoparticles from the rest of the mixture, needs to be done by centrifuging or filtering.

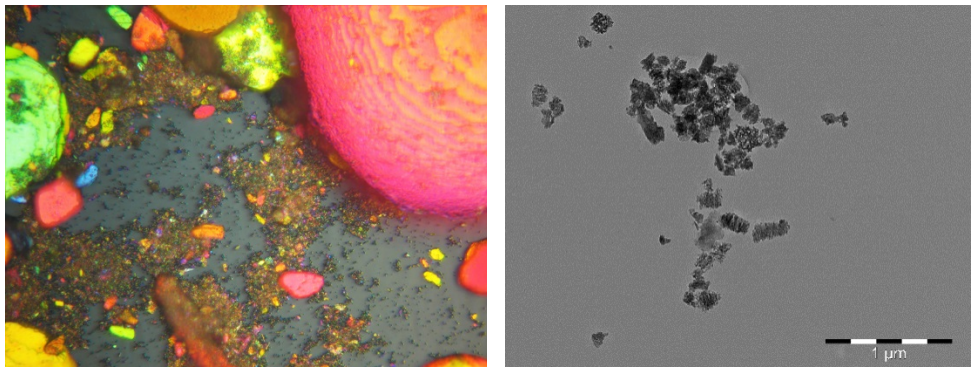

Figure 6. (Left) Microscope image (multiple images combined, no in scale) is from unfractioned PSi particles with multilayer structure clearly seen. (Right) Centrifuged and filtered PSi nanoparticles imaged with TEM.

Lithographic methods have also evolved towards the nanoscale, but the size of these particles is still around 1 μm [75]. The benefit of this method, also in nanoscale, is very robust control over the geometry of the particles which, can vary from hemispherical [68] to discoidal [76]. Recently, the colloidal lithographic method [77] and the imprinting method [78] have been developed, which might offer more cost effective PSi patterning methods in the nanoscale.

2.4 Mesoporous silica nanoparticles

The fact that there is an another silicon based mesoporous material is easily causing confusions. This material is mesoporous silica — not silicon. The discovery of mesoporous silica also occurred during the last half of the 20th century. In 1968, when chemists were already familiar with the sol-gel method, where through hydrolysis and polymerization, tetraethyl orthosilicate (TEOS) was turned into silica (SiO_2) [79], Stöber *et al.* [80] decided to modify the process and use an alkaline solution to catalyze the reaction. They managed to create extremely monodisperse silica colloids with controllable particle size from 0.05 μm to 2 μm. The final size of formed silica particles depended on the concentration of components and the type of the used silicon alkoxide precursor. After this, temperature was also shown to play a role in the process [81].

There is evidence that mesoporous silica was actually fabricated right after Stöber's publication in 1971, but the porosity was not noticed [82]. Thus, the actual discovery of the material dates to the beginning of 1990s [83] to the laboratory of Mobil Research and Development Corporation in New Jersey, USA. They named the material MCM-41 according to the company's naming tradition. The porosity was generated with self-assembling nanoscale templates, which were covered by polymerizing silicates. Templating was done with the surface-active molecules (surfactants), which in aqueous solution have a tendency to cluster together to form micelles, as they are called.

Surfactants have a hydrophobic end which tries to avoid contact with water and a hydrophilic end which favors the water contact. When the concentration of these molecules in water is high enough, they are entropically driven to form clusters where the hydrophobic parts are shielded from the aqueous environment. Depending on the concentration and the dimensions of the surfactant, they may form spheres, rods, or layers. The dimensions of the surfactant's hydrophilic and hydrophobic end can be used for the determination of the so called packing parameter $v/a_0 l_c$, where v and l_c are the volume and effective length of the hydrocarbon chain, and a_0 is the optimal surface area per molecule [84]. The

smaller the hydrophobic part on the molecule is, the more probable the formation of a spherical micelle. When the size of this end is increased, the cylinder becomes the preferred shape, which follows the lamellar structure (Figure 7).

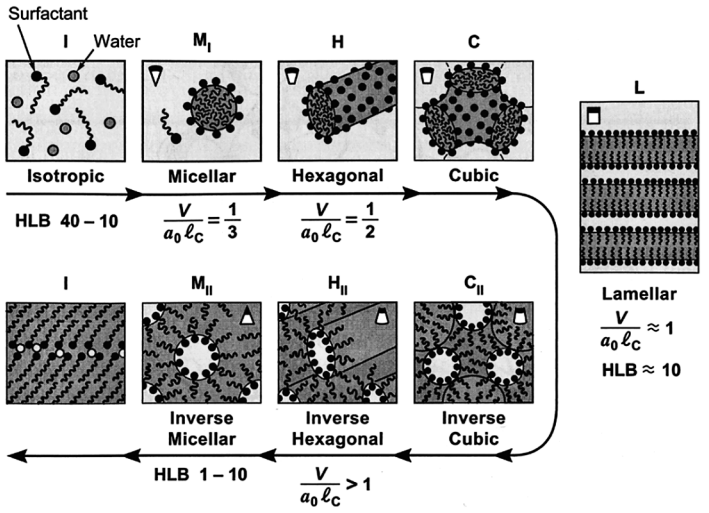

Figure 7. The self-assembled structures with different surfactant packing parameter and hydrophilic-lipophilic balance (HLB) number. Reprinted from [85] with permission from Elsevier (© 1994).

There are several synthesis routes for the formation of silica particles, but for the fabrication of mesoporous nanoparticles, alkaline synthesis with a cationic surfactant is preferred [86]. In the alkaline environment, electrostatic interaction between negatively charged silica species and positively charged template surfactants yields to the formation of silica walls around the self-assembled (liquid crystal) structures. Particle formation starts with fast nucleation silicates and continues with a slower growing period. Two of the most important parameters for a monodisperse suspension and size control are low concentration of silicate precursors and high pH. The alkaline environment is preferred so that the attractive interaction between the formed particles can be avoided, as it typically yields to the coalescence of particles into increasingly larger structures (so called Ostwald ripening). Different chemical additives, called particle growth quenchers, can also be used to control particle size.

Basic synthesis of silica yields the negatively charged surface caused by the silanol groups [86]. By co-condensation of alcoxysilanes together with orga-

nosilanes (with amine or carboxylic acid parts), the variation of surface functionalities can be achieved. Alternatively, silica particles can be functionalized post-synthesis via siloxane bonds as explained in Chapter 2.2.3.

3 Biomedical applications of porous silicon

The diverse collection of techniques available for a fabrication of PSi has generated diverse forms of materials [87]. Porous silicon can be used as a nanoparticle suspension, a microparticle powder, a membrane, or a layer. As silicon is widely used as a material in microelectronics, PSi can be easily integrated to electrical, optical or mechanical devices. In this section, I will limit the discussion to particle based biomedical applications. This casts off almost completely the important application area in biomedical fields, biosensors, but does not mean that the field is insignificant or passive. Significant amount of PSi research takes place aiming towards biosensor applications [88,89].

For PSi particles, the drug delivery devices are the most important and widely studied applications [34,90]. These can be broadly divided into three categories depending on the benefit that porous matrix can offer: the possibility to control (typically to sustain) the drug release, to provide a stabilizing matrix for amorphous drug form, and to act as a vehicle for drug delivery, allowing longer drug circulation time or accumulation towards a certain target.

3.1 Sustained and protected delivery of peptides

Peptides are small chains of amino acids, which differ from proteins only by chain length. Maximum chain length for a peptide is from 50 to 100 amino acids. It is a small molecule compared to proteins, yet typically much bigger than conventional small molecular drugs. Physicochemical properties of peptides can vary a lot, but there are still some common pros and cons compared to conventional drugs.

Typical disadvantages of peptide drugs are the poor metabolic stability, rapid clearance from the blood circulation, and poor permeability through biological membranes [91]. Despite these limitations, a number of peptide drugs are

steadily rising [92,93] because of their potency, specificity, and broad range of targets. In addition, the rise of biotechnological routes for the fabrication, such as cloning and fermentation, have increased the interest on peptides [94].

The sensitivity of typical peptide drugs and the harsh environment in the gastro-intestinal (gi) tract necessitates their parenteral administration. Subcutaneous (sc) and intravenous (iv) delivery are the most common methods, but the rapid clearance from the blood forces the use of frequent injections. This means that sustained release, with PSi particles for example, could be a relief for patients. The benefit of PSi particles, compared to many other particulate peptide delivery systems, is that the peptide loading can be made after the fabrication of particles, at room temperature, and in mild solvents. This is not the case with most polymeric and liposomal particles, where the drug needs to be incorporated into the delivery system during the particle synthesis.

In studies of peptide delivery with PSi, the sc administration is the most used approach, and evidence of sustained release has been found. The first *in vivo* study was done by Kovalainen (née Kilpeläinen) *et al.* with THCPSi microparticles. Ghrelin antagonist [95] and Melanotan II [96] were used as model peptides. In both studies, they observed a prolonged action of model peptides, attributed to sustained release. In addition, no toxic effects were observed and THCPSi microparticles were considered a good candidate as a sustained delivery vehicle. In a subsequent study, three different surface chemistries were tested and peptide YY (3-36), later PYY, was used as a model drug [61]. In this study, the sustained release was observed with all surface chemistries, and in addition, they observed an improved absolute bioavailability, up to 98 % in the case of TOPSi microparticles. This is 2.5-fold increase compared to the 38 % bioavailability of sc injected PYY solution. Significant differences between surface chemistries were also observed since THCPSi and UnTHCPSi microparticles could not overcome the bioavailability of the pure PYY solution. On the other hand, these hydrophobic particles showed slower release compared to TOPSi. Similar studies were made also with PYY and PSi nanoparticles (Paper III), but they are discussed in more detail in the results.

Oral delivery is naturally simple and has the highest degree of compliance, and numerous methods have been proposed to overcome the problems in gi tract [97]. Chemical modification of peptides is one of the most popular methods, but, since maintaining the therapeutical efficacy is obviously important, a trial and error approach might be time-consuming [94]. Another, quite general, strategy is to add additives such as absorption enhancers, enzyme inhibitors, or particle carriers to the formulation. The problem in this approach is the potential toxicity of the additives. Potential toxicity might also be a challenge for the PSi

based delivery, but the idea that the mesoporous matrix could provide protection and control over the release has tempted researchers, although the task is challenging. The first hints of enhanced permeation of insulin through typical intestinal cell line model, Caco-2, was obtained by Foraker *et al.* in 2013 [65]. The next studies mainly considered stability of proteins on loading and release [98,99], and the idea of chitosan functionalization as a mucoadhesive coating of PSi [100].

Recently, an especially large contribution to this topic have been made by Francisca Araújo and Neha Shrestha from Helder Santos's research group [101–107]. They have linked chitosan mainly to UnTHCPSi nanoparticles and, in studies with epithelial cell models, noticed the increased mucoadhesion, increased cell uptake, and enhanced permeation of peptide drugs when compared to peptide solution. Peptides, which were mainly used, were insulin and glucagon-like peptide-1 (7-37), later GLP-1, although some preliminary experiments were made with PYY also. In order to create a pH sensitive polymer coating around the particles to avoid the release and degradation of peptides in the stomach, they have used the microfluidic synthesis or airflow reactor (AFR). They have also successfully added the DPP4 protease inhibitor to the enteric coating to ensure the protection against the enzymic degradation in a stomach. After promising *in vitro* results, they showed *in vivo* that this coating can protect the cargo in the stomach, and that the underlying mucoadhesive coating still works after the enteric layer has dissolved. This multifunctional GLP-1 delivery system resulted in a 32% reduction in blood glucose levels and a 6-fold enhancement in pancreatic insulin content, as compared to the pure GLP-1 + DPP4 solution, when studied *in vivo* with a type 2 diabetic rat model.

The benefit of iv administration is the 100 % bioavailability, but the problem of rapid clearance from the blood circulation is the biggest stumbling block of this delivery route. De Rosa *et al.* found that agarose coating protected the bovine serum albumin (BSA) which was loaded on PSi microparticles [108]. In our study (Paper III), PSi nanoparticles were sustaining the release of PYY, but the release was still significantly faster compared to sc administered nanoparticles. This was attributed to faster dissolution of peptides in circulation caused by competitive adsorption of blood proteins. One interesting, but less studied branch of peptide delivery is the use of PSi particles as vaccine adjuvants and an antigen delivery device. Microparticles might have an active role in vaccines as a substitute of pathogen-associated molecular patterns (PAMPs), which are used in antigen based, subunit vaccines. Indeed, it has been shown that antigenic peptides, delivered with PSi microparticles, enhances MHC class I presentation by human monocyte derived dendritic cells to CD8 T lymphocytes [109].

3.2 Stabilization of amorphous drug form

Since the first study on ibuprofen delivery with MCM-41 microparticles [110] in 2001, the most studied drug delivery application of mesoporous materials has been the delivery of small molecule drugs. This has been shown to work also with PSi films [111] and PSi microparticles [67].

The value of the application is that the vast majority of new small molecular entities for oral administration suffer poor bioavailability arising from poor aqueous solubility [112]. The amorphization is a promising tool to overcome the dissolution issue, but the stabilization of the amorphous form is challenging [113]. Salonen *et al.* [67] found that the release rate depends on the type of the drug, PSi increases the solubility of poorly soluble drugs and decreases the solubility of already soluble drugs. This has been attributed to two different phenomena. For drugs with good solubility, the long pores with relatively large surface area are slowing dissolution and diffusion of the drugs. In case of poorly soluble drugs, the enhanced dissolution has been attributed to the amorphous state of a drug caused by the confined space inside the pores [114,115].

The better dissolution of poorly soluble drugs has been mostly studied *in vitro*, but one of the rare exceptions has been made by Wang *et al.*, who studied the effect of enhanced dissolution to *in vivo* absorption [116]. They used indomethacin as a model drug because its oral permeability is high, but its dissolution hinders the bioavailability. They found that oxidized PSi microparticles were able to increase the bioavailability of a drug to 100 % when it was 54 % for the pure drug and 77 % for the commercial formulation Indocid. In addition, they found excellent *in vivo–in vitro* correlation between dissolution experiments and absorption.

3.3 Passive and active targeting

The most recent application of PSi particles has mainly emerged after the size of particles was decreased into the nanoscale, which enabled the intravenous administration and tumor targeting [69,70]. This is probably the most studied application among all pharmaceutical nanoparticles because of the enhanced permeability and retention (EPR) on tumor vasculature [117]. This natural ability of tumor tissue to absorb nutrients from circulation makes it possible to accumulate nanoparticles to the tissue if long enough circulation time is achieved. The biggest threat for long circulation is mononuclear phagocyte system (MPS) which

includes liver, spleen, lungs, and bone marrow. The avoidance of this system has been an issue of nanoparticle based drug delivery for more than 30 years [118]. To some extent, nanoparticles can avoid the recognition of immune system (opsonization) and subsequent phagocytosis of macrophages in MPS organs via the steric stabilization [119]. Steric stabilization is typically achieved with a neutrally charged and hydrophilic polymeric coating. One of the first nanodrugs on market, Abraxane, licensed in 2005 for the treatment of refractory malignant breast cancer [120], is utilizing this kind of "stealth" coating. The conventional hydrophobic chemotherapeutic agent paclitaxel nanoparticle is covered with albumin, which is the most common protein in circulation and thus works as a Trojan horse in the system.

Despite the significant efforts, long circulation time has been hard to achieve with pure tuning of the surface chemistry of PSi nanoparticles [121–123]. Instead, some evidences has been found that the particle shape and size might affect the distribution [124]. Especially promising are disc shaped particles which seem to interact with neuroblastoma cells and accumulate into the tumor [76,77].

The exploitation of the EPR effect on targeting nanoparticles is typically referred as passive targeting. The use of specific molecular markers to deliver the cargo to the site of action is called active targeting. The marking can be made with antibodies [125,126] or peptides [127–129] which are overexpressed on the surface of target cells. These markers can also enhance the cellular uptake [130] and this way facilitate the delivery of active molecules inside the cell. Here, the probability of adsorptive endocytosis might further increase with positively charged surface chemistry [131,132], but a lot of different interactions need to be considered before that.

3.4 Other delivery routes

Besides oral, sc, and iv administration routes, a few other interesting ways to use PSi in treatment of diseases have been studied. Actually, one of the most advanced biomedical application of PSi particles does not include the drug at all, but biodegradable and ^{32}P isotope containing PSi microparticles are placed with injection directly into the tumor [133]. In this, so called brachytherapy, the aim is to keep the radioactive source bound in the particle inside the tumor and this way expose the surrounding healthy tissue to a minimum amount of radiation. The phosphorus 32 isotope is close to the ideal therapeutic radionuclide due to the long, two-week half-life and positron emitting decay. After promising *in vitro* results [66], the development was carried on with human patients [134], which

followed Phase IIa clinical trials [133]. The data from clinical studies showed doubling overall survival rates compared to standard care. Approximately half of the patients were alive after 18 months, whereas typically more than 80 % of patients die during 12 months. This technology was developed by pSiMedica and is now licensed to OncoSil Medical Limited under the trademark OncoSil. During the writing of this thesis, the FDA has just accepted global pivotal studies under IDE (investigational device exemption), and the approval of CE mark for the commercial launch is awaited in UK, EU, and Australia[6].

Another delivery route of PSi is the intravitreal delivery. In order to treat retinal diseases such as age-related macular degeneration and proliferative vitreoretinopathy, there are many difficult to reach drug targets inside the eye. Sustained release DDSs are needed because frequent injections into the eye are expensive and lowers the patient compliance rates. Sustained release from PSi particles or films has been achieved in intravitreal delivery with covalent bonding of a drug and subsequent degradation driven release [135], for example.

The possibility to exploit of the tunable fabrication methods and optical properties and the visual monitoring of the drug release during the treatment, is a benefit of PSi based DDS [136,137]. The flexible fabrication techniques are also exploited in another emerging application. Chiappini *et al.* have [138,139] recently developed PSi nanoneedles with precise microfabrication techniques and metal assisted chemical etching for highly localized delivery of nucleic acids or quantum dots.

[6] Oncosil Investor Presentation - Aug 2016 (22.8.2016). OncoSil Medical announcements can be found on the Australian Stock Exchange (www.asx.com.au) under the code “OSL”.

4 Characterization and properties of mesoporous nanoparticles

4.1 Dry state properties

The complex and variable structure of PSi provides a variety of physicochemical properties but is a challenge for characterization at the same time. Few of the most influential techniques for the study of PSi include electron microscopes (EM), nitrogen sorption, Fourier transform infrared spectroscopy (FTIR), and X-ray photoelectron spectroscopy (XPS).

The main advantage of EM measurements is the direct characterization of PSi morphology in micron-scale and nanoscale [140]. Especially important has been the scanning electron microscope (SEM). The knowledge of the fabrication parameters' impact on the final structure of PSi has significantly increased along with the development of better imaging techniques, such as SEM (Figure 3). The drawback of electron microscopes is the small statistical significance. In a typical cross section image, there might be 50 pores in a 1 μm row, but when the whole sample is macroscopic, 1 cm^2 for example, there is in total 250 billion pores.

A powerful way to overcome this issue and to characterize porous materials is gas sorption. If the previous mentioned sample is 10 μm thick and the pore diameter is 15 nm, the amount of surface area in the pore walls is more than 1000 times bigger than the apparent 1 cm^2 surface area of the sample. With the gas sorption method, the actual surface area in a sample is determined by utilizing the affinity of gas molecules (typically nitrogen) to the surface of material. By measuring precisely the volume of injected gas and pressure on the test tube, adsorption of the gas molecules can be observed, and with predictions from the Brunauer-Emmet-Teller (BET) theory, the surface area can be calculated [141]. By continuing the gas injection into the sample tube near ambient pressure (and near the condensation temperature of nitrogen), the capillary effect eventually fills the pores with liquid nitrogen. When the gas pressure is decreased during the so

called desorption branch, the capillary effect causes a hysteresis loop to form in the adsorption-desorption isotherm. From the shape of this loop (Figure 8), the pore morphology, as well as pore size, can be determined [142]. One of the most used theories for the determination of pore size distribution is the so called Barret-Joyner-Halenda (BJH) theory [143].

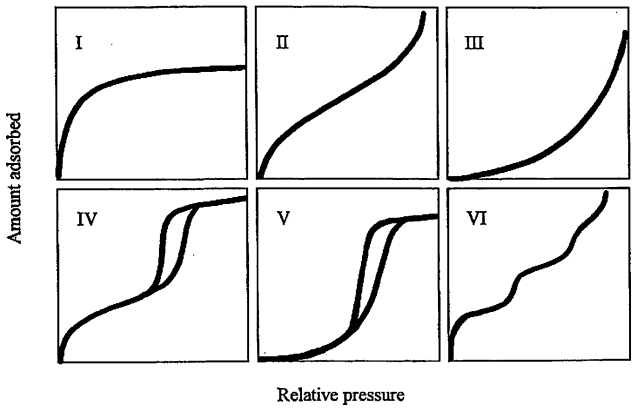

Figure 8. Shape classification of gas sorption isotherms. The hysteresis loop, especially in IV, is usually associated to the filling and emptying of the mesopores by capillary condensation. Image is Donohue's adaptation [144] from IUPAC's classification [145]. Reprinted with permission from Elsevier (© 1998).

Thermal analysis and calorimetry provide a way to characterize PSi, especially for drug delivery purposes. Thermogravimetry (TG) measures the amount of mass loss during heating, and as the loaded drug usually decomposes and desorbs completely at high temperatures (< 700 °C) the mass loss can be used for the estimation of the loading degree [146,147]. In differential scanning calorimetry (DSC), the energetics of phase transformations are studied and the drug's physical form inside the pores can be determined. This has opened new insights to various amorphous forms of drugs inside the pores [115,148] and shown the importance of well controlled drug loading since the crystallization to the external surface of particles is undesired [149].

A convenient way to analyze the surface chemistry of PSi is the infrared spectroscopy (IR) or Fourier transform infrared spectroscopy (FTIR). Although silicon absorbs light strongly in the shorter wavelengths of the visible spectrum, it is almost transparent in the IR area. In addition, the high surface area assures the sufficient concentration of surface groups when the surface species, Si—H and Si—O, are characterized [150].

4.2 Medium dependent characterization

The problem with all previous mentioned techniques is that they are not compatible with wet samples. When nanoparticles are placed in an aqueous medium, the system changes from a static material studied in vacuum without "context," to a dynamic part of the bigger system. Constant thermal motion of the medium keeps particles in motion in such a vigorous way that colloids with small enough particle size (and a few other limitations, as will be seen) can be considered stable. In this context, stability is considered a stability against gravitation, sedimentation, or in some cases, against agglomeration.

The physics in the world of nanoparticles has been studied long before the term nanoscience was even known. Many different disciplines, physics, chemistry, mathematics, and biology, have contributed to building the models of the nanoscale world. Unfortunately, the discussion between these fields has turned out to be challenging at times and many overlapping definitions are confusing the field. These models concern different kinds of forces, which are manifested in different ways depending on the length scale. Forces can be divided into long-range and short-range categories (Table I), where the latter typically means forces affecting less than 1 nm distance from the surface. In the case of nanoparticles, especially when stability issues are considered, the long-range forces are more important.

One of the earlier attempts to shine a light to the world of nanoparticles or colloidal particles was made in the field of colloidal sciences. These models are especially beneficial for the studies of nanoparticles because they mostly consider the long-range forces. Many of the theories are well known, but they are not usually included in the curriculum of the physics master's studies. Nevertheless, I have found these concepts useful so we will shortly go through a few of the main phenomena dominating the surroundings and interactions of nanoparticles. The introduction to these concepts in Chapters 4.2.1-4.2.5 is obtained from the several text books considering surface charging and zeta potential [15,151,152], stability against agglomeration and long-range colloidal forces [15,153], Brownian motion [154], light scattering [155–157], and isotonic solutions [158].

Table I. Different types of interparticle forces in liquids[a]*

Type of the Interaction	Other Names (subclasses)	Attractive or Repulsive	A body or surface force
Van der Waals	Dispersion, dipole-induced-dipole, charge-fluctuation, ion-correlation[b], Debye, Keesom, Casimir	Either: attractive	Weak but ubiquitous body force. Force can change sign at some finite distance.
Electrostatic	Coulomb, ionic, salt-bridge, dipolar, hydrogen-bonding, charge-transfer, double-layer[b]	Either: repulsive, attractive between electro-neutral	Strong, long-ranged force arising in polar solvents. Usually a surface force.
Solvation	Structural, epitacial, hydration (in water), depletion[b], hydrophobic[c]	Either, incuding oscillatory	Surface force that modifies the local liquid structure
Entropic	Steric, osmotic, thermal fluctuation, polymer brindging, depletion[b], double-layer[b]	Usually repulsive	Surface force that arises from the confinement of solvent or solute molecules between the surfaces
Short-range physical	Adhesive, cohesive, surface tension, wetting, capillary	Usually attractive	Can be either a body or surface force
Short-range chemical	Covalent, quantum mechanical, metallic exchange, steric, hard core, Born	Either: ultimately repulsive at small distances	Strong short-ranged surface forces, largely independent of the suspending liquid medium
Specific	Complementary (electrostatic or geometric), host-guest, lock-and-key, lig-and-receptor, antibody-antigen	Attractive (specific but not necesarily strong)	Single or multiple noncovalent bond arising from perfect fit of ion or molecule into host pocket or lattice site.
Nonequilibrium	Viscous (drag), friction, shear, lubrication, hydrodynamic, energy dissipating, hysteretic	Either (depends on externally applied forces)	Involves continuous or transient motion of molecules or particles. Heat generating.

[a] Unless specifically mentioned, the interactions refer to the pair-potentials of like particles.
[b] Forces that are difficult to classify unambiguously, or that are made up of two equally important contributors
[c] Classification still unknown or controversial

* Reprinted from [159] with permission from Elsevier (© 2011)

4.2.1 Surface charge and zeta potential

A polar medium, such as water, leads to the rise of surface charging of a particle, even if the surface is neutral in the dry state. This is typically caused by the ionization of the surface groups, uneven ion adsorption from medium, or uneven ion dissolution on a particle surface. The most relevant surface charging mechanism, in our point of view, is ionization, which in many cases is pH dependent. The pH point where the average surface charge is neutral is called the point of zero charge (PZC). This is very easy to confuse with the isoelectric point, which actually means almost the same thing for proteins, but in the case of nanoparticles, the situation is different. Proteins' charge is mostly caused by amine (e.g. $-NH_3^+$) or carboxyl groups (—COOH), and the point where the total charge is zero is called the isoelectric point (pI). In the case of nanoparticles, the isoelectric point (IEP) is defined as pH value, where zeta potential goes to zero. Luckily, the abbreviations for these physical quantities are typically different and hereinafter, the (calculated) isoelectric point of proteins or peptides is abbreviated as (pI) and (measured) isoelectric point in the case of particles as (IEP).

Zeta potential is a quantity that is defined as movement of the particle under the applied electric field in a (electrolyte) solution. As stated above, all particles have surface charge (σ_0) which means that they also have surface potential (Ψ_0). These properties are causing their movement under applied electric field. In the presence of a polar medium and ions, the so called electrical double layer (EDL) is formed around the particle as a consequence of uneven distribution of free charges around the charged particle in solution (according to the Gouy-Chapman model). In addition, some counterions are adsorbed transiently, or specifically on the surface, which causes the formation of a Stern or Helmholtz layer. Potential on the surface, right next to the adsorbed layer, is called Stern potential (Ψ_d) (Figure 9). In a technical point of view, the actual surface charge behind the layer of tightly attached adsorbed ions cannot be distinguished when the measurement is electrokinetic, i.e. by measuring the movement of the particle under the applied electric field. Stern potential is typically very close to this so called slipping plane, but in order to make a difference between these planes, the electrokinetically obtained quantity is called zeta potential (ζ). Because of the zeta potential's sensitivity to adsorption, it is a compelling research method for the characterization of charged molecules such as peptides and proteins [160].

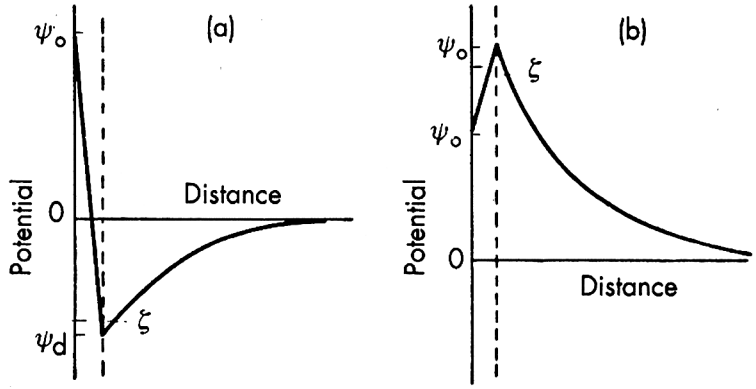

Figure 9. Two possible, but not the most typical, scenarios on what happens to electric potential as a function of distance from the surface when (a) polyvalent counter-ions and (b) surface active co-ions are adsorbed. Dashed line represents the Stern plane in average distance of adsorbed ions and zeta potential (ζ) is the electrokinetically measured quantity on its own slip plain. Reprinted from [152] with permission from Elsevier (© 1994).

4.2.2 Diffusion

When studying pollen particles under the microscope, one will clearly see a phenomenon dictating the wet world of nanoparticles. Particles are under constant movement. This was observed also by botanist Robert Brown in 1827, after whom the phenomenon was named as Brownian motion. Later the motion was explained by the constant random impacts caused by thermal motion of molecules in solution. Because these collisions are random, the average movement of many particles is zero, but for one particle the movement, diffusion, can and will happen. According to Einstein and Smoluchowski, the displacement $\boldsymbol{R}(t)$ can be described by the simple relationship

$$\langle \big(\boldsymbol{R}(t)\big)^2 \rangle = Dt \tag{1}$$

Here D is diffusion coefficient (or constant), t is time and $\boldsymbol{R}(t)$ is the particle displacement vector. When a particle is suspended in a medium, viscosity causes a movement-opposing force and the translational diffusion coefficient D_t can be described with the Stokes-Einstein equation

$$D_t = \frac{k_B T}{6\pi\eta d_h} \tag{2}$$

where k_B is Bolzmann's constant, T is temperature, η is the medium viscosity and d_h is the hydrodynamic diameter of the moving object. This way, by observing the movement of particles in solution, with known temperature and viscosity, it is possible to calculate particles' translational diffusion coefficient and get the value for the hydrodynamic diameter. Because the hydrodynamic diameter is calculated from the movement of the particle, it is only a close approximation of the actual particle size. This is an analogue to zeta potential and surface potential. In the Stokes-Einstein equation, a few approximations are made and one of them is that the particle is assumed spherical and rigid. In other words, the hydrodynamic diameter describes the diameter of a spherical particle, which has the same diffusion coefficient as the studied particle. Another similarity with zeta potential is that the adsorbed layer moves with the original particle and thus affects the diffusion.

4.2.3 Biorelevant and pharmacorelevant fluids

In biological applications, the prediction of nanoparticle behavior gets complex. There is, for example, enormous selection of biomolecules that are circulating in

our veins. Biological molecules are typically big and flexible, which means it is likely that there are parts that favor surface interactions. In addition, there are more combinations of physicochemical properties that are promoting adsorption than restraining it [161]. Some predictions can be made when we know the hydrophobicity and the charge of the surface, and the protein. Hydrophobic surfaces typically attract proteins and so do the oppositely charged surfaces. Protein labile structures can also increase the probability of adsorption.

Another compelling property of a biological fluid is its osmotic pressure, which due to the ions present all over the body, is quite high. Osmotic pressure is important because the cell membrane acts as a semipermeable membrane. It allows water molecules to diffuse freely through it, which means that osmotic pressure tends to seek a balance on both sides of the membrane. If osmotic pressure is higher outside the cell, the solution is hypertonic and water starts to flow out causing the cell to shrink. This kind of solution typically contains too much salt, or the drug concentration is high. The solution with too low an osmotic concentration is called hypotonic, and it results in water flow into the cell. This causes swelling of the cell and in extreme cases lysis, braking of the cell membrane. When the solution is compatible with cells in terms of osmotic pressure, it is called isotonic. Tonicity, as a term, differs from osmotic pressure because the situation is not as simple as explained in all cases. There are some substances that diffuse through the cell membrane which complicates predicting behavior of the cell.

Since osmotic pressure cannot be readily measured, it is often characterized by connecting it to freezing-point depression. Freezing-point depression of the well-known isotonic saline solution (0.9 % NaCl) is 0.52 °C. By finding the same freezing point depression, the unknown isosmotic concentration of the solution can be determined [162].

4.2.4 Stability against agglomeration

The long-range interactions, van der Waals interaction, and double-layer interaction (or electrostatic force) are dictating the stability of colloids according to theory, described by Derjaguin and Landau [163], and Verwey and Overbeek [164]. This, so called DLVO theory, explains the stabilizing effect of usually repulsive double-layer interactions against the attractive van der Waals interactions (Figure 10). The net DLVO interaction forms a primary minimum near the surface, and if the charge is high enough, an energy barrier is formed right outside the minimum. In certain cases, a secondary minimum can also appear farther away from the surface. Secondary minimum typically causes the agglomeration of the particles. In this work, we follow the proposal of Nichols *et al.* [165]

that agglomeration means the attachment of the particles in a reversible and easily dispersible manner, as is the case with this secondary minimum. Aggregation is instead a strong (and even chemical) interaction which, is impossible to be break without extreme force.

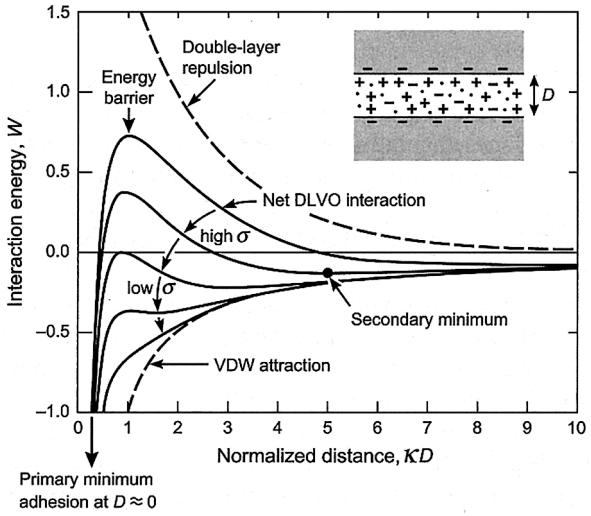

Figure 10. Interaction energy of two approaching surfaces (inset) as a function of distance as modeled by DLVO theory. Reprinted from [153] with permission from Elsevier (© 2011).

In simple solvents and electrolytes, the DLVO theory satisfactorily describes the stability of colloidal solutions, but in a more complex solution, if there is longer polymers on the surface, or if the surface is hydrophobic, the stability is not as much a straightforward phenomenon. In this case, the most relevant group of interactions affecting stability are solvation forces. These forces depend on the properties of the surface but also the medium. In this context, the most important, well studied, and unknown phenomenon is hydrophobicity, the strongly repulsive force between certain kind of surfaces and water molecules. Hydrophobicity has originally meant the low solubility and unexpectedly strong interaction between hydrocarbons in water. Hydrophobicity was extended to surfaces, when it was discovered that the mutual interaction between two surfaces could be higher than van der Waals forces predict, and water droplets have a large contact angle on hydrophobic surfaces. The latter gives an easy way to estimate the hydrophobicity by measuring the contact angle between surfaces and water droplets. When the angle is high enough (> 90°) the surface is generally considered

hydrophobic, although different definitions can be found depending on a research field.

The hydrophobic effect and insufficient electrostatic repulsion can both lead to unstable colloidal suspension in water, which can be avoided with so called steric stabilization. This typically means that the attachment of hydrophilic polymers or proteins to the particle surface changes the surface interaction with the surroundings in a more solvent favoring direction. Hydrophilic large molecules form a "hairy" layer around the particle, and when these layers are overlapping while two particles are approaching each other, they are causing a repulsive force.

4.2.5 Light scattering

Dynamic light scattering (DLS) makes use of the light's tendency to reflect or refract when travelling through interfaces of two phases with different refractive index. In the case of colloidal particles, this phenomenon is called light scattering. When the measurement is made in certain angle, light intensity either increases or decreases depending on the position of adjacent scattering objects. If particles are in constant movement, which is the case in colloidal suspensions, the very fast intensity fluctuations occur and the phenomenon is called DLS. Since the intensity fluctuations arise because of the Brownian motion of nanoparticles, it enables the convenient determination of the translational diffusion coefficient (equation 2). This way, the average size or even size distribution of nanoparticles is possible to be determined.

The measurement of fast intensity fluctuations and calculation of diffusion coefficients from obtained data is not a straightforward task, and DLS has benefitted from the recent technological advancements. These are, for example, the development of the digital autocorrelator, fast and cheap CCDs, and lasers, as well as the increase of calculation power from computers. The benefits of new DLS instruments include fast and non-invasive measurements and statistically significant results.

The direction of scattered light depends on the size and shape of the scattering object. As a rule of thumb, the bigger the particle is, the more it scatters light forward. In the so-called Rayleigh scattering zone, the size of the particle is much smaller than the wavelength of incident light ($R < \lambda/20$), and the angular dependence disappears. When operating above the Rayleigh regime, the light scattering is rigorously explained by the Mie theory. In this regime, the close relative of DLS is so called static light scattering (SLS). With this technique, the angular pattern of time averaged scattered light is collected and from the results,

the particle shape and size can be determined. Both of these light scattering techniques, DLS and SLS, give a different kind of approximation for particle size, and comparing them may be beneficial.

4.3 Importance of biorelevant physicochemical properties of PSi

The balance between nanoparticles' toxicity and functionality are a delicate matter in DDSs. A good example of this is that on the one hand, passively targeted nanoparticles are trying to avoid the immune system and on the other hand, adjuvants for vaccine therapies are trying to activate it [166]. This highlights the importance of understanding the effects of particle properties to the physiological response. Walkey *et al.* [167] described the design of nanoparticles with two different causal relationships: synthetic identity determines the biological identity, which in turn determines the physiological response (Figure 11). Synthetic identity is defined by dry state properties like size, shape, and chemical composition and biological identity by wet state properties like hydrodynamic size, aggregation, and protein adsorption.

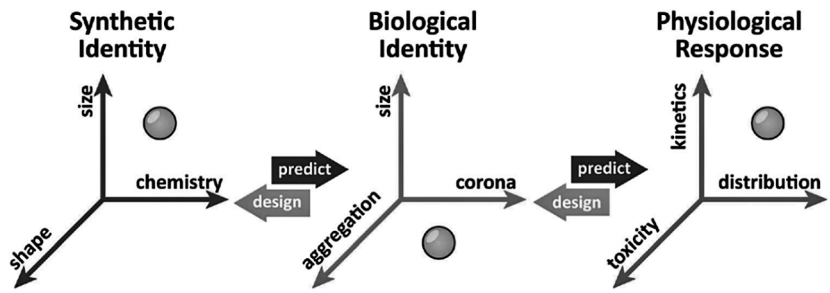

Figure 11. Design and prediction cycle as proposed by Walkey *et al.* [167]. Figure adapted with permission from The Royal Society of Chemistry.

4.3.1 Biodegradation of PSi

Besides the calcification, Canham *et al.* observed biodegradation of PSi [31,168], which was soon noticed to depend on the porosity and pH [169]. The finding was encouraging because of the fact that the degradation product of silicon is silicic acid [170]. This is the most common form of silicon in humans and has been found to be an essential nutrient [171,172]. Although silicic acid has been shown

to be absorbed by the gi tract, it is also rapidly excreted via the urinary pathways and does not accumulate in the body [173]. There is some evidence that silicic acid may have some additional health benefits, e.g. against Alzheimer's disease [174].

The degradation of PSi in biological environments (biodegradation) is rather well studied property. Besides higher pH increasing the dissolution rate, Anderson *et al.* [169] noticed that the lowest dissolution took place in a low porosity (62%) film, but surprisingly the film with medium porosity (83%) dissolved more during 24 h than the film with the highest porosity (88 %). So, the dissolution was not increasing monotonically as a function of porosity, and the difference was attributed to the film microstructure. The more recent studies on biodegradation of PSi microparticles attribute the faster dissolution to larger pore size [45,108,175]. Another structure related parameter is, naturally, the dimensions of the studied sample. The time of biodegradation could vary from days [108] to hours [69] when the particle size is decreased from the micronscale (~3 μm) to the nanoscale (~130 nm). This is understandable, since the concentration of silicic acid in saturated solutions is not high (~100 μg/ml), and the diffusion of the degradation products inside the porous matrix is slow. This was observed already by Anderson *et al.* [169], when they noted that dissolution seems to take place only on top of PSi layer.

The chemistry of PSi surfaces has a significant role in biodegradation. In biomedical applications, the freshly etched (as-anodized) hydrogen terminated surface turns into a native oxide surface when exposed to water. This surface is more stable than the as-anodized surface but in many cases degrades still too fast [69]. Conveniently, the diverse surface treatment arsenal enables the production of more stable surfaces for biomedical applications. When the degradation of PSi microparticles was studied in intravitreal gel inside rabbit eyes [136], the big differences were found between different surface chemistries. As-anodized particles degraded completely in a month, whereas thermal oxidation doubled the degradation time. In the case of hydrosilylated particles, only half of them were degraded when the experiment ended after four months. Jalkanen *et al.* [44] studied the degradation of multilayered PSi optical structures with different surface treatments in a strongly alkaline 1 M NaOH solution. Hydrosilylation protected the surface for 2-3 hours if the surface was hydrophobic (decene terminated). Hydrophilic (undecylenic acid terminated) surfaces did not differ significantly from thermally oxidized surfaces, and the structure was completely dissolved in less than 10 minutes. The best degradation resistance was on thermally carbonized samples, which started to show some signs of distortion after 5 hours but needed approximately 14 hours to dissolve completely.

The fact that the dissolution mechanism (Figure 12) is strongly pH dependent is important in the biological point of view since the typical pH inside human systemic circulation is slightly basic at a pH of 7.4. In addition, increasing the temperature from laboratory conditions to body temperature (37 °C) accelerates dissolution [169]. It has been observed that proteins (FBS, Fetal Bovine Serum) might also accelerate the degradation of PSi microparticles [45]. Tzur-Balter *et al.* noticed that, for example, a tumor microenvironment affects the degradation of PSi microparticles, which they attributed to increased oxidative stress compared to healthy tissue. In the summary, they also highlight the need to study the material performance in the right context [176]. When the behavior of the material can be tested in relevant conditions, the degradation can be tuned by adjusting surface coatings with PEG [45] or dextran [69], for example.

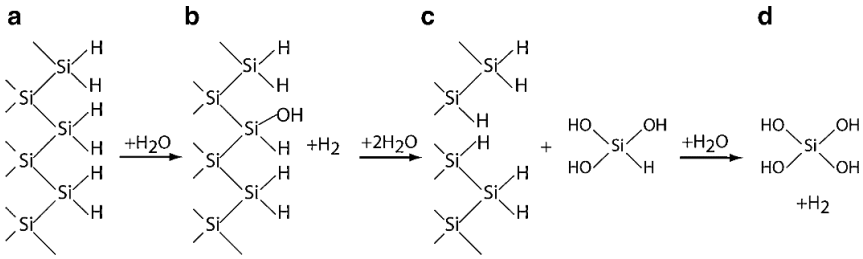

Figure 12. Proposed mechanism for porous silicon degradation in aqueous solutions [170]. (a) A Si—H-terminated surface immersed in H_2O. (b) The Si-H bond undergoes hydrolytic attack and is converted to Si—OH and produces a hydrogen molecule. (c) The Si—OH at the surface polarizes and weakens the Si—Si backbonds, which are then attacked by H_2O, producing $HSi(OH)_3$. (d) In solution, the $HSi(OH)_3$ molecule is quickly converted to $Si(OH)_4$ releasing a second hydrogen molecule. Figure has been redrawn and reprinted from [177] with permission of Springer International Publishing Switzerland (© 2014).

4.3.2 From PSi biocompatibility to biointeractions

Besides the PSi biocompatibility with bone, PSi has been found to be compatible with the subcutaneous tissue of guinea pigs [178] and conjunctiva in rat eyes [179]. On rats' abdominal walls, PSi implants induced foreign body reactions comparable to the response of the well-known bio-inert material titanium [180]. PSi films have been found to be good substrates also for cell adhesion and culturing [181,182], although surface chemistry can affect the cell attachment and growth [183] as well as the denaturation of some proteins [99,184].

The general target of biocompatibility studies for biomedical nanoparticles is to be able to predict their pharmacokinetics, biodistribution [185,186], and toxicity [187]. The possibility to modify nanoparticles' physicochemical properties leads to rapid expansion of the available combinations, and the study of all these would be time- and resource-consuming. Nanoparticles' interplay with cells is one of the most determining factors in inflammatory responses, biodistribution, and toxicity *in vivo* [188,189]. This interplay is mediated by different interfaces which Nel *et al.* divided into two different categories: the quite well known solid-liquid interface (which properties are presented on chapter 4.2) and the less known and far more complex nano-bio interface, where the final interaction between nanoparticle and cell surface happens [190].

The role of electrostatic interactions on cellular uptake has been studied in many reports, and the importance of high absolute zeta potential for cell uptake has been observed [191–194]. This has also been noticed in toxicity studies where a strong interaction of particles with the cell membrane might induce toxic effects [190]. The same behavior has been observed with PSi nanoparticles with significant surface chemistry dependent differences in toxicity [195]. The APSTCPSi nanoparticles with high positive zeta potential seem to cause the most toxic effects, which is seen in several different indicators. Also, hydrophobicity of THCPSi and UnTHCPSi particles caused cytotoxic signals. Hydrophilic and negatively charged TOPSi and TCPSi nanoparticles rarely cause any toxicity. The same was observed in *in vivo* studies with the exception that also THCPSi nanoparticles seemed to be bio-safe in addition to TOPSi and TCPSi.

The importance of neutral and hydrophilic surfaces has been recognized when the target is to avoid the macrophages and create long circulating delivery systems [119]. Recently, the importance of the collection of blood proteins around the nanoparticle, *i.e.*, formation of so called protein corona, has been recognized, and the area is under expanding research efforts. Quite commonly, protein corona is divided to hard and soft corona with long and short exchange times [196–198]. The adsorption of hard corona proteins is typically also considered to be non-reversible (Figure 13) [199].

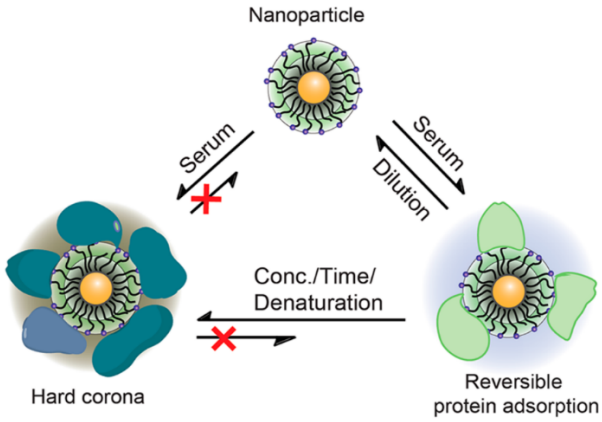

Figure 13. Evolution and nature of hard (on left) and soft (on right) protein corona [199]. This is an unofficial adaptation of an article that appeared in an ACS publication. ACS has not endorsed the content of this adaptation or the context of its use.

In the studies of protein corona, the hydrodynamic diameter and zeta potential are playing a big role [198]. These measurements can readily give information about the presence and size of the protein corona, but in order to produce models for structure-activity relationship, more quantitative data about the composition of the corona is needed. Here the important instrument is a mass spectrometer, which is often utilized with liquid chromatography (LC-MS). Walkey *et al.* [188] studied the protein corona "fingerprint" and cell association of 84 different gold and silver nanoparticle formulations in respect to particle size, surface chemistry, and composition of the primary particle. From the results, they developed a model that predicts the uptake and takes into account nanoparticles properties and the protein corona fingerprint. The main finding of the study was that the protein corona fingerprint predicted the uptake quite well. The more surprising finding was that despite the similar physicochemical parameters between two different materials, like size and surface chemistry, the composition of primary particles was still an important factor. The uptake prediction model that worked for gold nanoparticles could not predict the uptake of silver nanoparticles. They also noted that despite the fact that nanoparticles' exposure to serum causes zeta potential to shift to the average zeta potential of serum components (which in this case was -7.8 ± 2.6 mV). Zeta potential was the most important physicochemical parameter affecting the composition of protein corona and thus cell uptake.

The importance of zeta potential to the cell uptake has also been observed with PSi particles [132]. Serda *et al*. studied the uptake of PSi particles by endothelial cells (HUVEC) and macrophages (J773) with and without serum on the cell medium. Original zeta potential differences (-43 mv, 15 mv and -4 mV) were levelled off (-32 mV, -40 mV and -28 mV) when serum was added on nanoparticles. Curiously, addition of serum did not affect the uptake in the same way but increased the differences between surface chemistries for both cell types.

The impact of the hydrophobicity of nanoparticles on protein corona formation and composition is also significant. Increasing hydrophobicity increases protein affinity to the surface and thus the density and thickness of the corona [167], but Zhu *et al.* [200] noted an inverse linear correlation between the hydrophobicity index and cellular uptake. They treated gold nanoparticles with albumin and noted that it bound to the surface more tightly when the surface was hydrophobic. The avoidance of cellular uptake of hydrophobic nanoparticles was attributed to this albumin binding ability. In his dissertation, Rytkönen [201] studied the composition of protein corona around hydrophilic THCPSi nanoparticles. It was found that hydrophilic coatings with PEG [122] or hydrophobin [123] caused the amount of adsorbed corona proteins to decrease. With hydrophobin, also the composition of the corona changed. In both cases, the binding of serum albumin decreased when the surface was hydrophilic which is in accordance with the previous mentioned results [200].

4.3.3 Size, agglomeration and dose

The need to study the agglomeration primarily arises from the importance of nanoparticle size in biomedical applications [202,203] and toxicity [190]. The strong size dependency has also been found from PSi particles, and, in agreement with other studies, smaller size seems to promote the accumulation of particles on non-MPS organs [124]. In addition, the particles' discoidal shape seems to enhance size dependence of observed particle accumulation on breast tumors in mice when compared to spherical silica beads [76]. Size dependent behavior and subsequent toxicity for Caco-2 cells was observed by Santos *et al.* [204]. The cytotoxicity was studied in terms of mitochondrial disruption, ATP depletion, ROS production, and cell apoptosis. The lowered toxic concentration threshold was observed when particle size decreased from 75 μm to 1.2 μm. In a subsequent study by Bimbo *et al.*, the cytotoxicity was confirmed for small microparticles, but when the size was decreased to an average size of 142 nm and 188 nm, cytotoxicity decreased [70].

One of the practical issues masking the impact of nanoparticles properties to biological system is issues on dosing [205,206]. Firstly, the question of metrics

is not as straightforward as one could expect because the proposed units, including μg/ml, cm^2/ml, μg/cm^2 or particles/ml, all have their pros and cons, but in the case of nanoparticles units cannot be easily converted. Other important and closely related issues are nanoparticle dispersibility and colloidal stability. Particle agglomeration, which affects particle size distribution and may cause sedimentation, depends on the medium and storing time.

Most of the toxicological studies consider a 24 hour time period, and during this time, gold nanoparticles might change their form from dispersion of nanoparticles (30 and 60 nm) to gel like macroscopic networks [207]. Another outcome of agglomeration is sedimentation, which has been shown to cause toxicity of nanomaterials in a cell culture medium [208]. On the other hand, the change of size during the agglomeration can be also exploited, as demonstrated by Liu *et al.* [209] who designed particles that agglomerated as a response of pH decrease on tumor sites. This way, they enabled interaction between normally long circulation particles and tumor tissue. Another positive impact of a biorelevant medium is the increase of the stability against the agglomeration in cell cultures [210,211], which may happen when hydrophobic nanoparticles are coated with proteins, for example. The effect of agglomeration was also noticed by Sarparanta *et al.*, with hydrophilic and slightly negatively charged hydrophobin coated THCPSi particles [123]. They observed that the coating affects nanoparticles' colloidal stability in plasma, composition of protein corona, and biodistribution. However, the differences in protein corona could not explain the nanoparticles' different biodistribution, which was attributed to the change of size consequent of agglomeration.

4.3.4 Adsorption, loading and release

The excellence of mesoporous nanoparticles over non-porous ones is in their ability to carry and release active molecules or particles with different sizes from small crystalline drugs [67] to bigger peptides [93], oligonucleotides [212], proteins [213], and even to secondary nanoparticles [214].

One of the benefits of small molecular drug delivery inside PSi is the amorphous nature of the poorly soluble drug and consequent increase in dissolution rate [115,148,215]. This behavior has been attributed to the physical confinement [114] of drug molecules in the pores, which is naturally dependent on pore dimensions. The pore size was noticed to have an effect on loading and release in many studies. The bigger pores typically increase the loading and release rate [175,214,216,217] with the limitation that the larger pore diameter may cause recrystallization of the loaded drug [218]. When the aim has been to prolong the drug release, it has been achieved via smaller pore size and longer diffusion

length or by increasing the interaction between surface and drug molecules. If the adsorption is irreversible or chemical, the release of the drug is controlled by controlling the degradation of the carrier [135,219]. Here the surface chemistry, and again pore size, are in major roles as explained before. As also stated before, degradation of PSi depends on the pore size, particle size, and surface chemistry, the same parameters that are also affecting diffusion [67,215,219].

Before going to loading experiments in more detail, it would be better to define two concepts. The amount of drug compared to total mass of the formulation ($i.e., m(drug)/m(total)$) is called the loading degree. The amount of loaded drug compared to amount of drug available in loading solution (*i.e.* $m(drug\ inside\ particle)/m(drug\ in\ initial\ solution)$) is called the loading efficiency.

The common strategy to achieve the optimal carrier properties with PSi is to keep the pore size and particle size constant and adjust electrostatic and hydrophobic interactions between the surface and the drug molecules [90,220]. Tasciotti *et al.* studied the loading of so called secondary state nanoparticles into PSi microparticles and observed improvement in loading when zeta potentials of microparticles and nanoparticles were opposite [214]. The same observation was made by Huotari *et al.* [221], when the loading degree of negatively charged GLP-1 peptide in PSi microparticles was higher with positively charged surface than with negatively charged surface. In addition, the loading degree decreased from 45 % to 24 % when the pH was increased to 9.0, where the surface of originally positively charged PSi turns negative. By keeping the concentration of the loading solution low, electrostatic interactions between the PSi surface and the drug molecule might also enable slower, degradation driven, release of payload [69].

Surface adsorption based loading is a tempting approach, especially with biological cargoes when the molecules may be expensive and efficient use of the carrying material is not that important an issue. Charged and hydrophobic sections in biomolecules typically enable the efficient loading (Figure 14), even though the immersion method is used. As an example, Rytkönen *et al.* got a sufficient 14 % loading degree with oligonucleotides [212] and Kovalainen *et al.* [61,93] were able to load PYY with a 7 % loading degree, while both of these loadings were made with a 100 % loading efficiency without waste of drug. More basic research on the role of surface chemistry on protein adsorption onto PSi surface has been done by Jarvis *et al.* [99]. They noticed that the hydrophobicity of native porous silicon surfaces increased the adsorption of studied proteins (al-

bumin, lysozyme, and papain) but also caused structural rearrangements. A hydrophilic oxide surface instead decreased the adsorbed amount of proteins, but the protein structure remained undisturbed.

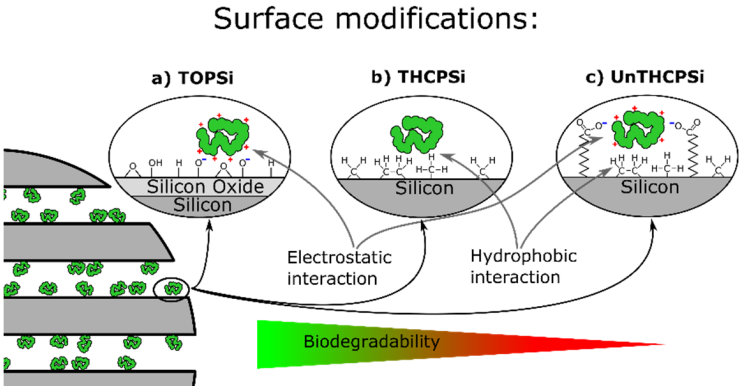

Figure 14. Surface modifications, peptide-surface interactions and biodegradation in peptide delivery as explained by Kovalainen *et al.* [93]. Figure is constructed from the original material with the permission of Dr. Riikonen.

The structural changes, when the driving force of biomolecule adsorption is a strong hydrophobic interaction, have been found with other materials also [222–224]. This kind of interaction is problematic in a drug delivery point of view because of the possible denaturation of the drug molecule and irreversible of adsorption [225]. Since the early studies on protein adsorption, it has been known that in order to achieve maximum protein adsorption onto the surface, maximizing electrostatic interaction between the surface and peptide is not necessarily the best approach. The high charge of the adsorbate also increases the repulsion between proteins and thus decreases the packing density when adsorption happens [226] (Figure 15).

The same behavior has been discovered when loading biomolecules inside mesoporous materials [227,228]. In an enzyme immobilization point of view, Vinu *et al.* have studied the adsorption of lysozyme (pI ≈ 11) [227] and cytochrome c (pI = 9.8) [229] into mesoporous (silica and carbon) materials. For both peptides, the results were the same and the best loading capacity was observed at pH near the protein isoelectric point. Later, Sang *et al.* calculated that the high loading degree on isoelectric conditions is due to the multilayered packing of peptides in mesopores [228].

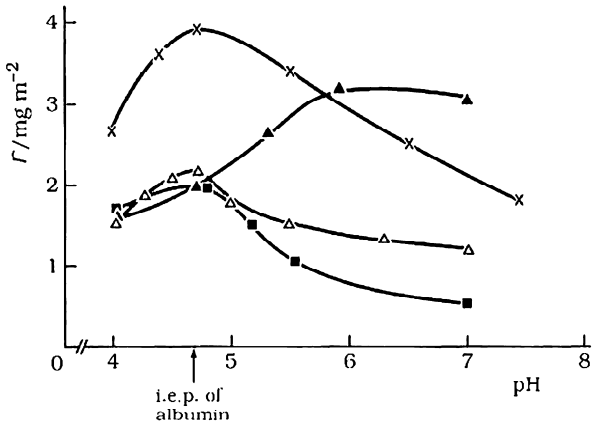

Figure 15. pH dependent plateau adsorption of human serum albumin on negatively charged polystyrene (PS) (Δ), positively charged PS (▲), negatively charged silver iodide (X) and uncharged poly(methylene oxide) (■). Reprinted from [230] with permission from Elsevier (© 2005).

In summary, we have gone through characterization from the dry state to the wet environment in this chapter. We have seen the importance of the "contex," the environment that the nanoparticles encounter and how it affects their behavior. In order to make predictions, careful characterization with well-known methods is needed through the whole design process. This is a demanding task and requires fluent collaboration between disciplines, starting from very basic research, which has been emphasized in many writings lately [167,190,205,231]. In the words of Zhang and Rosenholm on their editorial on Therapeutic Delivery 2015 [232]:

> Changing the design for each paper for yet another proof-of-concept study will not add significantly to this body knowledge, but more systematic and mechanistic studies on MSN behavior in conjunction to biological systems toward deeper *in vitro–in vivo* correlation understanding are necessitated. Adding to this body of literature will facilitate timely translation of MSNs from bench to bedside.

5 Aims of the study

The general aims of this work were to evaluate the feasibility of PSi nanoparticles on peptide delivery purposes and to study the use of light scattering as a characterization method for these kind of studies. Under these main themes, the role of medium and other formulation components were studied.

In the first paper, the objective was to study the zeta potential of PSi nanoparticles in isotonic formulations and to characterize the impact of peptide payload on zeta potential. The second objective was to test the zeta potential, and isoelectric point measurements on the PSi surface characterization purposes. The surface chemistry characterization potential of zeta potential measurements was utilized later in the second paper, where the aim was to enable and characterize the amine functionalization of TCPSi.

Peptide loading into PSi nanoparticles, as well as the release of peptides, was studied in the third and fourth papers. The aim of the third paper was to find out the suitability of PSi nanoparticles for sc and iv peptide (PYY3-36) delivery and, by altering the surface chemistry, to understand the effect of surface chemistry on peptide release rate and bioavailability. In addition, interactions driving adsorption and loading of peptide (GLP-1) into PSi nanoparticles was planned to study in fourth paper in order to find optimal peptide loading conditions, and to find explanations for the behavior of PSi nanoparticles during *in vivo* studies.

In the fifth paper, we wanted to explore the conventional light scattering methods and how they can be used for more versatile characterization of nanoparticle properties, like size, stability, and porosity. The secondary aim of the study was to understand why electron microscopy results sometimes differ drastically from light scattering results.

6 Experimental

6.1 Materials

6.1.1 PSi nanoparticle fabrication

PSi was anodized to boron doped p^+-type Si-wafers with (100) orientation and with a resistivity of 0.01–0.02 Ω cm (supplier Cemat Silicon or Siegert). A solution of hydrofluoric acid (HF, 38%) and ethanol was used as an electrolyte with a 1:1 volumetric ratio. Electrochemical etching of a multilayer PSi film was carried out by applying two different current densities successively. The lower etching current density of 50 mA/cm^2 was used as a work pulse to form a mesoporous structure for nanoparticles. This was followed by a high current density pulse of 200 mA/cm^2, which is expected to lead to the formation of a brittle fracture layer in between the mesoporous layers. After the higher current pulse, a brief pause was applied to allow the stabilization of concentration gradients in the electrolyte.

The hydrogen terminated surface of the anodized PSi was stabilized using three different surface treatments. Thermally oxidized porous silicon (TOPSi) was obtained by heating the anodized films in air at 300 °C for two hours. Thermal hydrocarbonization of PSi (THCPSi) was made in constant acetylene/N_2 flow at 500 °C. By continuing the treatment in acetylene/N_2 flow at room temperature (RT) and by subsequent annealing the material at 800 °C N_2 flow, surface hydrogen completely dissociates, and thermally carbonized porous silicon (TCPSi) was formed.

Further functionalization of the THCPSi films was carried out by covalently attaching 10-undecylenic acid to the surface hydrocarbons. The fresh THCPSi films were immersed in 120 °C undecylenic acid for 4 hours. The functionalization of the TCPSi surface was made first, by immersing the films in an etching electrolyte in order to create hydroxide groups on the surface and subsequently milling the films by using an APTES-toluene solution as the medium.

These functionalized particles are referred to as UnTHCPSi and APSTCPSi, respectively.

After the surface treatments, the freestanding PSi films were wet ball-milled in a Fritsch Pulverisette 7. Ethanol was used as a grinding medium for the UnTHCPSi, TCPSi and TOPSi films. In the case of APSTCPSi, the functionalization was carried out during the milling in a 5-10 % APTES-toluene solution. With THCPSi, particular attention was paid to avoiding oxidation by using 1-decene as a grinding medium.

Fractioning of the nanoparticles from the polydisperse mixture of PSi and grinding medium was done with a centrifuge. The diverse stability behavior arising from the different surface chemistries dictated the selection of the centrifugation medium. An attempt was made to keep the particle size distributions of the PSi nanoparticles constant by altering the centrifugation parameters so that the particle size distribution of the supernatant was within the desired limits. Typically centripetal accelerations from 1 500 g to 3 000 g were applied for the fractioning and the supernatant was collected. The fractioning step was made several times to the initial milled suspension and the collected supernatants were combined. Significantly higher accelerations from 10 000 g to 17 000 g were applied to discard the smallest particle fraction (< 100 nm), to concentrate the suspension and to change the dispersion medium. During these washing steps, nanoparticles were pelleted at the bottom of the tube and the supernatant was discarded. The particles were redispersed with ultrasound when necessary, and ethanol was used as a storage medium.

6.1.2 Silica nanoparticle fabrication

Silica nanoparticles were fabricated for Paper V in order to achieve more variations to pore morphology, orientation, and particle size. Syntheses were made bottom-up via controlled nucleation and growth of silica structure around self-assembled template of surfactants. Details of the syntheses conditions are tabulated in Table II. In the case of hollow MSN, the synthesis details have been published by Sen Karaman *et al.* [233]. In the case of P-MSN, pores are aligned parallel to each other, while in R-MSN pores are radial, pointing towards the center of the particle. With H-MSN, the core is hollow and radial porous structure is formed on the shell.

Table II. Summary of silica nanoparticles' preparation conditions

Sample	Base solution	Additives		Temp.	Mixing	Extraction	Storing
S-SN	EtOH/ammonia	TEOS+ FITC	1 mol% APTES	RT	Stirring, over night	-	Dried
L-SN	EtOH/ammonia	TEOS+ FITC	10 mol% APTES	RT	Stirring, over night	-	Dried
R-MSN	CTAB/DI water/ EtOH/ammonia	TEOS	10 mol% APTES	RT	Stirring, over night	3x30 min @ (NH4)(NO3) - EtOH	Acetone
P-MSN	CTAB/DI water /ethyleneglygol /ammonia	TEOS	20 mol% APTES	50°C	Stirring 2h + static over night	3x30 min @ HCl - EtOH	Acetone
H-MSN	CTAB/di-water/ NaOH/ethanol	TEOS	10 mol% APTES / 1.2 mol % Decane / 1.8 mol % (1, 3, 5) Trimethylbenzene	RT	Stirring, over night + hydro-thermally treated at 70°C for 48h.	Calcination at 550°C for 2.5 h.	Dried

6.1.3 Peptide properties

The peptides used in experiments were the gastrointestinal peptides GLP-1 (7-37) and PYY 3-36, later GLP-1 and PYY, which both are released endogenously [234] and have promising applications in diabetes and obesity treatment [235]. Two different versions of GLP-1 were used in these studies, which causes a small difference in isoelectric (pI) points. In Paper I, pIs of GLP-1 and PYY were calculated to be 5.4 and 7.7, respectively. In Paper IV, the acetylated GLP-1 was used and the pI was at pH 4.6. Amino acid sequences of peptides are shown in Table III.

Table III. Amino acid sequences of used peptides

Name	Sequence
GLP-1 (7-37)	H-A-E-G-T-F-T-S-D-V-S-S-Y-L-E-G-Q-A-A-K-E-F-I-A-W-L-V-K-G-R-G
PYY (3-36)	I-K-P-E-A-P-G-E-D-A-S-P-E-E-L-N-R-Y-Y-A-S-L-R-H-Y-L-N-L-V-T-R-Q-R-Y
GLP-1 (7-37) acetylated	Ac-H-A-E-G-T-F-T-S-D-V-S-S-Y-L-E-G-Q-A-A-K-E-F-I-A-W-L-V-K-G-R-G

The theoretical charge of amino acids in different pH values were calculated with the modified Henderson-Hasselbalch equation for positive (3) and negative (4) amino acids [236]. Total charge of peptides was approximated by summing these charges together. Amino acid dissociation constants were obtained from Lehninger Principles of Biochemistry [237].

$$Z_+ = \frac{1}{1 + 10^{\mathrm{pH}-\mathrm{pK_a}}} \quad (3)$$

$$Z_- = \frac{-1}{1 + 10^{\mathrm{pK_a}-\mathrm{pH}}} \quad (4)$$

6.2 Methods

6.2.1 Dynamic light scattering

On papers I, II, and IV, particle size was characterized by dynamic light scattering (DLS) measurements with the Malvern Zetasizer Nano ZS. The instrument collects data at the one back-scattering angle of 178°. By optimizing the laser light intensity and penetration depth to the suspension, multiple scattering can be avoided and the concentration of suspension can be selected more freely. By analyzing the autocorrelation function of collected intensity data, the diffusion constant(s) of nanoparticles is measured. The non-negative least squares (NNLS) algorithm [238] with a higher smoothing parameter, the so-called general purpose mode, was used for the deconvolution of the diffusion constants' distributions. The CUMULANTS algorithm [239] was used for calculations of the average diffusion constant.

The hydrodynamic diameter was calculated according to the Stokes-Einstein equation (2). All the measurements were made in ethanol, with the exception of THCPSi nanoparticles which were measured in dimethyl-formamide (DMF) or 5 w% ethanoic succinic acid solution. These media were selected in order to stabilize THCPSi nanoparticles.

6.2.2 Multiangle light scattering measurements

In Paper V, multiangle LS measurements were made with Brookhaven Instrument's BI-200SM goniometer, a BIC-TurboCorr digital pseudo-cross-correlator, and a BI-CrossCorr detector, including two BIC-DS1 detectors. Either a red or a blue laser was used depending on the nanoparticles' absorbance. In the case of silica nanoparticles, absorption of visible light is low, but in the case of PSi nanoparticles, absorbance increases strongly when shorter wavelengths are used. The unwanted effects of highly absorbing materials were minimized by using a red, 637 nm laser (A BIC Mini-L30 diode laser). In case of silica nanoparticles, a blue, 488.0 nm laser (Coherent Sapphire laser 488-100 CDRH) was used. LS measurements were made from scattering angles of 30° to 150° with a 5° interval.

In DLS experiments, pseudo-cross-correlation functions of scattered light intensity were collected using the self-beating scheme [155]. Correlation functions were analyzed with the CUMULANTS algorithm and a hydrodynamic radius (R_h) was calculated from D_t of nanoparticles according to the Stokes-Einstein equation (2).

Temperature was set to 20 °C and controlled with a Lauda RC 6 CP thermostat. Viscosity of methanol was 0.591 cP and refractive index was 1.332. The effective hydrodynamic radius (R_h^{eff}) was measured at a fixed scattering angle (θ) and fixed mass concentration of particles (c). The true hydrodynamic radius can then be obtained by extrapolating R_h^{eff} to a zero angle and zero concentration. Our experiments reveal negligible effect of particles' concentration on D_t and thus on R_h^{eff}. Therefore, herein R_h refers to R_h^{eff} extrapolated to a zero angle.

SLS was used for determining the radius of gyration (R_g) for the nanoparticles. Normalized scattering intensity from the particles $P(q)$, i.e. the scattering function, is defined as

$$P(q) = P(\theta) = \frac{I(\theta)}{I(\theta = 0°)} \tag{5}$$

where,

$$q = \frac{4\pi n_0}{\lambda} \cdot sin\left(\frac{\theta}{2}\right) \tag{6}$$

is the scattering vector, n_0 is the refractive index of the medium, and λ is the laser wavelength in vacuum. In other words, $P(q)$ is calculated by subtracting the scattering of the medium from the total scattering intensity and normalizing this value to the intensity at the extrapolated angle, $\theta = 0°$. The Debye-Bueche [240,241] or Guinier [242] scattering functions were found to be the most suitable for R_g determination.

Pure solvents used in LS experiments were filtered with a 0.2 μm syringe filter (Pall Acrodisc CR 13 mm with PTFE membrane). Cuvettes were first rinsed with methanol and then dried in a filtered compressed air stream. In order to reduce the adsorption of positively charged silica particles onto the negatively charged glass surface, a cuvette was silanized with a 5 vol-% mixture of APTES ((3-aminopropyl)triethoxysilane) and toluene. Background scattering of the medium, methanol, was measured and subtracted. Samples were diluted with methanol to as low a concentration as possible in order to avoid agglomeration and multiple scattering. The sample was drawn into a syringe and filtered with

a 0.45 μm syringe filter (VWR International 13 mm with PTFE membrane) in order to avoid dust particles. The exception to the filtering step was made with bigger H-MSNs in which case the diluted suspension was used as it was.

6.2.3 Electrophoretic light scattering

The electrophoretic mobility of the PSi nanoparticles with different surface chemistries and nanosuspension media was measured with the electrophoretic light scattering (ELS) method using the Malvern Zetasizer Nano ZS. Zeta potential, ζ, was calculated from the electrophoretic mobility u_e with the equation

$$u_e = \frac{2}{3}\frac{\epsilon}{\eta\zeta f(\kappa a)} \tag{7}$$

where the permittivity, ϵ, and viscosity, η, are the properties of the medium, and $f(\kappa a)$ is the so-called Henry's function which depends on the particle radius, a, and the Debye length, κ^{-1} [243]. The Debye length can be understood as the thickness of the electric double layer, which is inversely proportional to the ionic strength [244].

The value of $f(\kappa a)$ varies from 1.0 for low ionic strength and/or small particles to 1.5 for high ionic strength and/or large particle size. Henry's function values for each medium were calculated with Ohshima's approximation [245].

$$f(\kappa a) = 1 + \frac{1}{2}\left\{1 + \left[\frac{5}{2\kappa a(1 + 2e^{-\kappa a})}\right]\right\}^{-3} \tag{8}$$

Zeta potential characterization of a pure nanoparticle suspension was made as a function of pH with the IEP titrations. The nanoparticle concentration was 50 – 100 μg/ml, and de-ionized (DI) water was used as a medium. In Paper II, IEP values were measured in a weak, 1 mM NaCl solution. HCl and NaOH were used as titrants, and the addition of new ions to the nanosuspension was taken into account in Henry's function. Each data point is the average of at least three individual measurements. The IEPs were determined by interpolating the titration curve in a linear fashion to the pH point at which zeta potential reaches a zero value.

6.2.4 UV-Vis adsorption

Peptide concentration measurements were made with an ultraviolet-visible (UV-Vis) range spectrophotometer (Labrox, Finland). For the peptide loading experiments, GLP-1 was dissolved in ultrapure DI water (Millipore Direct-Q 5 UV). An ethanol based suspension of PSi nanoparticles was centrifuged, washed, and changed to DI water. Loading experiments were made by combining peptide solution, DI water, buffer solution, and a nanoparticle suspension, in this order, to a 1.5 ml low retention Eppendorf centrifuge tube. After mixing, particle concentration was 1 mg/ml and the buffer was diluted by half. Peptide concentration was adjusted by changing the ratio of peptide stock solution and DI water. Adsorption was let to equilibrate for 1.5 to 2 hours. Particles were centrifuged down and the sample from the supernatant was applied to the well-plate for a UV absorbance measurement. All the measurements were made twice and average values with mean absolute deviations are reported. Statistical analysis with the Independent-Sample T-Test was made with IBM SPSS Statistics 22.

Absorbance was measured at the wavelength of 280 nm, where peptides' aromatic side chains phenylalanine (F), tyrosine (Y) and tryptophan (W) have an absorption peak. Concentration dependence of the absorbance obeyed the linear Beer-Lambert law after the proper reduction of the baseline caused by citric acid in the buffer and occasional residues of PSi nanoparticles.

6.2.5 Nitrogen sorption

Specific surface area (SSA_{BET}) and pore volume (V_P) were obtained from the dried nanoparticle samples with nitrogen sorption measurements (Micromeritics TriStar 3000) at -196°C. The SSA_{BET} was calculated according to the BET theory [141]. Pore volume (V_p) was calculated from the maximum nitrogen adsorption near the normal pressure [246]. If necessary, the pore diameter (D) was calculated from these values by assuming cylindrical pores, when $D = \frac{4 \cdot V_p}{SSA_{BET}}$.

6.2.6 TEM

Size and shape of nanoparticles was analyzed with TEM (JEM-1400 Plus, JEOL Ltd.) with 120 kV acceleration voltage. ImageJ 1.50 [247] was used for particle analysis with following procedure.

The original 8-bit greyscale image was turned to binary scale by adjusting the threshold with the "Threshold" tool. The threshold selection method was fixed inside one particle batch, as the same thresholding method was impossible to use on all samples due to the contrast differences arising from the size and

density of nanoparticles. Particles were selected with the "Analyze particles" tool. The smallest particles ($area < 400$ nm^2, $r \lesssim 12$ nm) were filtered out in order to exclude the false particle identifications from the image noise and defects in the supporting grid. In the case of silica nanoparticles, circularity measurement was used in order to exclude agglomerates from the analysis. The complicated morphology of the PSi nanoparticles made this method less convenient, and in this case, the agglomerated particles were identified visually.

In order to retain comparability of TEM to LS measurements, all samples, except H-MSN, were filtered with a 0.45 μm syringe filter (VWR International 25 mm with PTFE membrane).

7 Results

7.1 Nanoparticles used in studies (All papers)

For all papers, nanoparticles were characterized with ELS. One-angle backscattering DLS measurements were made in Papers I, III and IV and multiangle DLS in Paper V. For microparticles on Paper II, DLS is not a suitable method and the particle size distribution was characterized by sieving (d_s). The surface area and pore volume were determined with N_2-sorption measurements. Characterization results are reported on Table IV and, in case of Paper V, on Table VI.

Table IV. Used nanoparticles (in Papers I-IV) and their characterization results

	d_H nm	PdI	d_s µm	IEP	ζ mV	SSA_{BET} m^2/g	V_p cm^3/g	d_p	Contact angle
Paper I									
TOPSi	132	0.120		2.6[c]					
THCPSi	129[a]	0.167[a]		4.6[c]					
UnTHCPSi	164	0.103		3.8[c]					
TCPSi	146	0.090		3.3[c]					
APSTCPSi	153	0.116		8.4[c]					
Paper II									
TCPSi			< 25	2.6[d]		256	0.87		
APSTCPSi			< 25	7.7[d]		222	0.84		
Paper III									
TOPSi	140	0.145			- 47.8[e]	163	0.591	15.3	
THCPSi	133[b]	0.158[b]			- 40.5[e]	202	0.598	11.8	
UnTHCPSi	158	0.115			- 31.4[e]	230	0.706	12.3	
Paper IV									
TCPSi	147	0.109				183	0.54		13° ± 3°
APSTCPSi	166	0.055		9.0[f]		227	0.77		52° ± 5°

Used medium was DMF(a), 5 w% SA-EtOH(b), DI water(c), 1 mM NaCl(d), 10 mM phosphate buffer, pH 7.5(e), 1 mM NaH_2PO_4(f).

7.2 Zeta potential as surface characterization method (Papers I, II, IV)

In order to study zeta potentials and IEPs, the PSi nanoparticles with various surface chemistries were fabricated. One aim of the study was to measure the IEPs of these surface chemistries for the first time (Paper I). Titrations were made with several different nanoparticle batches, from which obtained IEPs are reported in Table IV. Typical titration curves can be seen in Figure 16a. For the peptide loading studies (Paper IV), the effect of McIlvane buffer to zeta potential was measured and charge of GLP-1 peptides was calculated (Figure 16b).

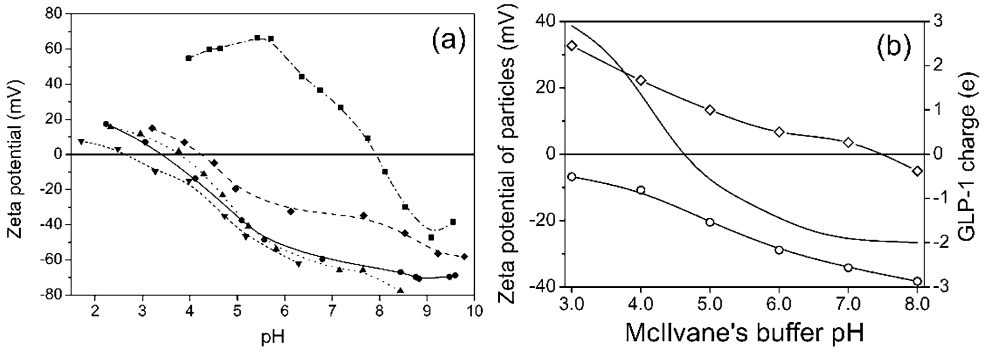

Figure 16. (a) Titration curves for an IEP determination of PSi nanoparticles with different surface chemistries (■) APSTCPSi (◆) THCPSi (●)TCPSi (▲)UnTHCPSi (▼) TOPSi. (b) Zeta potential of TCPSi (○) and APSTCPSi (◊) nanoparticles in different buffer solutions and the calculated charge of GLP-1 peptide.

The lowest IEPs, 2.6 and 3.3, can be found from TOPSi and TCPSi, respectively. The high treatment temperature of TCPSi enables the dissociated acetylene to absorb into the PSi crystal structure, leading to the formation of a thin surface oxide layer on the top of silicon carbide layer. The TCPSi and APSTCPSi surface chemistries were later characterized with various methods in Paper II. The IEPs for TOPSi and TCPSi are consistent with the IEP of silica, which is generally assumed to be in between of 2 and 3, due to the presence of surface silanol groups [248]. The observed differences between the IEPs of TOPSi and TCPSi could be due to the differences in the surface oxide structure. Unexpectedly, IEP results were also obtained for THCPSi nanoparticles. The surface of this material is terminated by hydrocarbon groups [53], which cannot be ionized, thus a pH independent behavior of surface charge should have been observed. However, we managed to measure an IEP of 4.6 for the THCPSi in a repeatable fashion.

This behavior could be due to the formation of surface silanol at the ball-milling stage of PSi films.

IEP measurements also verified the successful functionalization of carbonized surfaces. IEP was increased from 3.3 to 8.4 after the amine functionalization of TCPSi. This was expected because the functionalization is typical for silica particles, and it is explained by the decrease of the number of free silanol groups and by the presence of the primary amine groups on the surface [249]. Further confirmation of the result was obtained with IEP measurements of PSi microparticles in Paper II. The smaller shift was observed when THCPSi surface was functionalized with undecylenic acid. The shift was explained by the reaction of undecylenic acid with hydrophobic and neutral $-CH_x$ groups on the particle surface. This means that these surface groups are reacting with the unsaturated end of the molecule, and the carboxylic acid ($-COOH$) is pointing outward. This yields a negatively charged and pH dependent surface termination.

In order to keep the pH constant during the peptide adsorption experiment in Paper IV, McIlvane's buffer solutions were used. Zeta potential is sensitive to the ionic strength of the medium, which is why the nanoparticles' IEP in buffers was measured for the studied TCPSi and APSTCPSi particles (Figure 16b). When compared to previously mentioned results in weak electrolytes, IEPs shifted from pH 8.4 to pH 7.4 with APSTCPSi and from pH 3.3 to pH < 3.0 with TCPSi. In addition, absolute zeta potential of both particles decreased throughout the pH range and it was especially pronounced in the case of APSTCPSi. The fact that IEP shifted toward the same direction with both surfaces gives reason to suspect that some specific (non-electrostatic) adsorption of negatively charged ions takes place on the buffer. Besides nanoparticles' zeta potential, Figure 16b also shows the theoretical net charge of GLP-1 in different pH conditions.

In Paper II, we showed that zeta potential measurements could be used for *in situ* aqueous (chemical) stability studies (Figure 17). The loss of amine termination was studied with two different surface chemistries, APSTCPSi and APSTOPSi, the former surface is thermally carbonized and latter thermally oxidized before the silanization.

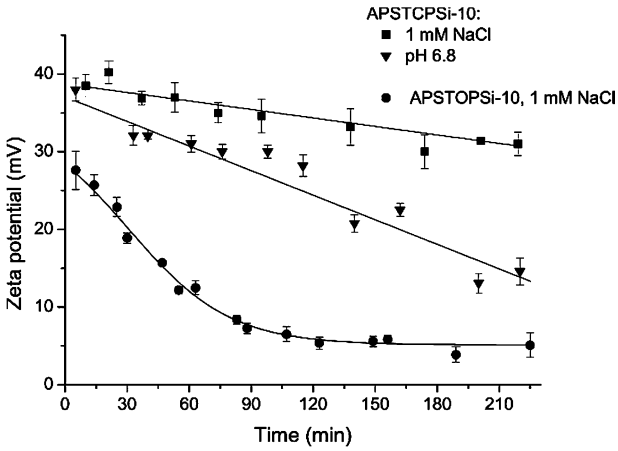

Figure 17. Aqueous stability of zeta potential of APSTCPSi-10 in distilled water and in pH 6.8 phosphate buffer and APSTOPSi-10 in distilled water as a function of time.

Zeta potential of all surfaces decreased as a function of time, which was attributed to the detachment of the positively charged amine groups on the surface. The APSTCPSi surface was found to be more stable against the degradation as the detachment of the amine groups lasted several hours in the aqueous electrolyte solution. The zeta potential of the APSTCPSi-10 decreases by 20 % from its initial value in approximately 4 hours. Conversely, the APSTOPSi-10 appeared to undergo a fast hydrolysis, and in the same time frame, zeta potential was reduced by 70%. In a pH 6.8 buffer solution, the hydrolysis rate of APSTCPSi increased when compared to the electrolyte solution. The PSi particles typically cause an electrolyte pH shift to a slightly acidic direction, and in the buffer solution, pH 6.8 is significantly higher. Zeta potential decrease appeared to be slower than with the oxidized sample, falling approximately 50 % from the initial value in 4 hours, suggesting that the surface should be stable enough in aqueous conditions to be used, e.g., in intravenous drug delivery applications.

7.3 Effect of isotonic media and peptide adsorption to zeta potential (Papers I, IV)

In order to study the effect of formulation components to zeta potential of a nanoparticle suspension and its colloidal stability, nanoparticles were dispersed into several different isotonic media (Figure 18) and nanoparticles' zeta potential was measured (Paper I). Zeta potential was found to be strongly dependent on

the isotonic medium. The analysis of the results were made by keeping in mind the practical $|\zeta| > 30$ mV limit for an electrostatically stable suspension[7].

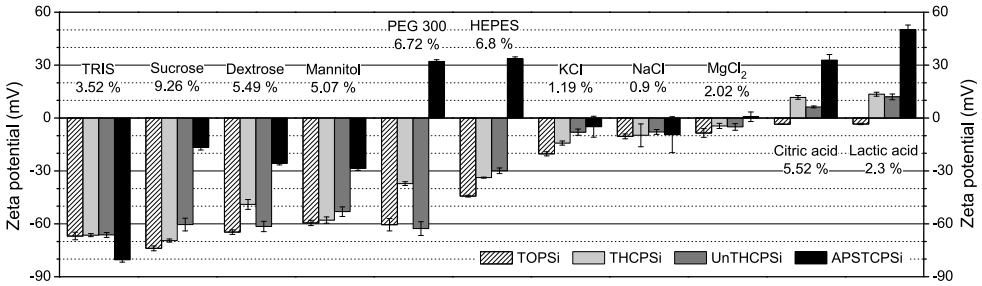

Figure 18. Zeta potential of PSi nanoparticles in different isotonic media.

As a highly basic compound, TRIS (2-Amino-2-hydroxymethyl-propane-1,3-diol) caused the disappearance of special characteristics of the surface chemistries, with respect to zeta potential. Slightly acidic sucrose, dextrose and mannitol generated a good isotonic medium for negatively charged nanoparticles, but for positively charged APSTCPSi these additives reversed the zeta potential. A somewhat unexpected result was the almost indistinguishable effect of PEG 300. Adsorption of neutral molecules on the charged surface should cause the movement of the slip plane away from the surface causing a decrease of the absolute value of the zeta potential [244]. The absence of this effect was attributed to the small molecular weight of PEG molecule and the subsequent small shift of the slip plane. HEPES (4-(2-hydroxyethyl)-1-piperazineethanesulfonic acid) shifted the zeta potential of TOPSi and UnTHCPSi slightly towards neutral but maintained the zeta potential on a sufficiently high level. All salt solutions were very poor media for PSi nanoparticles, because the high ion concentration screens the surface charge and shifts the zeta potential practically to zero. The more acidic solutions of citric and lactic acid maintain the positive zeta potential of the APSTCPSi nanoparticles but are at the same time very poor media for negatively charged particles.

In order to evaluate the role of loaded peptides on zeta potential of functional nanoparticle drug delivery formulations (in Paper IV and in Paper I) and to test the feasibility of zeta potential in adsorption characterization, zeta potential of nanoparticles was measured as a function of peptide concentration and

[7] Malvern's technical note: Zeta potential - An introduction in 30 minutes, online citation 13.12.2016, http://www.malvern.com/en/support/resource-center/technical-notes/TN101104ZetaPotentialIntroduction.aspx

pH. Relative changes of zeta potential on different pH buffers are shown in Figure 19.

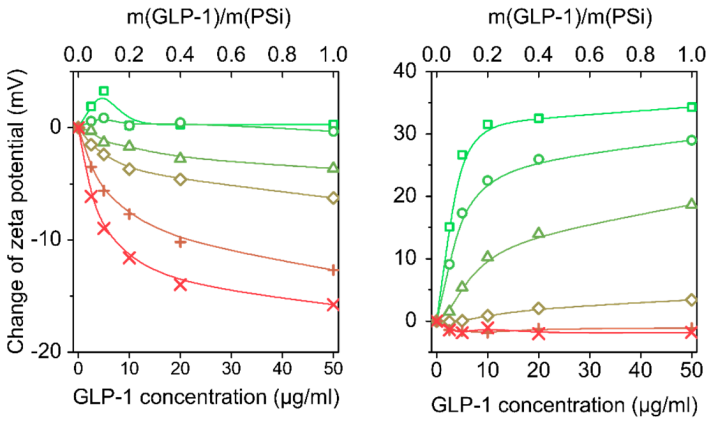

Figure 19. Change of zeta potential as a function of peptide GLP-1 concentration. Positive APSTCPSi nanoparticles are on the left and negative TCPSi nanoparticles on the right. Concentration of nanoparticles was 50 µg/ml. pH varies from 3.0 (green) to 8.0 (red).

These results show that zeta potential is very sensitive to peptide adsorption and highlights the sensitivity of ELS measurements in the adsorption studies. The change of zeta potential during the adsorption is a product of the charge density of one peptide and the number of adsorbed peptides on the surface. This can be seen in Figure 19. The change of zeta potential is largest when the peptide and particle are oppositely charged. For APSTCPSi, this is at pH 8.0, when the peptide is negatively charged and particle is neutral and for TCPSi at pH 3.0, when peptide is positively charged and particle is neutral. The biggest change of zeta potential takes place at low concentrations, which is probably due to the screening effect of the first peptide layer that is formed on the particle surface.

The effect of peptide loading on the zeta potential of the PSi nanoparticles was also studied with two oppositely charged peptides, PYY and GLP-1. The peptide to particle mass ratio was 1:1. The effect of peptide adsorption on the zeta potential of PSi nanoparticles with different surface chemistries is presented in Table V. The shift was largest for the THCPSi nanoparticles. The original zeta potential in the corresponding pH was slightly negative (-15 mV), increased up to +40 mV when PYY was added, and decreased to -44 mV when GLP-1 was added.

Table V. Measured zeta potentials of PSi nanoparticles compared to loaded nanoparticles

Particle	Zeta potential (mV)		
	unloaded[a]	PYY	GLP-1
THCPSi	- 15 ± 6	40	- 44
UnTHCPSi	- 54 ± 4	13	- 53
TCPSi	- 46 ± 3	4.4	- 53
APSTCPSi	> 57	59	6.1

[a] Zeta potential of nanosuspension in corresponding pH conditions estimated from the pH titrations (Figure 16).

In order to design good, agglomeration resistant suspensions, the selection of the isotonic medium for each peptide-loaded nanoparticle could be made based on the previously obtained information about the effect of each isotonic media on the nanoparticles. The concept is illustrated in Figure 20. The change of zeta potential is drastic when the payload is added to the THCPSi nanoparticles. The addition of isotonic solution to the formulation can be done so that the sufficiently high (for a stable suspension) zeta potential is maintained.

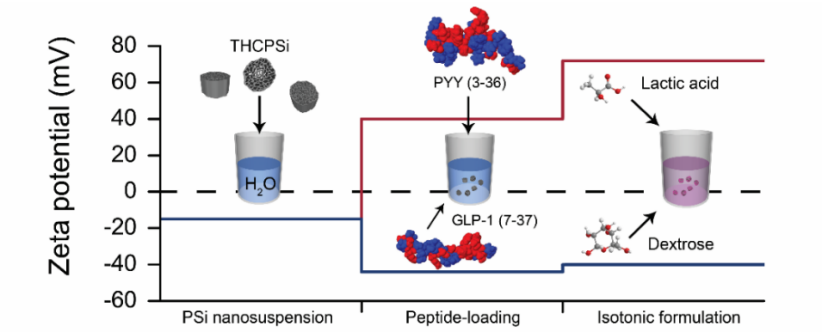

Figure 20. Example of the effect of loaded peptides to nanoparticles zeta potential and selection of the isotonic medium.

7.4 Studies on the interactions during the peptide loading (and release) (Papers III, IV)

In Paper III, PSi nanoparticles were used for the first time in peptide delivery *in vivo*. Subcutaneously injected (sc) PSi nanoparticles sustained the release of the peptide PYY over the 4 day measurement time (Figure 21a). The reference sc injected peptide solution was eliminated from circulation after 12 hours. In other words, nanoparticles were able to prolong the half-life of PYY from 26 min to more than 20 hours. More hydrophobic surface chemistries, especially UnTHCPSi, sustained the release longer than hydrophilic TOPSi, but the difference was not large. All the sc PSi nanoparticles increased the relative bioavailability and showed over 80 % absolute bioavailability.

The importance of the administration route was significant, which was noted when similar nanoparticles with PYY loading were delivered intravenously (Figure 21b). This time, the half-life increased marginally from 12 min to 20 min, 26 min, and 46 min for THCPSi, TOPSi, and UnTHCPSi nanoparticles, respectively. Here, the differences between surface chemistries were even smaller than with sc injection and the order different. THCPSi nanoparticles released the cargo fastest and showed lowest absolute bioavilability when compared to PYY solution. The faster iv release was attributed to competitive protein adsorption on systemic circulation.

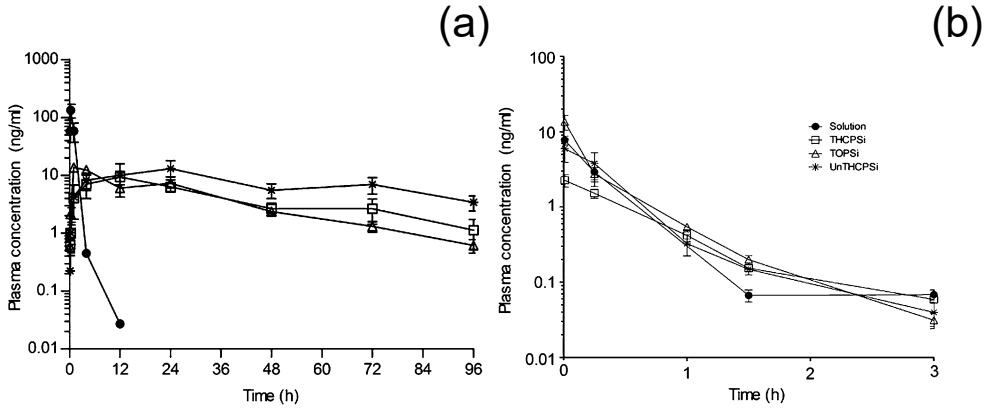

Figure 21. PYY plasma concentrations in mice after sc delivery (a) and iv delivery (b) in THCPSi (□), TOPSi (Δ) and UnTHCPSi (∗) nanoparticle formulations compared to PYY solution. In sc delivery n = 5-6 for each nanoparticle and n= 4 for solution. In iv delivery n = 6-10. Results are calculated mean ± standard error of the mean.

Peptide loading efficiency was also studied and results can be seen in Figure 22. The loading seems to take place quite fast, and after 30 min, the plateau is reached. The peptide affinity seems to be higher toward hydrophobic UnTHCPSi and THCPSi surfaces than toward hydrophilic TOPSi surface. The peptide to nanoparticle ratio was 2:5 ($m_{peptide}/m_{PSi} = 0.4$) in this study. Another *in vitro* test, where the ratio was adjusted to 2:25 (0.08), was made and loading efficiency of >99.5 % for hydrophobic and >96 % for hydrophilic nanoparticles was observed. For the *in vivo* studies, the PYY:PSi ratio was adjusted to 2:125 (0.016) in sc administration and 2:1250 in iv administration. Though it should be safe to say that, in these cases, the loading efficiency was close to 100 %.

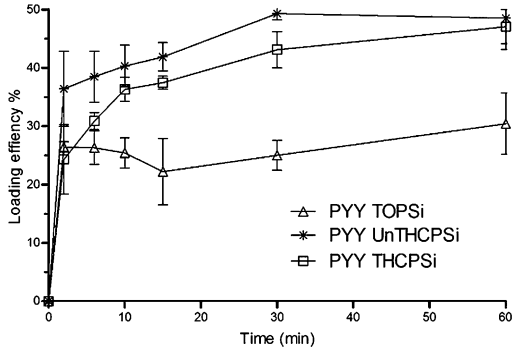

Figure 22. Loading efficiency (mean ± standard deviation, n=4) of PYY to PSi nanoparticles as a function of time. Peptide concentration was 1 mg/ml and PSi concentration 2.5 mg/ml. Remaining peptide amount in loading solution was measured with HPLC.

In vivo peptide release differences between surface chemistries and significantly different release rates between administration routes, together with the observed strong affinity of GLP-1 and PYY toward the PSi surfaces in Paper I, raised the question of the interactions between peptides and nanoparticles and optimal loading conditions. Thus in Paper IV, adsorption and loading of peptide GLP-1 was studied as a function of pH and concentration. The low concentration was used in order to understand the interaction between surfaces and peptides (Figure 23). At the lowest concentration, there is no clear difference in adsorption at different pH conditions (except at pH 3.0) for APSTCPSi particles, but for TCPSi nanoparticles, the difference is clear. Since both surface chemistries show a pH dependent charging behavior, the differences should also be seen in APSTCPSi, if the driving interaction would be electrostatic. The observation that APSTCPSi is more hydrophobic (Table IV) could explain the pH independent adsorption behavior. Either the driving force of GLP-1 adsorption on APSTCPSi

is the hydrophobic interaction or the adsorption is driven by the changes on the peptide structure, which may also be increased by the adsorbent's hydrophobic nature [230]. Results also show that the adsorption efficiency is almost 100 % for APSTCPSi nanoparticles when the peptide to nanoparticle ratio is 1:5 (0.2) or lower, as presented in Figure 23. The situation is also the same for TCPSi particles with the smallest concentration when the ratio is 1:20 (0.05). This is in line with the adsorption efficiency studies on Paper III, where near 100 % adsorption efficiency was observed with the ratio 2:25 (0.08).

Nanoparticle loading with the maximum peptide concentration is shown as a function of pH in Figure 23c. The impact of pH to the loading process is clear. The strongest loading takes place at pH 5.0 for positively charged APSTCPSi nanoparticles and from pH 4.0 to 5.0 for negatively charged TCPSi nanoparticles. The pI of GLP-1 is at pH 4.6 so the results confirm the hypothesis and previous findings with mesoporous silica observing the strongest loading near the pI value of the loaded component [228].

At pH 4.0, negatively charged TCPSi nanoparticles adsorbed positively charged peptide about 27 % more than positively charged particles, which may be due to the electrostatic interaction between the peptide and the particle surface. A more pronounced effect of opposite charges can be seen in pH values below and above GLP-1's pI. At pH 3, the peptide's and APSTCPSi nanoparticles' charges are highly positive while the charge of TCPSi is negative or neutral. At this pH, loading to the TCPSi is moderate, while there is no loading at all in the APSTCPSi nanoparticles. Similar effect can be seen on the other side of the peptide's pI where neutral or weakly positive APSTCPSi is a better adsorbent for negatively charged peptide. Loading was 30 %, 75 % and 102 %, better on APSTCPSi compared on TCPSi at pH values 6.0, 7.0, and 8.0, respectively.

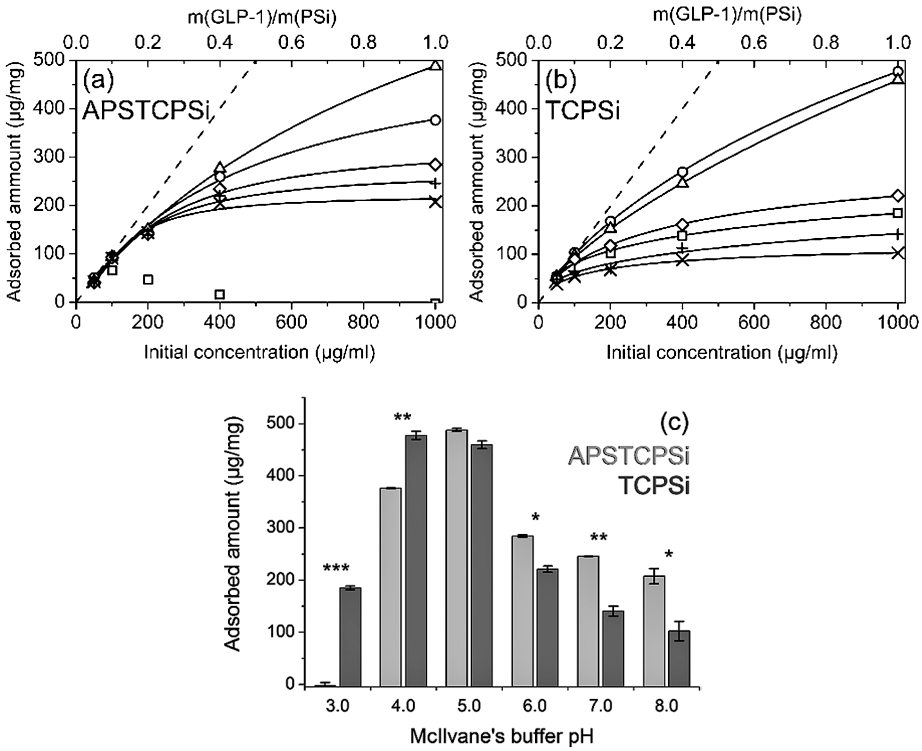

Figure 23. Adsorbed peptide amount on PSi nanoparticles. The experiment was made as a function of initial peptide concentration with two different particles (a) APSTCPSi and (b) TCPSi and six different buffer pHs 3.0 (□), 4.0 (○), 5.0 (Δ), 6.0 (◊), 7.0 (+) and 8.0 (x). Lines are fitted using the general Langmuir-Freundlich equation. The last of the graphs above is plotted in order to better compare the differences (c). The concentration of particles and peptides was the same 1 mg/ml. The level of significance between the TCPSi and APSTCPSi was set at probabilities of *$p < 0.1$, **$p < 0.05$ and ***$p < 0.01$.

In order to evaluate the amount of adsorbed peptides the following simple calculation can be made. As GLP mostly consist of a long α-helix its shape is elongated [250] and is here approximated as an elliptic cylinder. The length of the cylinder is 4.9 nm and ellipsis axes are 1.1 nm and 1.5 nm. Thus if the longer side of peptide adsorbs on the surface, the minimum area it covers is 5.4 nm^2. This information, together with the molecular mass and SSA_{BET} of PSi nanoparticles, can be used for the calculation of theoretical adsorbed amount. In the case of monolayer, the adsorbed amount would be 240 µg/mg for APSTCPSi and 190 µg/mg for TCPSi. As can be seen in Figure 23c, loaded peptide amount near the pI is more than double compared to theoretical calculation. The adsorption of lysozyme ($M \approx 15$ kDa), papain (23 kDa) and HAS (65 kDa) has before found

to form less than a monolayer which was attributed to the big size of the proteins and thus significantly smaller accessible surface area compared to nitrogen sorption methods [99]. GLP-1 is smaller molecule ($M \approx 3.4$ kDa) than these previous mentioned. This means that the first adsorbed layer on surface is thinner and the surface characteristics may still affect the adsorption. This could explain the formation of multilayer which is in line with previous results with mesoporous silica [228].

In summary, the adsorption at low concentrations seems to be driven by different interactions than at high concentrations. We attributed this difference to strong hydrophobic interactions between surface and peptide at low concentrations, which enables the high, 100 % loading efficiency. When peptide concentration is increased to near the concentration of particles, the peptide-peptide interaction dominates the loading and the neutral charge of the peptide enables the high packing density and thus, higher loading degrees.

The different adsorption behavior at small concentrations gave us a reason to study differences in desorption also. TCPSi nanoparticles were loaded in a 1:1 peptide solution at different pHs. Centrifuged nanoparticles were dispersed into a pH 7.0 buffer solution, and the amount of peptide released after two hours was measured with a UV-Vis spectrophotometer. The release dynamics were also tested, and the maximum release was achieved after 90 minutes. Results showed that the amount of released peptide is less than the loaded amount, indicating that there is a portion of irreversibly adsorbed peptides still attached to the nanoparticles. The amount of released peptide was taken into account and the adsorption behavior of GLP-1 to TCPSi nanoparticles is shown in Figure 24a with the irreversible layer highlighted. In order to verify the irreversible adsorption, we made a new desorption experiment with two cycles (Figure 24b). First in pH 7.0 and second in the same buffer with or without ethanol spiking. 20 vol-% ethanol on the solution increased the amount of released peptide and suppressed the irreversible amount to half, which implicates that a significant amount of apparently irreversibly adsorbed peptide was not covalently bonded on the surface.

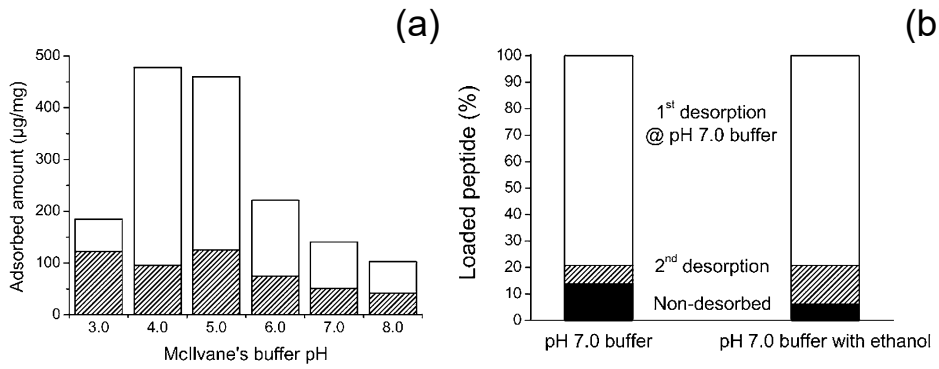

Figure 24. Irreversibly (dashed) and reversibly adsorbed payload on TCPSi nanoparticles in fist test with single release medium (a) and with second test with second desorption round in two different media (b).

The payload is typically reported as a loading degree. If the optimal pH 4.0 is used, the loading degree of the formulation is 32 %. If the irreversibly loaded peptides are subtracted from the payload, the loading degree is 26 %, which is still very good for biological drugs. Although irreversible adsorption is not reported in the context of mesoporous nanoparticles before Paper IV, it is not an uncommon observation when peptide adsorption on flat surfaces is studied. For example, Pinholt *et al.* observed irreversible adsorption in the case of another proglucagon originating peptide, GLP-2 [222].

7.5 Size, porosity and agglomeration: characterization challenges of DLS (Paper V)

Characterization of nanoparticle size is crucial for applications and toxicity studies, but not a straightforward task. In order to tackle this problem, the thorough light scattering study for mesoporous nanoparticles was made.

Two different silicon based materials, PSi and mesoporous silica, were used. The size of nanoparticles was measured first with TEM, and a clear difference on particle shape between silica and PSi nanoparticles can be observed (Figure 25). The morphology of PSi nanoparticles is irregular. The particle size distribution was found to be similar in all studied particle batches, and the data fits reasonably well to a log-normal distribution.

In the case of silica nanoparticles, the TEM pictures showed a spherical shape of particles, differences in pore structure, and the clear size difference. Log-

normal distributions fit well to the data. Sample R-MSN shows the narrowest particle size distribution and sample H-MSN the widest. Porosity and pore orientation of silica nanoparticles was confirmed. On P-MSN, pores are aligned parallel to each other while in R-MSN pores are radial, pointing towards the center of the particle. H-MSN has a hollow core and radial porous structure in the shell. S-SN and L-SN were small and large non-porous nanoparticles used as references in the study.

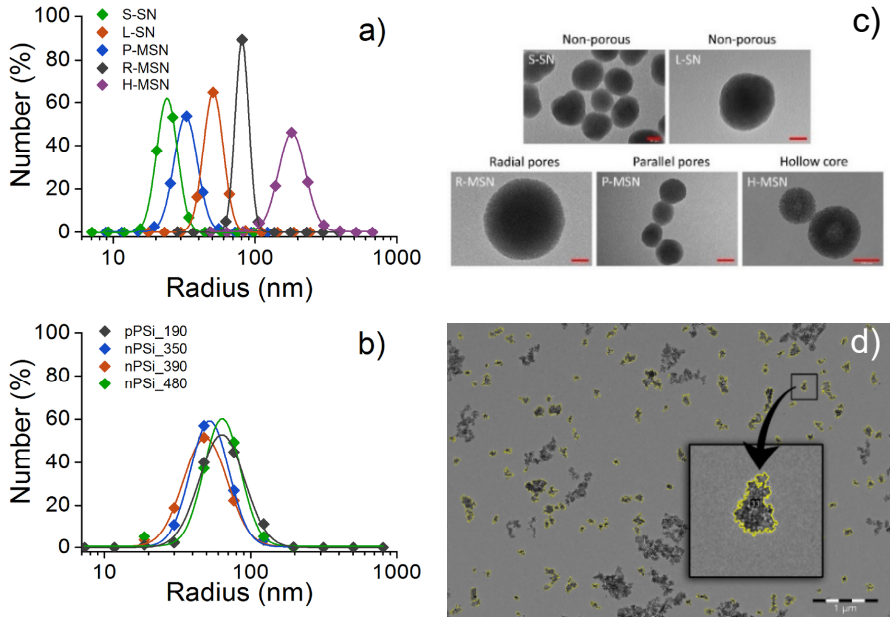

Figure 25. Particle size distribution of studied silica nanoparticles (a) and PSi nanoparticles (b). The example pictures of TEM results on respective order (c,d). Red scale bar represents 20 nm (S-SN, L-SN and R-MSN), 50 nm (P-MSN) and 200 nm (H-MSN).

In order to measure the radius of gyration R_g, the Debye-Bueche fit was used for the SLS result analysis of PSi nanoparticles (Figure 26a) as well as P-MSN, L-SN and S-SN samples. The scattering of R-MSN and H-MSN more resembled a scattering of spherical nanoparticles, enabling the use of a Guinier plot (Figure 26d). In the case of H-MSN, a Guinier plot was done to q^2–values below $5 \cdot 10^{-4}\ nm^{-2}$. Scattering behavior above this value resembles the scattering of non-porous hollow silica nanoparticles and is typical for core-shell particles [251],

but does not fit to the Guinier model. Hydrodynamic sizes (R_h) of studied nanoparticles were obtained with multiangle DLS measurements (Figure 26a,b). The values of R_h and R_g are tabulated in Table VI.

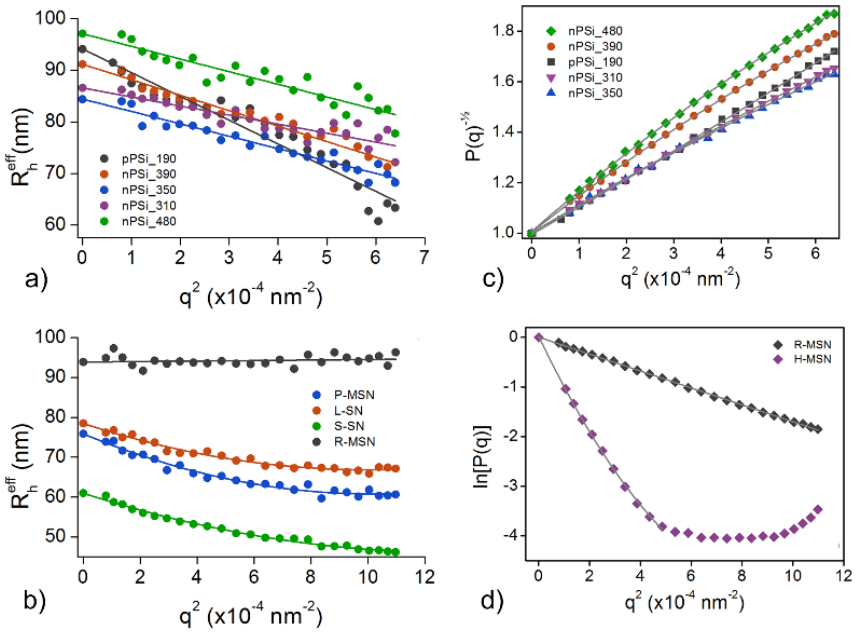

Figure 26. Measured DLS results and fits for PSi (a) and silica (b) nanoparticles. Example of SLS results and fits for the determination of R_g with Debye-Bueche (c) and Guinier (d) models.

The decrease of R_h^{eff} as a function of scattering angle (and scattering vector) was observed for all PSi samples as well as L-SN, S-SN, and P-MSN samples. That was attributed to a well-known phenomenon relating to the polydispersity of the suspension under investigation and particle size itself [156]. The polydispersity effect arises from the fact that large particles ($R > \lambda/20$) are scattering more light on low rather than high angles, which means that in polydisperse samples, the effect of big particles is more important on low angles. The only limitation for this is if the hydrodynamic size of all the particles are below the limit ($\lambda/20$), which is not the case with these nanoparticles. Thus polydispersity has an effect to the angular dependence of R_h^{eff}. This observation was used in order to quantify and compare the polydispersities between the samples.

All measured radiuses are tabulated on Table VI with the structural parameter (R_g/R_h) and overestimations between the hydrodynamic radius and

TEM primary particle radius (R_h/R_e). This overestimation was significant for almost all samples. In the case of silica nanoparticles, the variation of the error between particle types was considerable as the smallest error (13 % overestimation) was measured for the H-MSN sample and highest (148 %) for the S-SN sample. For the PSi nanoparticles, the variation was smaller, ranging from 31 % to 65 %.

Table VI. Measured sizes of PSi and silica nanoparticles along with structural characteristics

	Pore morphology	SSA_{BET} m^2/g	R_e nm	GSD	R_h nm	R_g nm	R_h/R_e	R_g/R_h
pPSi_190		190	72.1	0.36	94.1	80.2	1.31	0.85
nPSi_390		390	55.3	0.35	91.2	93.5	1.65	1.03
nPSi_350		350	57.5	0.30	84.4	81.8	1.47	0.97
nPSi_310		310			86.6	81.3		0.94
nPSi_480		480	69.3	0.29	97.1	98.8	1.40	1.02
P-MSN	parallel pores		33.6	0.19	75.9	78.6	2.26	1.04
S-SN	solid		24.6	0.17	61.0	68.0	2.48	1.11
L-SN	solid		52.1	0.16	78.5	74.1	1.51	0.94
R-MSN	radial pores		81.8	0.11	93.9	73.0	1.15	0.78
H-MSN	hollow		190.7	0.22	215.1	179.5	1.13	0.83

When comparisons between the DLS and TEM radiuses are made, it must be noted that these techniques and particle size distributions are fundamentally different. The TEM size distribution is based on the number of the particles, whereas the DLS distribution is based on the intensity of scattered light, which weights the distribution towards larger sizes. Some error is therefore expected. For a polydisperse sample, this error may be significant, so first we need to study the polydispersity.

In the studied samples, the polydispersity may arise in two different ways: from the initial particle size distribution or agglomeration in the presence of a medium. The intrinsic polydispersity can be quantified with a geometric standard deviation (GSD) of the size distribution from TEM studies. The agglomeration caused polydispersity should be seen in the slope of R_h^{eff} as explained before. In the case of PSi nanoparticles, which all have a wide size distribution, no correlation to either of these were found. For silica particles, there is a weak correlation on R_h^{eff} and error, which is a first hint of the agglomeration.

The easiest way to analyze the morphology of the nanoparticles is to compare the ratio of radius of gyration and hydrodynamic radius, R_g/R_h. Investigation of this value, with respect to the size error, reveals interesting behavior of silica nanoparticles and the correlation is clear (Figure 27a). The bigger the error is, the larger is R_g/R_h, also. Noteworthy is also the result that R_g/R_h does not correlate with the porosity of silica nanoparticles. This confirms the agglomeration of silica nanoparticles [252,253]. This is a significant observation, since the common assumption is that the hydrodynamic radius and polydispersity index, obtained from the one angle DLS measurement with CUMULANTS-analysis could reveal if agglomerates are present. This is the deduction that we have also made during the preparation of nanoparticle samples.

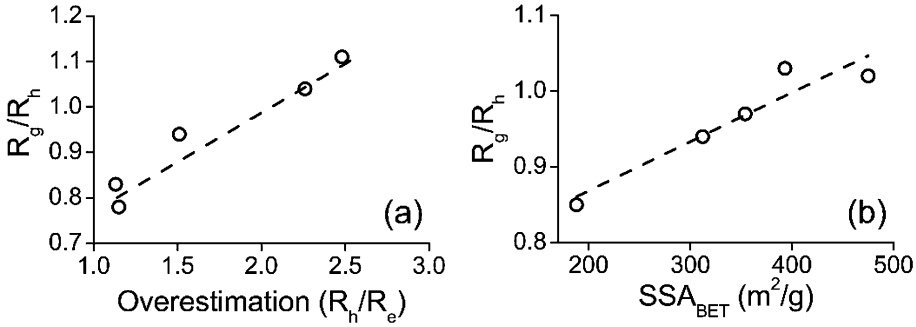

Figure 27. Correlation of structure parameter R_g/R_h compared to overestimation in the hydrodynamic diameter for silica nanoparticles (a) and to SSA_{BET} with PSi nanoparticles (b).

Differences between the TEM radius and hydrodynamic radius were less pronounced in the case of PSi nanoparticles, but still clear. A clear difference to silica nanoparticles was that the standard deviation correlates with the DLS slope, which emphasizes the polydispersity of primary particles, not agglomerates. Unexpectedly, a strong correlation between R_g/R_h and specific surface area, SSA_{BET} (Figure 27b) was found in PSi nanoparticles. The difference could arise from the distribution and size of scattering centers in the PSi matrix as similarly observed with silica aggregates [253]. This was a very interesting result and needs further studies because it could give a way to characterize porosity of PSi nanoparticles in solution. Unfortunately, an explanation for the error between DLS and TEM was not found because of conflicting or weak correlations. Both of the LS radiuses, R_g and R_h, seem to overestimate the nanoparticles radiuses when compared to the TEM radius, but by comparing these together, the correlation between R_g/R_h

and SSA_{BET} shows that LS studies can be used in order to make more rigorous particle size analysis.

8 Conclusions

One of the aims of this thesis was to study the zeta potential of PSi nanoparticles in isotonic formulations and characterize the impact of peptide payload to zeta potential. Zeta potential measurements, and especially IEP measurements, were made and reported for the first time for PSi nanoparticles with different surface chemistries. These measurements were found useful for surface chemistry characterization studies. The IEP results indicate the preservation of the special characteristics of the surface chemistries during the complex fabrication process of PSi nanoparticles. The results also indicate successful surface functionalization, highlighting the importance of the surface chemistry when controlling the zeta potential of PSi nanoparticles in the biologically relevant pH area. In addition, zeta potential was found to be useful for *in situ* degradation studies of surface coating.

When it is desired to maintain the PSi nanosuspensions' biocompatibility , one of the concerns is the stability of the suspension. It must be kept in mind that zeta potential is not an intrinsic property of nanoparticles, but as we have demonstrated, it is also affected by the other formulation components, like an isotonic medium and the loaded peptides. This effect is significant, and the impact of these components to the stability is critical. The studied peptides, GLP-1 and PYY, had opposite effects to zeta potential of PSi nanoparticles. Especially for the neutral and hydrophobic THCPSi nanoparticles, zeta potential was completely determined by the adsorbed peptide. The selection of isotonic medium also plays a role and they can be used in order to adjust zeta potential to the desired direction. Concentrated electrolytes, such as isotonic salt solutions, caused a drastic drop of zeta potential, and those media cannot be recommended to electrostatically stabilized nanoparticles. Low molecular weight PEG and HEPES provided sufficient zeta potential for a stable formulation of all studied nanoparticles.

One of the general aims was to find out the suitability of PSi nanoparticles for sc and iv peptide delivery, and by altering the surface chemistry, understand

the effect of surface chemistry on peptide release rate and bioavailability. PSi nanoparticles were found to be suitable for PYY delivery in sc administration *in vivo*. In sc delivery, PSi improved the delivery showing sustained release with high absolute bioavailability. The surface chemistry affected the delivery, and hydrophobic carriers showed more prolonged release. When nanoparticles were administered intravenously, nanoparticles' effect to sustain the release was almost nonexistent. This was attributed to competitive adsorption of blood proteins and rapid clearance from the circulation.

Interactions driving adsorption and loading of peptide (GLP-1) to PSi nanoparticles was studied in order to find optimal peptide loading conditions, and to find explanations for behavior of PSi nanoparticles *in vivo* studies. At low concentrations, both hydrophobic and electrostatic interactions were observed depending on the surface chemistry. The electrostatic effect seemed to be present in the adsorption at higher concentration, but the highest loading degrees were obtained when the peptide charge was near zero. Thus, we have concluded that the electrostatic attraction between the peptide and the surface is overemphasized when the objective is to maximize the loading degree. We also noted that strong interaction between the peptide and the nanoparticle could lead to irreversible adsorption. This highlights the importance of peptide-peptide interaction in the pores because the peptides that are firstly adsorbed on porous silicon may form a protective layer and facilitate the easy desorption. When the conditions are selected carefully, large amount of easily desorbing peptides can still be loaded into porous silicon nanoparticles. With the optimal loading pH, the loading degree was 32 %, and after subtracting the irreversibly loaded layer, the loading degree was still 26 %.

When adsorption and loading studies are reflected with the *in vivo* studies, some contemplations can be made. It is possible that the low peptide concentrations in loading solutions that were used in *in vivo* studies, had caused the strong interaction between particle surface and peptide. This would have been especially likely with hydrophobic surfaces. Since in *in vivo* studies hydrophobic nanoparticles are releasing peptides at the slowest rate, the strong interaction could be the explaining factor. Particle dissolution might also play a role in this behavior since TOPSi degrades faster than THCPSi or UnTHCPSi. The irreversible layer, which was observed in loading experiments, may only desorb when particles are dissolving.

In the fifth paper, we wanted to show how conventional light scattering methods can be used for a rigorous characterization of medium sensitive nanoparticles properties, like size, stability, and porosity. The size of silicon based mesoporous nanoparticles were measured with three different techniques, TEM,

DLS, and SLS. The primary particle radius, R_e, was measured with TEM, hydrodynamic radius, R_h, with DLS, and radius of gyration, R_g, with SLS. Recently DLS has become the most common method to characterize nanoparticle size and big differences between DLS and TEM sizes have been observed. These differences are normally attributed to the fundamental difference between intensity and number weighted particle size distributions and the differences between dry and hydrodynamic radii of particles. We studied the sizes of PSi nanoparticles and MSN and, as expected, we also observed remarkable differences between the hydrodynamic radius and primary particle radius. The overestimation of DLS varied from 13 % to 148 %.

The overestimation, in the case of the silica nanoparticles, was attributed to agglomeration of primary particles. This was the case despite the careful selection of the dispersion medium and monitoring the size with one angle DLS. If the porosity plays a role on the measurement, we were not able to distinguish it because of the strong agglomeration effect. The overestimation affected the structure parameter, R_g/R_h, so that the overestimation between DLS and TEM also led to the high structure parameter. This was attributed to the fractal nature of the agglomerates. In the case of PSi nanoparticles, the clear correlation between R_g/R_h and the specific surface area was observed, which could be due to the shape of the primary particle and the distribution of scattering centers inside one nanoparticle. This behavior needs more studies, and in the future, might open new ways to characterize the porosity of PSi nanoparticles.

Overall, the results of this thesis highlight the importance to characterize nanoparticles in their native colloidal state. Even more important is to test and apply these characterization methods to biorelevant media. With this purpose, light scattering, and especially multiangle light scattering, instruments have shown their versatility and analytical power.

References

[1] M. Heikkilä, H. Häkkinen, K. Rissanen, and J. Toppari, *Pienestä Syntyi Suurta | Nano Came to Jyväskylä* (University of Jyväskylä, Nanotiedekeskus, Jyväskylä, 2014).

[2] R. P. Feynman, Eng. Sci. **23**, 22 (1960).

[3] C. Toumey, Nat. Nanotechnol. **4**, 783 (2009).

[4] R. P. Feynman, Phys. Rev. **56**, 340 (1939).

[5] K. E. Drexler, Proc. Natl. Acad. Sci. USA **78**, 5275 (1981).

[6] K. E. Drexler, *Engines of Creation* (Anchor Press, Doubleday, New York, 1986).

[7] G. Binnig, C. F. Quate, and C. Gerber, Phys. Rev. Lett. **56**, 930 (1986).

[8] D. M. Eigler and E. K. Schweizer, Nature **344**, 524 (1990).

[9] M. L. Walker, S. A. Burgess, J. R. Sellers, F. Wang, J. A. Hammer, J. Trinick, and P. J. Knight, Nature **405**, 804 (2000).

[10] R. A. L. Jones, *Soft Machines - Nanotechnology and Life* (Oxford University Press, Oxford, 2004).

[11] V. Weissig, T. Pettinger, and N. Murdock, Int. J. Nanomedicine **9**, 4357 (2014).

[12] V. Weissig and D. Guzman-Villanueva, Int. J. Nanomedicine **10**, 1245 (2015).

[13] A. S. Hoffman, in *Fundam. Pharm. Nanosci.*, edited by I. F. Uchegbu, A. G. Schätzlein, W. P. Cheng, and A. Lalatsa (Springer Science+Business Media, New York, 2013), pp. v–vii.

[14] D. Berti and G. Palazzo, in *Colloid. Found. Nanosci.*, edited by D. Berti and G. Palazzo (Elsevier, 2014), pp. ix–x.

[15] R. J. Hunter, *Foundations of Colloid Science*, 2nd ed. (Oxford University Press, Oxford, 2001).

[16] IUPAC, *Compendium of Chemical Terminology, the "Gold Book,"* 2nd ed. (IUPAC, Research Triagle Park, NC, 2009).

[17] A. F. Masters and T. Maschmeyer, Microporous Mesoporous Mater. **142**, 423 (2011).

[18] R. Jones, Nat. Nanotechnol. **4**, 785 (2009).

[19] A. Uhlir, Bell Syst. Tech. J. **35**, 333 (1956).

[20] D. R. Turner, J. Electrochem. Soc. **105**, 402 (1958).

[21] V. Lehmann, *Electrochemistry of Silicon* (Wiley-VCH Verlag GmbH, Weinheim, 2002).

[22] R. J. Archer, J. Phys. Chem. Solids **14**, 104 (1960).

[23] A. L. Dalisa, W. K. Zwicker, D. J. Debitetto, and P. Harnack, Appl. Phys. Lett. **17**, 208 (1970).

[24] Y. Watanabe and T. Sakai, Rev. Electr. Commun. Lab. **19**, 899 (1971).

[25] K. Imai, Solid. State. Electron. **24**, 159 (1981).

[26] Y. Watanabe, J. Electrochem. Soc. **122**, 1351 (1975).
[27] L. T. Canham, Appl. Phys. Lett. **57**, 1046 (1990).
[28] A. Halimaoui, C. Oules, G. Bomchil, A. Bsiesy, F. Gaspard, R. Herino, M. Ligeon, and F. Muller, Appl. Phys. Lett. **59**, 304 (1991).
[29] P. M. Fauchet, L. Tsybeskov, C. Peng, S. P. Duttagupta, J. von Behren, Y. Kostoulas, J. M. V. Vandyshev, and K. D. Hirschman, IEEE J. Sel. Top. Quantum Electron. **1**, 1126 (1995).
[30] T. I. Cox, in *Prop. Porous Silicon*, edited by L. Canham (INSPEC, The Institution of Electrical Engineers, London, 1997), pp. 290–310.
[31] L. T. Canham, Adv. Mater. **7**, 1033 (1995).
[32] S. Bayliss, L. Buckberry, P. Harris, and C. Rousseau, Thin Solid Films **297**, 308 (1997).
[33] L. Canham, in *Handb. Porous Silicon*, edited by L. Canham (Springer International Publishing Switzerland, Cham, 2014), pp. 3–9.
[34] J. Salonen, A. M. Kaukonen, J. Hirvonen, and V.-P. Lehto, J. Pharm. Sci. **97**, 632 (2008).
[35] H. A. Santos, E. Mäkilä, L. M. Bimbo, P. Almeida, and J. Hirvonen, in *Fundam. Pharm. Nanosci.*, edited by I. F. Uchegbu, A. G. Schätzlein, W. P. Cheng, and A. Lalatsa (Springer Science+Business Media, New York, 2013), pp. 235–275.
[36] M. J. Sailor, *Porous Silicon in Practice* (Wiley-VCH Verlag GmbH & Co. KGaA, Weinheim, 2011).
[37] A. Loni, in *Handb. Porous Silicon*, edited by L. Canham (Springer International Publishing Switzerland, Cham, 2014), pp. 11–22.
[38] V. Lehmann, R. Stengl, and A. Luigart, Mater. Sci. Eng. B **69–70**, 11 (2000).
[39] J. Riikonen, M. Salomäki, J. van Wonderen, M. Kemell, W. Xu, O. Korhonen, M. Ritala, F. MacMillan, J. Salonen, and V.-P. Lehto, Langmuir **28**, 10573 (2012).
[40] J. Salonen, V.-P. Lehto, and E. Laine, Appl. Phys. Lett. **70**, 637 (1997).
[41] D. B. Mawhinney, J. A. Glass, and J. T. Yates, J. Phys. Chem. B **101**, 1202 (1997).
[42] A. E. Pap, K. Kordás, G. Tóth, J. Levoska, A. Uusimäki, J. Vähäkangas, S. Leppävuori, and T. F. George, Appl. Phys. Lett. **86**, ID 041501 (2005).
[43] G. B. Alexander, W. M. Heston, and R. K. Iler, J. Phys. Chem. **58**, 453 (1954).
[44] T. Jalkanen, V. Torres-Costa, E. Mäkilä, M. Kaasalainen, R. Koda, T. Sakka, Y. H. Ogata, and J. Salonen, ACS Appl. Mater. Interfaces **6**, 2884 (2014).
[45] B. Godin, J. Gu, R. E. Serda, R. Bhavane, E. Tasciotti, C. Chiappini, X. Liu, T. Tanaka, P. Decuzzi, and M. Ferrari, J. Biomed. Mater. Res. Part A **94**, 1236 (2010).
[46] J. M. Buriak, M. P. Stewart, T. W. Geders, M. J. Allen, H. C. Choi, J. Smith, D. Raftery, and L. T. Canham, J. Am. Chem. Soc. **121**, 11491 (1999).
[47] M. P. Stewart and J. M. Buriak, Angew. Chemie - Int. Ed. **37**, 3257 (1998).
[48] R. Boukherroub, J. Wojtyk, D. D. M. Wayner, and D. J. Lockwood, J. Electrochem. Soc. **149**, H59 (2002).
[49] Y. J. Seo, H. J. Cheon, and D. J. Choi, J. Mater. Sci. Lett. **17**, 313 (1998).

[50] J. Salonen, V.-P. Lehto, M. Björkqvist, E. Laine, and L. Niinistö, Phys. Status Solidi A **182**, 123 (2000).

[51] G. Dufour, F. Rochet, F. C. Stedile, C. Poncey, M. De Crescenzi, R. Gunnella, and M. Froment, Phys. Rev. B **56**, 4266 (1997).

[52] J. Paski, M. Björkqvist, J. Salonen, and V.-P. Lehto, Phys. Status Solidi C **2**, 3379 (2005).

[53] J. Salonen, M. Björkqvist, E. Laine, and L. Niinistö, Appl. Surf. Sci. **225**, 389 (2004).

[54] J. Salonen, E. Laine, and L. Niinistö, J. Appl. Phys. **91**, 456 (2002).

[55] C. C. Cheng, P. A. Taylor, R. M. Wallace, H. Gutleben, L. Clemen, M. L. Colaianni, P. J. Chen, W. H. Weinberg, W. J. Choyke, and J. T. Yates, Thin Solid Films **225**, 196 (1993).

[56] M. Sarparanta, E. Mäkilä, T. Heikkilä, J. Salonen, E. Kukk, V.-P. Lehto, H. A. Santos, J. Hirvonen, and A. J. Airaksinen, Mol. Pharm. **8**, 1799 (2011).

[57] A. M. Tinsley-Bown, L. T. Canham, M. Hollings, M. H. Anderson, C. L. Reeves, T. I. Cox, S. Nicklin, D. J. Squirrell, E. Perkins, A. Hutchinson, M. J. Sailor, and A. Wun, Phys. Status Solidi A **182**, 547 (2000).

[58] A. Janshoff, K.-P. S. Dancil, C. Steinem, D. P. Greiner, V. S.-Y. Lin, C. Gurtner, K. Motesharei, M. J. Sailor, and M. R. Ghadiri, J. Am. Chem. Soc. **120**, 12108 (1998).

[59] M. Arroyo-Hernández, R. J. Martín-Palma, J. Pérez-Rigueiro, J. P. García-Ruiz, J. L. García-Fierro, and J. M. Martínez-Duart, Mater. Sci. Eng. C **23**, 697 (2003).

[60] B. Sciacca, S. D. Alvarez, F. Geobaldoa, and M. J. Sailor, Dalt. Trans. **39**, 10847 (2010).

[61] M. Kovalainen, J. Mönkäre, E. Mäkilä, J. Salonen, V.-P. Lehto, K.-H. Herzig, and K. Järvinen, Pharm. Res. **29**, 837 (2012).

[62] T. Jalkanen, E. Mäkilä, Y.-I. Suzuki, T. Urata, K. Fukami, T. Sakka, J. Salonen, and Y. H. Ogata, Adv. Funct. Mater. **22**, 3890 (2012).

[63] J. L. Heinrich, C. L. Curns, G. M. Credo, K. L. Kavanagh, and M. J. Sailor, Science (80-.). **255**, 66 (1992).

[64] R. A. Bley, S. M. Kauzlarich, J. E. Davis, and H. W. H. Lee, Chem. Mater. **8**, 1881 (1996).

[65] A. B. Foraker, R. J. Walczak, M. H. Cohen, T. A. Boiarski, C. F. Grove, and P. W. Swaan, Pharm. Res. **20**, 110 (2003).

[66] K. Zhang, S. L. E. Loong, S. Connor, S. W. K. Yu, S. Tan, R. Ng, K. M. Lee, L. Canham, and P. K. H. Chow, Clin. Cancer Res. **11**, 7532 (2005).

[67] J. Salonen, L. Laitinen, A. M. Kaukonen, J. Tuura, M. Björkqvist, T. Heikkilä, K. Vähä-Heikkilä, J. Hirvonen, and V.-P. Lehto, J. Control. Release **108**, 362 (2005).

[68] C. Chiappini, E. Tasciotti, J. R. Fakhoury, D. Fine, L. Pullan, Y. C. Wang, L. Fu, X. Liu, and M. Ferrari, ChemPhysChem **11**, 1029 (2010).

[69] J.-H. Park, L. Gu, G. von Maltzahn, E. Ruoslahti, S. N. Bhatia, and M. J. Sailor,

Nat. Mater. **8**, 331 (2009).

[70] L. M. Bimbo, M. Sarparanta, H. A. Santos, A. J. Airaksinen, E. Mäkilä, T. Laaksonen, L. Peltonen, V.-P. Lehto, J. Hirvonen, and J. Salonen, ACS Nano **4**, 3023 (2010).

[71] L. Bychto, Y. Makushok, V. Chirvony, and E. Matveeva, Phys. Status Solidi C **5**, 3789 (2008).

[72] Z. Qin, J. Joo, L. Gu, and M. J. Sailor, Part. Part. Syst. Charact. **31**, 252 (2014).

[73] T. Nissinen, T. Ikonen, M. Lama, J. Riikonen, and V.-P. Lehto, Powder Technol. **288**, 360 (2016).

[74] L. Russo, F. Colangelo, R. Cioffi, I. Rea, and L. De Stefano, Materials (Basel). **4**, 1023 (2011).

[75] D. J. Savage, X. Liu, S. A. Curley, M. Ferrari, and R. E. Serda, Curr. Opin. Pharmacol. **13**, 834 (2013).

[76] B. Godin, C. Chiappini, S. Srinivasan, J. F. Alexander, K. Yokoi, M. Ferrari, P. Decuzzi, and X. Liu, Adv. Funct. Mater. **22**, 4225 (2012).

[77] H. Alhmoud, B. Delalat, R. Elnathan, A. Cifuentes-Rius, A. Chaix, M. L. Rogers, J. O. Durand, and N. H. Voelcker, Adv. Funct. Mater. **25**, 1137 (2015).

[78] J. W. Mares, J. S. Fain, K. R. Beavers, C. L. Duvall, and S. M. Weiss, Nanotechnology **26**, 271001 (2015).

[79] L. L. Hench and J. K. West, Chem. Rev. **90**, 33 (1990).

[80] W. Stöber, A. Fink, and E. Bohn, J. Colloid Interface Sci. **26**, 62 (1968).

[81] C. G. Tan, B. D. Bowen, and N. Epstein, J. Colloid Interface Sci. **118**, 290 (1987).

[82] F. Di Renzo, H. Cambon, and R. Dutartre, Microporous Mater. **10**, 283 (1997).

[83] C. T. Kresge, M. E. Leonowick, W. J. Roth, J. C. Vartuli, and J. S. Beck, Nature **359**, 710 (1992).

[84] J. N. Israelachvili, in *Intermol. Surf. Forces*, 3rd ed. (Academic Press, 2011), pp. 535–576.

[85] J. Israelachvili, Colloids Surfaces A - Physicochem. Eng. Asp. **91**, 1 (1994).

[86] F. Hoffmann, M. Cornelius, J. Morell, and M. Fröba, Angew. Chemie - Int. Ed. **45**, 3216 (2006).

[87] L. Canham, in *Handb. Porous Silicon*, edited by L. Canham (Springer International Publishing Switzerland, Cham, 2014), pp. 733–740.

[88] S. Dhanekar and S. Jain, Biosens. Bioelectron. **41**, 54 (2013).

[89] A. Jane, R. Dronov, A. Hodges, and N. H. Voelcker, Trends Biotechnol. **27**, 230 (2009).

[90] E. J. Anglin, L. Cheng, W. R. Freeman, and M. J. Sailor, Adv. Drug Deliv. Rev. **60**, 1266 (2008).

[91] D. J. Craik, D. P. Fairlie, S. Liras, and D. Price, Chem. Biol. Drug Des. **81**, 136 (2013).

[92] P. Vlieghe, V. Lisowski, J. Martinez, and M. Khrestchatisky, Drug Discov. Today **15**, 40 (2010).

[93] M. Kovalainen, J. Mönkare, J. Riikonen, U. Pesonen, M. Vlasova, J. Salonen, V.-P. Lehto, K. Järvinen, and K.-H. Herzig, Pharmacol. Rev. **67**, 541 (2015).

[94] S. Frokjaer and D. E. Otzen, Nat. Rev. Drug Discov. **4**, 298 (2005).
[95] M. Kilpeläinen, J. Riikonen, M. A. Vlasova, A. Huotari, V. P. Lehto, J. Salonen, K. H. Herzig, and K. Järvinen, J. Control. Release **137**, 166 (2009).
[96] M. Kilpeläinen, J. Mönkäre, M. A. Vlasova, J. Riikonen, V.-P. Lehto, J. Salonen, K. Järvinen, and K.-H. Herzig, Eur. J. Pharm. Biopharm. **77**, 20 (2011).
[97] J. Renukuntla, A. D. Vadlapudi, A. Patel, S. H. S. Boddu, and A. K. Mitra, Int. J. Pharm. **447**, 75 (2013).
[98] C. A. Prestidge, T. J. Barnes, A. Mierczynska-Vasilev, I. Kempson, F. Peddie, and C. Barnett, Phys. Status Solidi A **205**, 311 (2008).
[99] K. L. Jarvis, T. J. Barnes, and C. A. Prestidge, Langmuir **26**, 14316 (2010).
[100] E. Pastor, E. Matveeva, A. Valle-Gallego, F. M. Goycoolea, and M. Garcia-Fuentes, Colloids Surfaces B - Biointerfaces **88**, 601 (2011).
[101] D. Liu, L. M. Bimbo, E. Mäkilä, F. Villanova, M. Kaasalainen, B. Herranz-Blanco, C. M. Caramella, V.-P. Lehto, J. Salonen, K.-H. Herzig, J. Hirvonen, and H. A. Santos, J. Control. Release **170**, 268 (2013).
[102] F. Araújo, N. Shrestha, M.-A. Shahbazi, P. Fonte, E. M. Mäkilä, J. J. Salonen, J. T. Hirvonen, P. L. Granja, H. A. Santos, and B. Sarmento, Biomaterials **35**, 9199 (2014).
[103] N. Shrestha, M.-A. Shahbazi, F. Araújo, H. Zhang, E. M. Mäkilä, J. Kauppila, B. Sarmento, J. J. Salonen, J. T. Hirvonen, and H. A. Santos, Biomaterials **35**, 7172 (2014).
[104] F. Araújo, N. Shrestha, M.-A. Shahbazi, D. Liu, B. Herranz-Blanco, E. M. Mäkilä, J. J. Salonen, J. T. Hirvonen, P. L. Granja, B. Sarmento, and H. A. Santos, ACS Nano **9**, 8291 (2015).
[105] N. Shrestha, M. A. Shahbazi, F. Araújo, E. Mäkilä, J. Raula, E. I. Kauppinen, J. Salonen, B. Sarmento, J. Hirvonen, and H. A. Santos, Biomaterials **68**, 9 (2015).
[106] N. Shrestha, F. Araújo, M. A. Shahbazi, E. Mäkilä, M. J. Gomes, M. Airavaara, E. I. Kauppinen, J. Raula, J. Salonen, J. Hirvonen, B. Sarmento, and H. A. Santos, J. Control. Release **232**, 113 (2016).
[107] N. Shrestha, F. Araújo, M.-A. Shahbazi, E. Mäkilä, M. J. Gomes, B. Herranz-Blanco, R. Lindgren, S. Granroth, E. Kukk, J. Salonen, J. Hirvonen, B. Sarmento, and H. A. Santos, Adv. Funct. Mater. **26**, 3405 (2016).
[108] E. De Rosa, C. Chiappini, D. Fan, X. Liu, M. Ferrari, and E. Tasciotti, Pharm. Res. **28**, 1520 (2011).
[109] A. Jiménez-Periáñez, B. Abos Gracia, J. López Relaño, C. M. Diez-Rivero, P. A. Reche, E. Martínez-Naves, E. Matveyeva, and M. Gómez del Moral, Clin. Dev. Immunol. **2013**, 362163 (2013).
[110] M. Vallet-Regi, A. Rámila, R. P. del Real, and J. Pérez-Pariente, Chem. Mater. **13**, 308 (2001).
[111] E. J. Anglin, M. P. Schwartz, V. P. Ng, L. A. Perelman, and M. J. Sailor, Langmuir **20**, 11264 (2004).
[112] L. Z. Benet, J. Pharm. Sci. **102**, 34 (2013).

[113] R. Laitinen, K. Löbmann, C. J. Strachan, H. Grohganz, and T. Rades, Int. J. Pharm. **453**, 65 (2013).

[114] C. Alba-Simionesco, B. Coasne, G. Dosseh, G. Dudziak, K. E. Gubbins, R. Radhakrishnan, and M. Sliwinska-Bartkowiak, J. Phys. Condens. Matter **18**, R15 (2006).

[115] E. Mäkilä, M. P. A. Ferreira, H. Kivelä, S.-M. Niemi, A. Correia, M.-A. Shahbazi, J. Kauppila, J. Hirvonen, H. A. Santos, and J. Salonen, Langmuir **30**, 2196 (2014).

[116] F. Wang, H. Hui, T. J. Barnes, C. Barnett, and C. A. Prestidge, Mol. Pharm. **7**, 227 (2010).

[117] I. Brigger, C. Dubernet, and P. Couvreur, Adv. Drug Deliv. Rev. **54**, 631 (2002).

[118] L. Grislain, P. Couvreur, V. Lenaerts, M. Roland, D. Deprez-Decampeneere, and P. Speiser, Int. J. Pharm. **15**, 335 (1983).

[119] G. Storm, S. O. Belliot, T. Daemen, and D. D. Lasic, Adv. Drug Deliv. Rev. **17**, 31 (1995).

[120] J. Cortes and C. Saura, Eur. J. Cancer Suppl. **8**, 1 (2010).

[121] T. Tanaka, B. Godin, R. Bhavane, R. Nieves-Alicea, J. Gu, X. Liu, C. Chiappini, J. R. Fakhoury, S. Amra, A. Ewing, Q. Li, I. J. Fidler, and M. Ferrari, Int. J. Pharm. **402**, 190 (2010).

[122] J. Rytkönen, R. Miettinen, M. Kaasalainen, V.-P. Lehto, J. Salonen, and A. Närvänen, J. Nanomater. **2012**, 896562 (2012).

[123] M. Sarparanta, L. M. Bimbo, J. Rytkönen, E. Mäkilä, T. J. Laaksonen, P. Laaksonen, M. Nyman, J. Salonen, M. B. Linder, J. Hirvonen, H. A. Santos, and A. J. Airaksinen, Mol. Pharm. **9**, 654 (2012).

[124] P. Decuzzi, B. Godin, T. Tanaka, S.-Y. Lee, C. Chiappini, X. Liu, and M. Ferrari, J. Control. Release **141**, 320 (2010).

[125] E. Secret, K. Smith, V. Dubljevic, E. Moore, P. Macardle, B. Delalat, M.-L. Rogers, T. G. Johns, J.-O. Durand, F. Cunin, and N. H. Voelcker, Adv. Healthc. Mater. **2**, 718 (2012).

[126] A. P. Mann, T. Tanaka, A. Somasunderam, X. Liu, D. G. Gorenstein, and M. Ferrari, Adv. Mater. **23**, H278 (2011).

[127] E. Ruoslahti, S. N. Bhatia, and M. J. Sailor, J. Cell Biol. **188**, 759 (2010).

[128] C. F. Wang, E. M. Mäkilä, C. Bonduelle, J. Rytkönen, J. Raula, S. Almeida, A. Närvänen, J. J. Salonen, S. Lecommandoux, J. T. Hirvonen, and H. A. Santos, ACS Appl. Mater. Interfaces **7**, 2006 (2015).

[129] P. J. Kinnari, M. L. K. Hyvönen, E. M. Mäkilä, M. H. Kaasalainen, A. Rivinoja, J. J. Salonen, J. T. Hirvonen, P. M. Laakkonen, and H. A. Santos, Biomaterials **34**, 9134 (2013).

[130] I. I. Slowing, B. G. Trewyn, and V. S.-Y. Lin, J. Am. Chem. Soc. **129**, 8845 (2007).

[131] Z. P. Xu, Q. H. Zeng, G. Q. Lu, and A. B. Yu, Chem. Eng. Sci. **61**, 1027 (2006).

[132] R. E. Serda, J. Gu, R. C. Bhavane, X. Liu, C. Chiappini, P. Decuzzi, and M. Ferrari, Biomaterials **30**, 2440 (2009).

[133] L. Canham and D. Ferguson, in *Handb. Porous Silicon*, edited by L. Canham

(Springer International Publishing Switzerland, Cham, 2014), pp. 901–907.
[134] A. S. W. Goh, A. Y. F. Chung, R. H. G. Lo, T. N. Lau, S. W. K. Yu, M. Chng, S. Satchithanantham, S. L. E. Loong, D. C. E. Ng, B. C. Lim, S. Connor, and P. K. H. Chow, Int. J. Radiat. Oncol. Biol. Phys. **67**, 786 (2007).
[135] H. Hou, A. Nieto, F. Ma, W. R. Freeman, M. J. Sailor, and L. Cheng, J. Control. Release **178**, 46 (2014).
[136] L. Cheng, E. Anglin, F. Cunin, D. Kim, M. J. Sailor, I. Falkenstein, A. Tammewar, and W. R. Freeman, Br. J. Ophthalmol. **92**, 705 (2008).
[137] H. Hou, A. Nieto, A. Belghith, K. Nan, Y. Li, W. R. Freeman, M. J. Sailor, and L. Cheng, Acta Biomater. **24**, 309 (2015).
[138] C. Chiappini, E. De Rosa, J. O. Martinez, X. Liu, J. Steele, M. M. Stevens, and E. Tasciotti, Nat. Mater. **14**, 532 (2015).
[139] C. Chiappini, J. O. Martinez, E. De Rosa, C. S. Almeida, E. Tasciotti, and M. M. Stevens, ACS Nano **9**, 5500 (2015).
[140] R. J. Martín-Palma and V. Torres-Costa, in *Handb. Porous Silicon*, edited by L. Canham (Springer International Publishing Switzerland, Cham, 2014), pp. 413–421.
[141] S. Brunauer, P. Emmett, and E. Teller, J. Am. Chem. Soc. **60**, 309 (1938).
[142] F. Rouquerol, J. Rouquerol, and K. Sing, in *Adsorpt. by Powders Porous Solids* (Elsevier, London, 1999), pp. 439–447.
[143] E. P. Barrett, L. G. Joyner, and P. P. Halenda, J. Am. Chem. Soc. **73**, 373 (1951).
[144] M. D. Donohue and G. L. Aranovich, Adv. Colloid Interface Sci. **76–77**, 137 (1998).
[145] K. S. W. Sing, Pure Appl. Chem. **57**, 603 (1985).
[146] V.-P. Lehto, K. Vähä-Heikkilä, J. Paski, and J. Salonen, J. Therm. Anal. Calorim. **80**, 393 (2005).
[147] J. Salonen, J. Paski, K. Vähä-Heikkilä, T. Heikkilä, M. Björkqvist, and V.-P. Lehto, Phys. Status Solidi A **202**, 1629 (2005).
[148] J. Riikonen, E. Mäkilä, J. Salonen, and V.-P. Lehto, Langmuir **25**, 6137 (2009).
[149] E. Mäkilä, H. Kivelä, N. Shrestha, A. Correia, M. Kaasalainen, E. Kukk, J. Hirvonen, H. A. Santos, and J. Salonen, Langmuir **32**, 13020 (2016).
[150] Y. H. Ogata, in *Handb. Porous Silicon*, edited by L. Canham (Springer International Publishing Switzerland, Cham, 2014), pp. 473–480.
[151] M. Kosmulski, *Surface Charging and Points of Zero Charge* (CRC Press, Taylor and Francis Group, Lublin, 2009).
[152] D. J. Shaw, *Introduction to Colloid and Surface Chemistry*, 4th ed. (Butterworth-Heinemann, Oxford, 1992).
[153] J. N. Israelachvili, *Intermolecular and Surface Forces*, 3rd ed. (Academic Press, 2011).
[154] R. A. L. Jones, *Soft Condensed Matter* (Oxford University Press, Oxford, 2002).
[155] B. Chu, *Laser Light Scattering: Basic Principles and Practice*, 2nd ed. (Academic Press, San Diego, 1991).
[156] P. A. Hassan, S. Rana, and G. Verma, Langmuir **31**, 3 (2015).

[157] R. Xu, *Particle Characterization: Light Scattering Methods* (Kluwer Academic Publishers, Hingham, 2000).
[158] A. T. Florence and D. Attwood, *Physicochemical Principles of Pharmacy*, 4th ed. (Pharmaceutical press, London, 2006).
[159] J. N. Israelachvili, in *Intermol. Surf. Forces*, 3rd ed. (Academic Press, 2011), pp. 205–222.
[160] D. Zadaka, A. Radian, and Y. G. Mishael, J. Colloid Interface Sci. **352**, 171 (2010).
[161] W. Norde, Colloids Surfaces B - Biointerfaces **61**, 1 (2008).
[162] Merck, *The Merck Index*, 13th ed. (Merck, New Jersey, 2001).
[163] B. Derjaguin and L. Landau, Acta Physicochim. URSS **14**, 633 (1941).
[164] E. J. W. Verwey and J. T. G. Overbeek, *Theory of the Stability of Lyophobic Colloids* (Elsevier Publishing Company, Amsterdam, 1948).
[165] G. Nichols, S. Byard, M. J. Bloxham, J. Botterill, N. J. Dawson, A. Dennis, V. Diart, N. C. North, and J. D. Sherwood, J. Pharm. Sci. **91**, 2103 (2002).
[166] D. F. Moyano, M. Goldsmith, D. J. Solfiell, D. Landesman-milo, O. R. Miranda, D. Peer, and V. M. Rotello, J. Am. Chem. Soc. **134**, 3965 (2012).
[167] C. D. Walkey and W. C. W. Chan, Chem. Soc. Rev. **41**, 2780 (2012).
[168] L. Canham, in *1st Annu. Int. IEEE-EMBS Spec. Top. Conf. Microtechnologies Med. Biol. Proc.* (IEEE, 2000), pp. 109–112.
[169] S. H. C. Anderson, H. Elliott, D. J. Wallis, L. T. Canham, and J. J. Powell, Phys. Status Solidi A **197**, 331 (2003).
[170] P. Allongue, J. Electrochem. Soc. **140**, 1018 (1993).
[171] E. Bissé, T. Epting, A. Beil, G. Lindinger, H. Lang, and H. Wieland, Anal. Biochem. **337**, 130 (2005).
[172] L. M. Jurkić, I. Cepanec, S. K. Pavelić, and K. Pavelić, Nutr. Metab. (Lond). **10**, ID 2 (2013).
[173] D. M. Reffitt, R. Jugdaohsingh, R. P. Thompson, and J. J. Powell, J. Inorg. Biochem. **76**, 141 (1999).
[174] S. Davenward, P. Bentham, J. Wright, P. Crome, D. Job, A. Polwart, and C. Exley, J. Alzheimer's Dis. **33**, 423 (2013).
[175] A. Tzur-Balter, J. M. Young, L. M. Bonanno-Young, and E. Segal, Acta Biomater. **9**, 8346 (2013).
[176] A. Tzur-Balter, Z. Shatsberg, M. Beckerman, E. Segal, and N. Artzi, Nat. Commun. **6**, 6208 (2015).
[177] S. P. Low and N. H. Voelcker, in *Handb. Porous Silicon*, edited by L. Canham (Springer International Publishing Switzerland, Cham, 2014), pp. 381–393.
[178] A. P. Bowditch, K. Waters, H. Gale, P. Rice, E. A. M. Scott, L. T. Canham, C. L. Reeves, A. Loni, and T. I. Cox, in *MRS Proc.* (1998), p. 149.
[179] S. P. Low, N. H. Voelcker, L. T. Canham, and K. A. Williams, Biomaterials **30**, 2873 (2009).
[180] A. Rosengren, L. Wallman, M. Bengtsson, T. Laurell, N. Danielsen, and L. M. Bjursten, Phys. Status Solidi A **182**, 527 (2000).

[181] S. Bayliss, P. Harris, L. Buckberry, and C. Rousseau, J. Mater. Sci. Lett. **16**, 737 (1997).
[182] V. Chin, B. E. Collins, M. J. Sailor, and S. N. Bhatia, Adv. Mater. **13**, 1877 (2001).
[183] S. P. Low, K. A. Williams, L. T. Canham, and N. H. Voelcker, Biomaterials **27**, 4538 (2006).
[184] K. L. Jarvis, T. J. Barnes, A. Badalyan, P. Pendleton, and C. A. Prestidge, J. Phys. Chem. C **112**, 9717 (2008).
[185] P. Aggarwal, J. B. Hall, C. B. McLeland, M. a Dobrovolskaia, and S. E. McNeil, Adv. Drug Deliv. Rev. **61**, 428 (2009).
[186] D. E. Owens and N. A. Peppas, Int. J. Pharm. **307**, 93 (2006).
[187] A. Nel, T. Xia, L. Mädler, and N. Li, Science (80-.). **311**, 622 (2006).
[188] C. D. Walkey, J. B. Olsen, F. Song, R. Liu, H. Guo, W. H. Olsen, Y. Cohen, E. Andrew, and W. C. W. Chan, ACS Nano **8**, 2439 (2014).
[189] C. F. Jones and D. W. Grainger, Adv. Drug Deliv. Rev. **61**, 438 (2009).
[190] A. E. Nel, L. Mädler, D. Velegol, T. Xia, E. M. V Hoek, P. Somasundaran, F. Klaessig, V. Castranova, and M. Thompson, Nat. Mater. **8**, 543 (2009).
[191] S. Patil, A. Sandberg, E. Heckert, W. Self, and S. Seal, Biomaterials **28**, 4600 (2007).
[192] C. Wilhelm, C. Billotey, J. Roger, J. N. Pons, J.-C. Bacri, and F. Gazeau, Biomaterials **24**, 1001 (2003).
[193] A. Asati, S. Santra, C. Kaittanis, and J. M. Perez, ACS Nano **4**, 5321 (2010).
[194] I. Slowing, B. G. Trewyn, and V. S.-Y. Lin, J. Am. Chem. Soc. **128**, 14792 (2006).
[195] M.-A. Shahbazi, M. Hamidi, E. M. Mäkilä, H. Zhang, P. V Almeida, M. Kaasalainen, J. J. Salonen, J. T. Hirvonen, and H. A. Santos, Biomaterials **34**, 7776 (2013).
[196] M. P. Monopoli, D. Walczyk, A. Campbell, G. Elia, I. Lynch, F. B. Bombelli, and K. A. Dawson, J. Am. Chem. Soc. **133**, 2525 (2011).
[197] D. Walczyk, F. Baldelli Bombelli, M. P. Monopoli, I. Lynch, and K. A. Dawson, J. Am. Chem. Soc. **132**, 5761 (2010).
[198] E. Casals, T. Pfaller, A. Duschl, G. J. Oostingh, and V. Puntes, ACS Nano **4**, 3623 (2010).
[199] D. F. Moyano, K. Saha, G. Prakash, B. Yan, H. Kong, M. Yazdani, and V. M. Rotello, J. Am. Chem. Soc. **8**, 6748 (2014).
[200] Z.-J. Zhu, T. Posati, D. F. Moyano, R. Tang, B. Yan, R. W. Vachet, and V. M. Rotello, Small **8**, 2659 (2012).
[201] J. Rytkönen, Mesoporous Silicon Particles Designed for Nanomedical Applications, University of Eastern Finland, 2014.
[202] N. Benne, J. Van Duijn, J. Kuiper, W. Jiskoot, and B. Slütter, J. Control. Release **234**, 124 (2016).
[203] T. Sun, Y. S. Zhang, B. Pang, D. C. Hyun, M. Yang, and Y. Xia, Angew. Chemie - Int. Ed. **53**, 12320 (2014).
[204] H. A. Santos, J. Riikonen, J. Salonen, E. Mäkilä, T. Heikkilä, T. Laaksonen, L.

Peltonen, V.-P. Lehto, and J. Hirvonen, Acta Biomater. **6**, 2721 (2010).
[205] B. Fadeel, A. Fornara, M. S. Toprak, and K. Bhattacharya, Biochem. Biophys. Res. Commun. **468**, 498 (2015).
[206] A. T. Florence, J. Control. Release **164**, 115 (2012).
[207] A. R. M. N. Afrooz, S. M. Hussain, and N. B. Saleh, J. Nanoparticle Res. **16**, 2771 (2014).
[208] E. C. Cho, Q. Zhang, Y. Xia, and X. Xia, Nat. Nanotechnol. **6**, 385 (2011).
[209] X. Liu, Y. Chen, H. Li, N. Huang, Q. Jin, K. Ren, and J. Ji, ACS Nano **7**, 6244 (2013).
[210] Z. E. Allouni, M. R. Cimpan, P. J. Høl, T. Skodvin, and N. R. Gjerdet, Colloids Surfaces B - Biointerfaces **68**, 83 (2009).
[211] R. C. Murdock, L. Braydich-Stolle, A. M. Schrand, J. J. Schlager, and S. M. Hussain, Toxicol. Sci. **101**, 239 (2008).
[212] J. Rytkönen, P. Arukuusk, W. Xu, K. Kurrikoff, U. Langel, V.-P. Lehto, and A. Närvänen, Mol. Pharm. **11**, 382 (2014).
[213] K. L. Jarvis, T. J. Barnes, and C. A. Prestidge, Adv. Colloid Interface Sci. **175**, 25 (2012).
[214] E. Tasciotti, X. Liu, R. Bhavane, K. Plant, A. D. Leonard, B. K. Price, M. M.-C. Cheng, P. Decuzzi, J. M. Tour, F. Robertson, and M. Ferrari, Nat. Nanotechnol. **3**, 151 (2008).
[215] T. Limnell, J. Riikonen, J. Salonen, A. M. Kaukonen, L. Laitinen, J. Hirvonen, and V.-P. Lehto, Int. J. Pharm. **343**, 141 (2007).
[216] P. Horcajada, A. Rámila, J. Pérez-Pariente, and M. Vallet-Regí, Microporous Mesoporous Mater. **68**, 105 (2004).
[217] Y. Zhang, Z. Zhi, T. Jiang, J. Zhang, Z. Wang, and S. Wang, J. Control. Release **145**, 257 (2010).
[218] J. Riikonen, A. Correia, M. Kovalainen, S. Näkki, M. Lehtonen, J. Leppänen, J. Rantanen, W. Xu, F. Araújo, J. Hirvonen, K. Järvinen, H. A. Santos, and V.-P. Lehto, Biomaterials **52**, 44 (2015).
[219] A. Tzur-Balter, A. Gilert, N. Massad-Ivanir, and E. Segal, Acta Biomater. **9**, 6208 (2013).
[220] A. Nieto, M. Colilla, F. Balas, and M. Vallet-Regí, Langmuir **26**, 5038 (2010).
[221] A. Huotari, W. Xu, J. Mönkäre, M. Kovalainen, K.-H. Herzig, V.-P. Lehto, and K. Järvinen, Int. J. Pharm. **454**, 67 (2013).
[222] C. Pinholt, S. J. Kapp, J. T. Bukrinsky, S. Hostrup, S. Frokjaer, W. Norde, and L. Jorgensen, Int. J. Pharm. **440**, 63 (2013).
[223] L.-C. Sang and M.-O. Coppens, Phys. Chem. Chem. Phys. **13**, 6689 (2011).
[224] C. Haynes and W. Norde, Colloids Surfaces B - Biointerfaces **2**, 517 (1994).
[225] C. Pinholt, R. A. Hartvig, N. J. Medlicott, and L. Jorgensen, Expert Opin. Drug Deliv. **8**, 949 (2011).
[226] W. Norde, Adv. Colloid Interface Sci. **25**, 267 (1986).
[227] A. Vinu, M. Miyahara, and K. Ariga, J. Phys. Chem. B **109**, 6436 (2005).
[228] L.-C. Sang, A. Vinu, and M.-O. Coppens, Langmuir **27**, 13828 (2011).

[229] A. Vinu, V. Murugesan, O. Tangermann, and M. Hartmann, Chem. Mater. **16**, 3056 (2004).
[230] W. Norde, J. Buijs, and J. Lyklema, in *Fundam. Interface Colloid Sci. Vol. V Soft Colloids*, edited by J. Lyklema (Academic Press, 2005), p. 3.1-3.59.
[231] A. Verma and F. Stellacci, Small **6**, 12 (2010).
[232] J. Zhang and J. M. Rosenholm, Ther. Deliv. **6**, 891 (2015).
[233] D. Şen Karaman, T. Gulin-Sarfraz, J. Zhang, and J. M. Rosenholm, Mater. Lett. **143**, 140 (2015).
[234] L. J. Karhunen, K. R. Juvonen, A. Huotari, A. K. Purhonen, and K. H. Herzig, Regul. Pept. **149**, 70 (2008).
[235] A. M. Wren and S. R. Bloom, Gastroenterology **132**, 2116 (2007).
[236] J. C. Cameselle, J. M. Ribeiro, and A. Sillero, Biochem. Educ. **14**, 131 (1986).
[237] D. L. Nelson and M. M. Cox, *Lehninger Principles of Biochemistry*, 3rd ed. (Worth Publishers, New York, 2000).
[238] I. D. Morrison and E. F. Grabowski, Langmuir **1**, 496 (1985).
[239] D. E. Koppel, J. Chem. Phys. **57**, 4814 (1972).
[240] W. Brown, *Dynamic Light Scattering: The Method and Some Applications* (Clarendon Press, Oxford, 1993).
[241] P. Debye and A. M. Bueche, J. Appl. Phys. **20**, 518 (1949).
[242] A. Guinier and G. Fournet, *Small-Angle Scattering of X-Rays* (John Wiley & Sons, New York, 1955).
[243] D. C. Henry, Proc. R. Soc. London Ser. A **133**, 106 (1931).
[244] A. V Delgado, F. González-Caballero, R. J. Hunter, L. K. Koopal, and J. Lyklema, J. Colloid Interface Sci. **309**, 194 (2007).
[245] H. Ohshima, J. Colloid Interface Sci. **168**, 269 (1994).
[246] J. Rouquerol, D. Avnir, C. W. Fairbridge, D. H. Everett, J. H. Haynes, N. Pernicone, J. D. F. Ramsay, K. S. W. Sing, and K. K. Unger, Pure Appl. Chem. **66**, 1739 (1994).
[247] C. A. Schneider, W. S. Rasband, and K. W. Eliceiri, Nat. Methods **9**, 671 (2012).
[248] G. A. Parks, Chem. Rev. **65**, 177 (1965).
[249] J. M. Rosenholm and M. Lindén, Chem. Mater. **19**, 5023 (2007).
[250] X. Chang, D. Keller, S. Bjron, and J. J. Led, Magn. Reson. Chem. **39**, 477 (2001).
[251] P. Ruckdeschel, M. Dulle, T. Honold, S. Förster, M. Karg, and M. Retsch, Nano Res. **9**, 1366 (2016).
[252] U. Kätzel, M. Vorbau, M. Stintz, T. Gottschalk-Gaudig, and H. Barthel, Part. Part. Syst. Charact. **25**, 19 (2008).
[253] U. Kätzel, R. Bedrich, M. Stintz, R. Ketzmerick, T. Gottschalk-Gaudig, and H. Barthel, Part. Part. Syst. Charact. **25**, 9 (2008).

Annales Universitatis Turkuensis

Turun yliopisto
University of Turku

ISBN 978-951-29-6811-4 (PRINT)
ISBN 978-951-29-6812-1 (PDF)
ISSN 0082-7002 (Print) | ISSN 2343-3175 (Online)

Painosalama Oy, Turku, Finland 2017